UNIVERSITA' DEGLI STUDI DI MILANO

Scuola di Dottorato di Ricerca in Scienze Biochimiche, Nutrizionali e Metaboliche

Direttore: Prof. Sandro Sonnino

Dottorato di Ricerca in Scienze Biochimiche XXVII ciclo

Coordinatore: Prof. Francesco Bonomi

INVOLVEMENT OF THE SPHINGOLIPID METABOLISM IN PROSTATE AND BLADDER CANCER MALIGNANCY

Docente guida: Prof. Sandro Sonnino

Tutor: Dr. Massimo Aureli

Tesi di Dottorato di

Valentina MURDICA

Matricola: R10183

Anno Accademico 2014-2015

Alla mia famiglia

Index

Summary

Sphingolipids (SLs) are cell membrane amphiphilic components, which reside in the external layer of the plasma membrane (PM), with the hydrophobic moiety, the ceramide (Cer), inserted into the membrane layer and the hydrophilic head group protruding toward the extracellular environment. As membrane components, SLs participate to modulate several cell processes, such as cell growth, motility, differentiation, morphogenesis, cell to matrix interaction and cell to cell communication. From this, it follows that a defect in SL metabolism can obviously lead to a great number of dysfunctions, ranging from neurodegeneration to cancer.

During my PhD course, I studied the different faces of SLs in cancer malignancy. In particular, I focused my attention on the involvement of SL as well as of their metabolism in the prostate and bladder cancer malignancy and in their response to the conventional therapies.

As well known, prostate cancer (PC) is the most common malignancy and second leading cause of cancer-related death in men. It is generally treated with radiotherapy and androgen ablation even if the onset of resistance is very frequent. Abiraterone is a new promising drug recently approved for the treatment of PC that seems to reduce this drawback inducing cell death also in androgen-resistant PC, nevertheless it mechanism of action is almost unknown. It is nowadays accepted that several pharmacological treatment as well as radiotherapy induce the ceramide-mediated apoptosis through the activation of the PM-associated SL-hydrolyses that generate in situ the formation of pro-apoptotic ceramide.

Based on these findings, this study addresses whether these enzymes are a target of abiraterone and of ionizing radiation in human PC. To this purpose, androgen-sensitive and androgen-insensitive PC cell lines were subjected to treatments with abiraterone and/or ionizing radiation and the activities of different PM-associated glycohydrolases as well as the ceramide level were evaluated. Interestingly, all the cell lines tested showed a marked increase in all the PM-associated glycohydrolases as well as in their ceramide content, especially after the combined treatment with abiraterone and ionizing radiation. These data demonstrate the involvement of the glycohydrolases in the mechanisms of abiraterone- and radiation- induced cell death in both androgen sensitive and insensitive PC cells and suggest that these enzymes, able to evocate the production of ceramide at the PM-level, could represent new potential therapeutic targets for prostate cancer.

Otherwise, part of my study are related to the involvement of the SL in the bladder cancer cell death induced by the treatment with antagonists of the cannabinoid receptor 2.

Bladder cancer (BC) is the most severe malignancy form of the genitourinary tract. Clinically, 75-80% of bladder neoplasms correspond to non-muscle-invasive bladder cancer (NMIBC) at diagnosis. After transurethral resection of the tumor followed by adjuvant chemotherapy, 30 to 50% of patients recur, and more than 15% of those undergo progression to muscle-invasive disease. Identification of novel potential targets to reduce recurrence and prevent disease progression represents a medical challenge for bladder cancer. Among the various putative novel biomarkers or targets recently described for urothelial carcinoma, the endocannabinoid system (ECS), expressed by the genitourinary organs, has recently gained particular attention. The ECS components such as CB1-CB2 receptors, and the endocannabinoid-degrading enzyme fatty acid amide hydrolase (FAAH) are present in the bladder at the epithelial level and play a role in regulating its functions. As recently shown, both clinical and experimental evidence has indicated a possible role of the ECS in modulating cancer proliferation, progression and metastasis in several types of neoplastic diseases, including, prostate and breast cancer. Interestingly, few information are available on the possible role of ECS components in proliferation and metastasis of human urothelial carcinoma, or on the mechanisms underlying progression to the muscle invasive phenotype. In this context, glycosphingolipids (GSL) play an important role. Indeed, aggressive, muscle-invasive BC is characterized by a different expression of the GM3 and Gb3 glycolipids, suggesting that the metabolism of GSL plays a role in controlling cell invasion and motility. Similarly, the known antiproliferative activity of cannabinoids in cancer models is reported to involve changes in GSL metabolism with accumulation of ceramide (Cer) via *de novo* synthesis and putative deregulation of the Cer/ sphingosine-1-phosphate (S1P) rheostat. Otherwise, the plasma membrane-associated enzymatic hydrolysis of GSL is activated and produces a signaling cascade that may modulate cytoskeletal changes via p-ERM and cell migration via Src. Into this picture though, it's important also to consider the already reported receptor-independent effects of cannabinoids, which may play an important role in our system. In my study I show a strong associations between the anti-metastatic properties of cannabinoids and GSL metabolism. This finding, together with the *in vitro* antiproliferative effect, the

in vivo efficacy on tumor progression, and the tumor-specific up-regulation of CB2 in primary bladder cancer may play a role in the identification of novel therapeutic and diagnostic targets for treating bladder cancer.

State of the Art

Sphingolipids

Sphingolipids (SL) are amphiphilic molecules residing in the external layer of the plasma membrane (PM) of mammalian cells [1] consisting in a hydrophobic moiety, ceramide (Cer), and in a hydrophilic headgroup from different origin. Cer is the most simple SL composed by a long chain amino alcohol like the 2-amino-1,3-dihydroxyoctadec-4-ene (sphingosine), connected to a fatty acid by an amide linkage. Of the four possible configuration of sphingosine, only the 2S,3R is present in nature [2,3]. Cer is the common precursor of complex SLs, which are synthesized by addition of polar molecules to the hydroxyl group in position 1 of the sphingoid base [4].

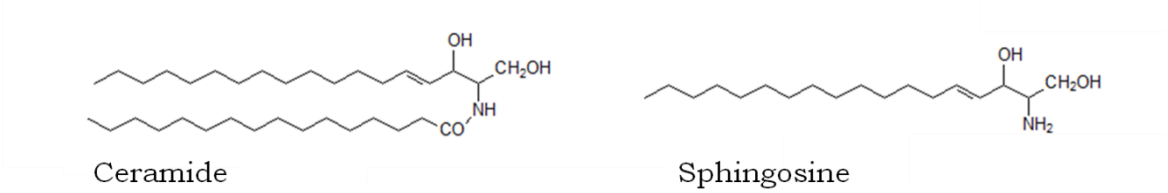

Figure 1. Structure of ceramide and sphingosine.

Hundreds of SL molecular species, differing in their polar head group, sphingoid base and fatty acyl moiety, have been described. Referring to the polar head group there is the phosphocholine, component of sphingomyelin (SM), and a very wide group of oligosaccharide chains, components of glycosphingolipids (GSLs) [5]. GSLs containing one or more sialic acid residues in the carbohydrate chain are referred to as gangliosides. Based on the sequences of the carbohydrate core residues, GSLs are classified into a number of series (including gala-, ganglio-, isoganglio-, lacto-, neolacto-, lactoganglio-, globo-, isoglobo-, and muco-series). Structural diversity in their carbohydrate chains is a hallmark of GSLs. At present, 172 neutral GSLs, 24 sulfated GSLs and 188 gangliosides with variations in the carbohydrate chain have been reported in a variety of vertebrate tissue and organs [6]. This complexity is increased many fold when heterogeneity in the lipophilic components is taken into consideration.

The glycolipids are clearly significant contributors to the structure of the outer leaflet of most eukaryotic cell membranes. The molar ratio of these molecules relative to the other major membrane lipids (phospholipids, cholesterol and glycerolipids) varies from being <0.5% in erythrocytes to about 6% in neurons. Thus, in neurons, SL are about the 12% of total lipids of external PM layer.

Sphingolipids neobiosynthesis

Sphingolipid biosynthesis in eukaryotic cells requires:

1) the intracellular formation of the membrane anchor ceramide [7];
2) The sequentially addition of the single carbohydrate residues or of the methyl choline [8-9].

Ceramide and Sphingomyelin neobiosynthesis

The begginig of the synthesis of the sphingoid bases (sphingosine, dihydrosphingosine) takes place via the condensation of *palmitoyl-CoA* and *serine* as shown in the Figure 2. This reaction occurs on the cytoplasmic face of the endoplasmic reticulum (ER) and is catalyzed by the pyridoxalphosphate-dependent enzyme, serine palmitoyltransferase (SPT). The product of this reaction is *3-ketosphinganine* (3-ketodihydrosphingosine). SPT is the rate-limiting enzyme of the sphingolipid biosynthetic pathway; an additional protein associates with the catalytic subunits to greatly enhance the activity of the enzyme complex as well as to confer acyl-CoA preference to the complex. Following formation of 3-ketosphinganine this compound is reduced to *sphinganine* (dihydrosphingosine) via the action of 3-ketosphinganine reductase (3-ketodihydrosphingosine reductase)[10-12]. Sphinganine is then acylated generating *dihydroceramide*. The acylation of sphinganine (also called dihydrosphingosine) occurs through the activities of six different ceramide synthases (CerS) in humans. These CerS enzymes introduce fatty acids of varying lengths [designated by the $-(CH_2)_n-$ in the structure] and degrees of unsaturation [13-15]. Dihydroceramide is then unsaturated in *ceramide* by the enzyme dihydroceramide desaturase 1 (DES1)[16-18]. The official designation for DES1 is delta(4)-desaturase, sphingolipid 1 which is encoded by the DEGS1 gene located on chromosome 1q42.11 that is composed of 5 exons encoding a protein of 323 amino acids.

The neo-synthesized ceramide could reach directly the membrane or it is used as common precursor for glycosphingolipids (GSL) or sphingomyelin (SM) biosynthesis. In both cases the ceramide reaches the Golgi apparatus by a not well defined mechanism [19], able to selectively address the synthesis of SM or GSLs. SM neobynthesis occurs via addiction of phosphocholine group to the hydroxyl group in position 1 of the sphingoid base of the ceramide.

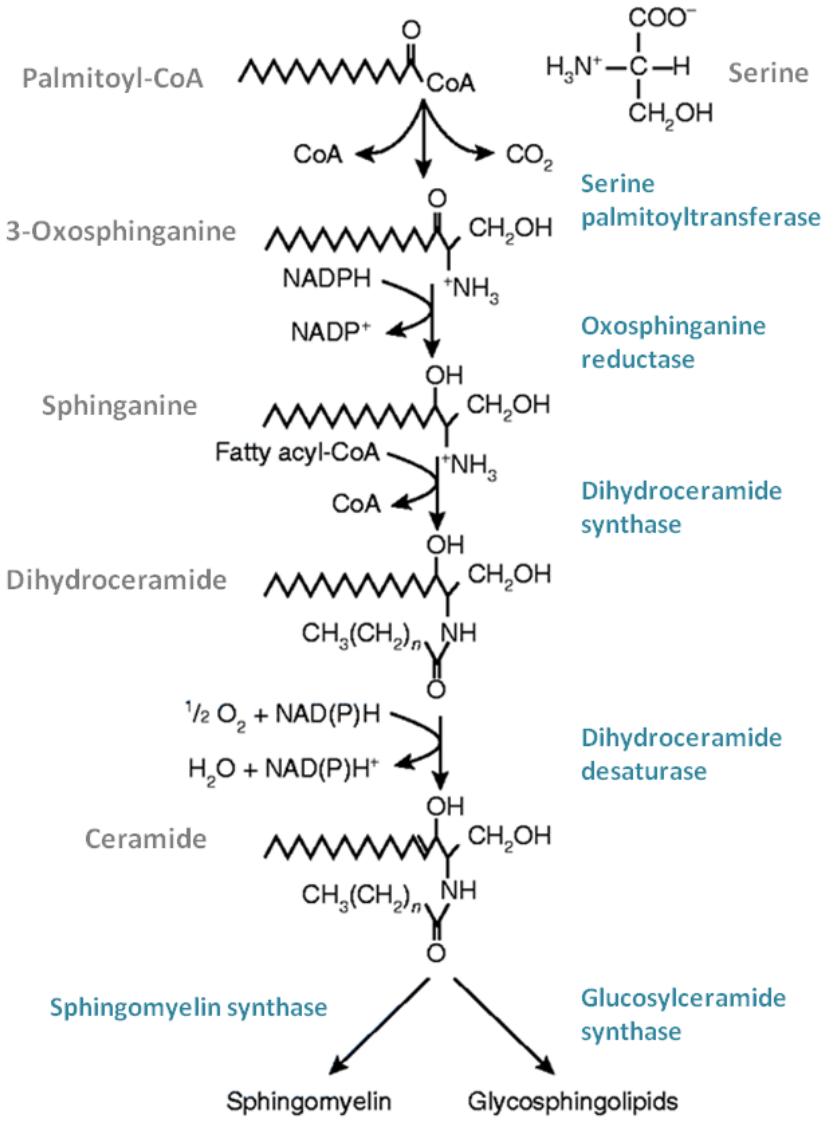

Figure 2. ***De novo*** **ceramide biosynthesis.**

Cer is also generated during the catabolism of SLs that occurs in lysosomes, and rapidly converted to sphingosine which is largely recycled. Cer synthase is able to use as substrate both sphingosine and sphinganine with similar efficiency [23-25], so Cer can be also formed by N-acylation of sphingosine produced by the catabolism of complex sphingolipids (Figure 3).

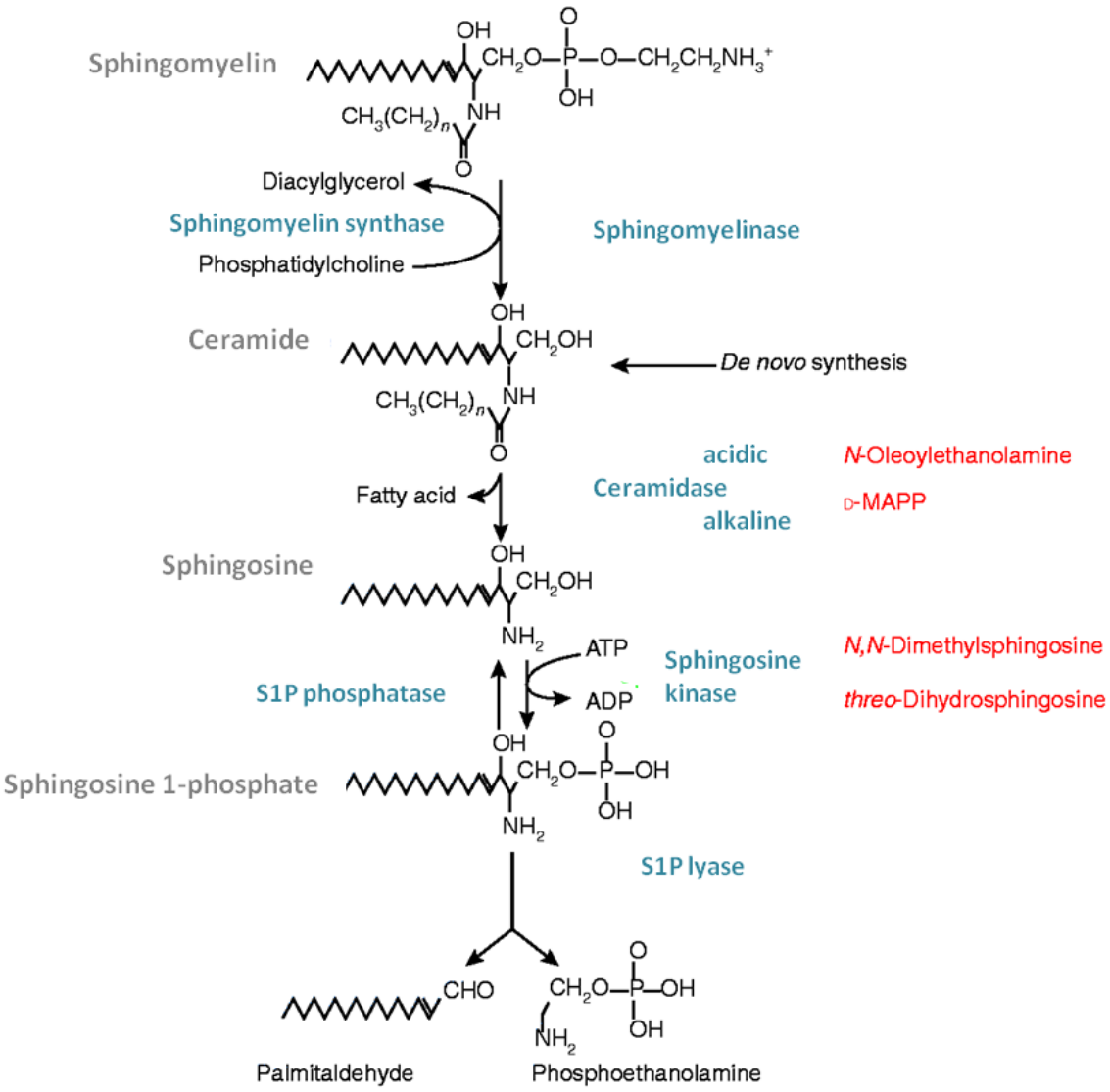

Figure 3. Ceramide from catabolism

Glycosphingolipid neobiosynthesis

Glucosylceramide (GlcCer) is the most common GSL precursors, formed by a ceramide glucosyltransferase activity localized at the cytosolic side of the early Golgi membrane [20]. Glucosylceramide can either directly reach the plasma membrane [21], presumably transported in a non-vesicular manner [REF], or be translocated to the luminal side of the Golgi, where it is further glycosylated by other glycosyltransferases to generate more complex glycosphingolipids. *Lactosylceramide* (LacCer), is formed by the addiction of a galactose moiety from UDP-Gal to GlcCer, catalyzed by galactosyltransferase. LacCer formation and also the reaction leading to higher glycosylated lipids occur on the luminal leaflet of Golgi membranes [22]; neo-synthesized GSLs move through the Golgi apparatus to the plasma membrane following the mainstream exocytotic vesicular traffic.

The biosynthesis of sialic acid-containing GSLs, the gangliosides, is catalyzed by glycosyltransferase in the lumen of the Golgi apparatus starting from the common precursors LacCer [8, 26, 27]. on the other hand the gangliosides GM3, GD3 and GT3, serve as precursors for the complex gangliosides of the 0-, a-, b-, and c-series (Figure 4). In adult human tissues, gangliosides from the o- and c-series are found only in trace amounts. The transferases which catalyze the first steps in ganglioside biosynthesis show high specificity towards their glycolipids substrates, i.e. for the formation of LacCer, GM3 and GD3. The relative amount of these GSLs in the steady state seems to determine the amount of o-series GSLs, which are derived only from LacCer, a-series gangliosides which are only derived from the ganglioside GM3, and b-series gangliosides which are only derived from ganglioside GD3. Sialyltransferase I and II are much more specific for their glycolipids substrates than sialyltransferases IV and V, or than galactosyltransferase-II and GalNAc transferase. It was assumed that different transferases catalyze the formation of homologous gangliosides of different series.

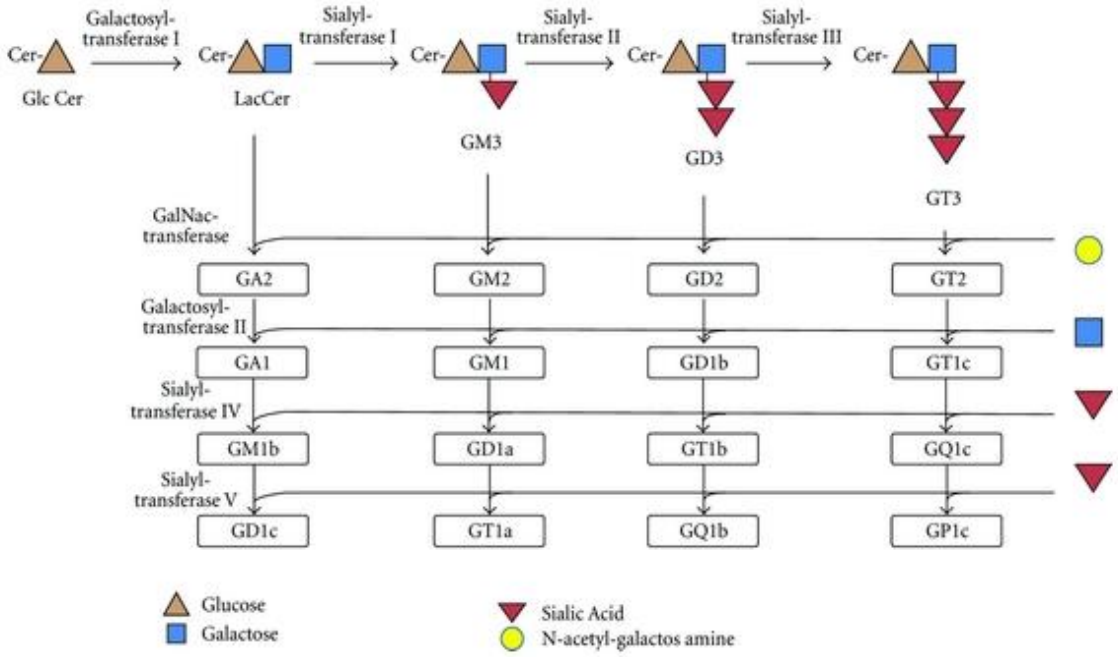

Figure 4. **Scheme of Gangliosides biosynthesis**. The formation of 0, a, b and c-series gangliosides is catalyzed by glycosyltransferases of Golgi membranes; all the enzymatic steps (except LacCer formation) take place at the luminal surfaces of the Golgi membranes.
"G" denotes "ganglioside", "A" denotes "asialo" or lacking sialic acid; "M" denotes "monosialo", "D" denotes "disialo" and the numbers indicate the carbohydrate sequence. Cer: ceramide; GlcCer: glucosylceramide; LacCer: lactosylceramide; GalNAc: N-acetylgalactosamine [143].

Catabolism

Another important point of regulation of plasma membrane SLs composition is the lipidic degradation which occurs in the lysosomes, where the SLs are transported by the endocytic vesicular flow through the early and late endosomal compartment to be catabolyzed (Figure 9).

Lysosomal glycosidases sequentially cleave the sugar residues from the non-reducing end of their glycolipid substrates. The resulting monosaccharides, sialic acids, fatty acids and sphingoid bases can leave the lysosomes and recycled or can be further degraded. In addition, the intra-lysosomal degradation of most, if not all, GSLs requires cofactors called "sphingolipid activator proteins (SAPs, or saposines)" [28]. Using the ganglioside GM1 as example of a GSLs lysosomal degradation, the first step is the removal of the galactose by the β-Galactosidase together with the GM2-AP or SAP-B [29], yielding GM2 (Figure 5).

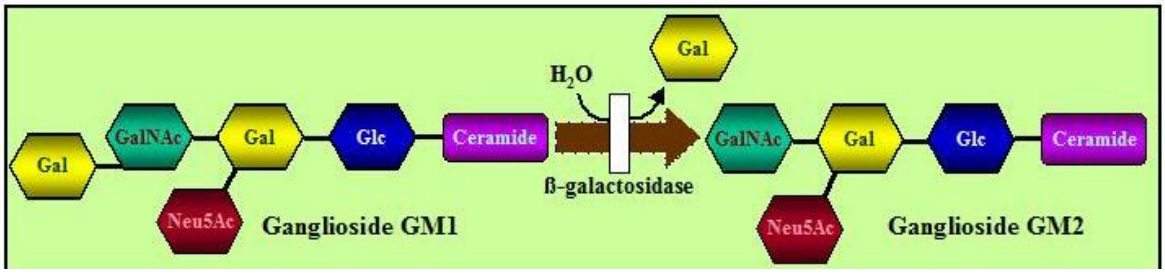

Figure 5. Reaction catalyzed by β-Galactosidase

The resulting gangliosides GM2 is catabolized to ganglioside GM3 and N-acetylgalactosamine by the β-Hexosaminidase isoenzymes Hex-A and GM2-AP (Figure 6).

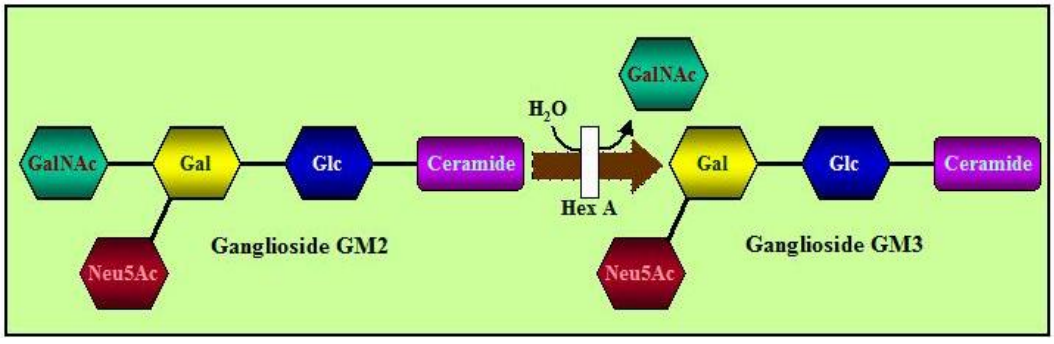

Figure 6. Reaction catalyzed by β-Hexosaminidase A.

In some cells and animals, sialic acid is removed from GM1 and GM2 by a specific sialidase (GM1 and GM2-sialidase) producing the corresponding a-sialo

derivatives GA1 and GA2, that, by the action of β-Galactosidase and β-Hexosaminidase or only β-Hexosaminidase respectively, are converted to LacCer. LacCer is produced also directly from GM3 by the action of a sialidase which cleaves this gangliosides into LacCer and sialic acid a reaction stimulated by SAP-B (Figure 7)[30].

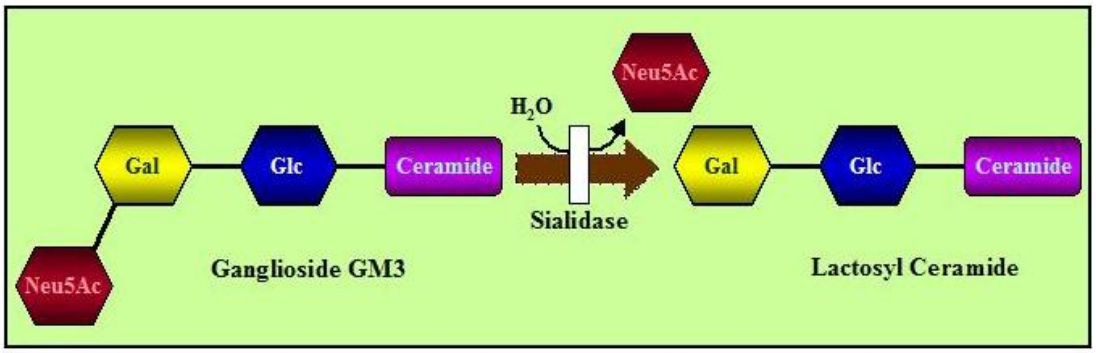

Figure 7. Reaction catalyzed by sialidases.

LacCer is then degraded to Cer by the sequential action of a β-Galactosidase (in the presence of either SAP-B or –C) and β-Glucosidases GBA1 and GBA2 (Figure 8)[31].

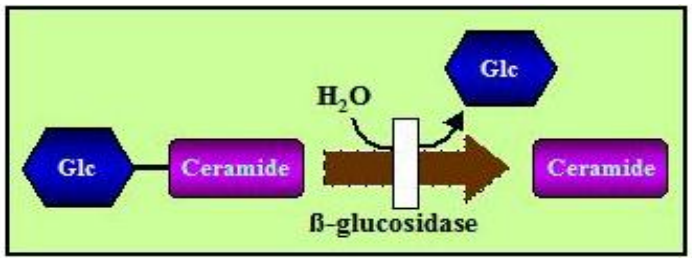

Figure 8. Reaction catalyzed by β-Glucosodase GBA1 and GBA2.

Cer is cleaved by acid ceramidase in the presence of SAP-D [32] into sphingosine and fatty acid. Together with the other cleavage products, there two metabolites are able to leave the lysosomes. An alternative pathway for ganglioside/GSLs degradation is the splitting of β-glucosidic linkage between glucose and Cer, with the formation of Cer and the oligosaccharide. The enzymes catalyzing this reactions, named “endoglycoceramidase” or “Cer glycanases” [33-38] appear to require, or to be markedly activated, by a specific activator proteins whose action would be essential *in vivo* conditions [33]. Endoglycoceramidases have been found to occur in some bacteria [33] and leeches [34]. Although described to occur in lactating mammary glands of rodents [36], the presence of this enzyme

in vertebrate and, particularly, mammalian tissues is yet to be definitely assessed. For the non-glycosylated SLs, like Cer and SM, non-lysosomal degradation steps are known which apparently do not need the assistance of an activator protein. SM is cleaved to Cer and phosphorylcholine; Cer later on is degraded into sphingosine and a fatty acid by ceramidase. Sphingosine moves into the cytosol where it can be phosphorylated to sphingosine-1-phosphate and further degraded to phosphoethanolamine and long chain aldehyde. But at the same time sphingosine-1-phosphate acts as metabolic regulator [39].

Enzymes that are capable to remove the fatty acid moiety from several sphingolipids (SM, gangliosides and some neutral GSLs) producing the corresponding lyso-derivatives were also described [39,40]. These enzymes, known as SL Cer N-deacylases, were detected in bacteria; no evidence was yet provided for their occurrence in vertebrates, however, it is known that in the brain of patients suffering from some sphingolipidosis where there is accumulation of lyso-GSLs [41], these accumulated compounds seems to be the products of proteins having this kind of enzymatic activity.

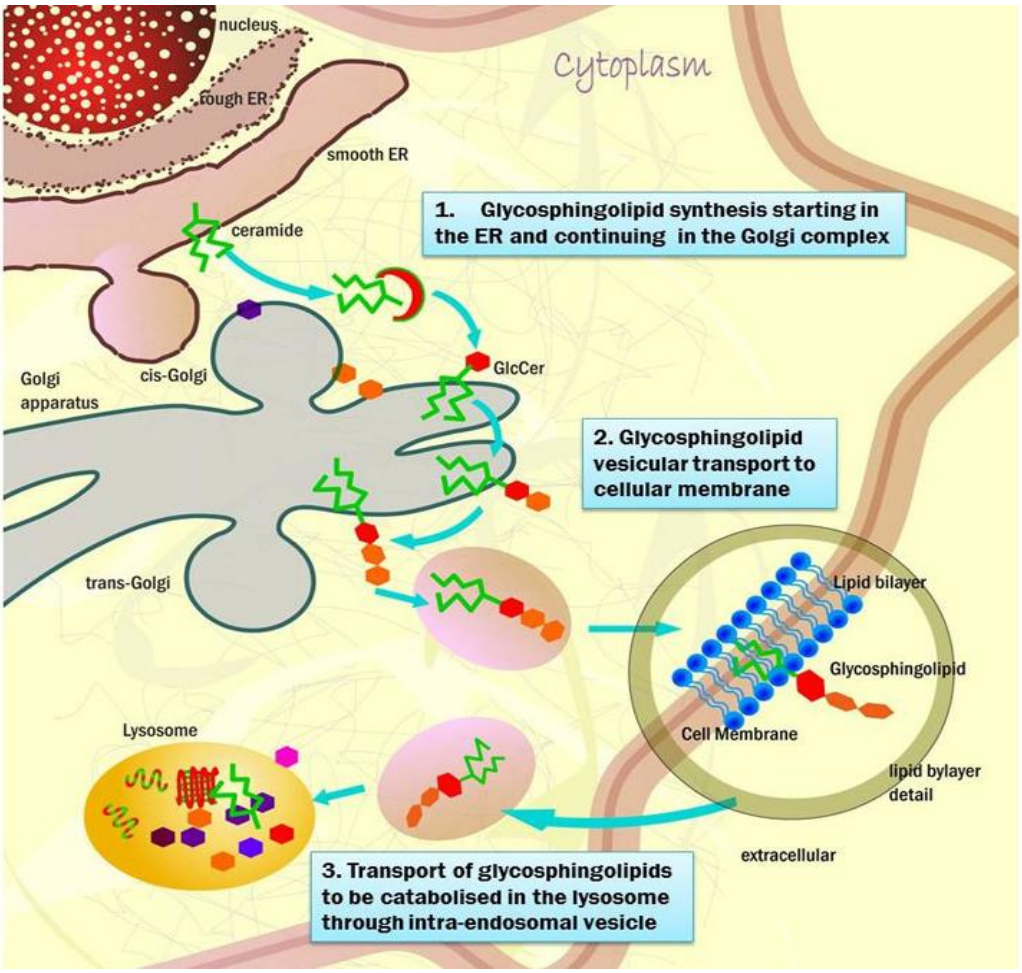

Figure 9. Intracellular sphingolipid metabolism and trafficking.

The regulation of GSL composition at the plasma membrane level

Changes in the GSL composition of the plasma membrane in a certain cell type would lead to very important biological consequences, this all mechanisms possibly contributing to these changes have a high functional significance. The classical view on sphingolipid metabolism implies the vesicular transport of neo-biosynthesized sphingolipids from the endoplasmic reticulum and the Golgi apparatus to the plasma membranes [47]. Changes in the activities of enzymes of the biosynthetic pathway have been associated with the changes in GSL expression which are associated with biological events such as neoplastic transformation or neuronal differentiation. However, other mechanisms could be responsible for a local regulation of the GSL composition of plasma membranes or restricted plasma membrane areas (Figure 10). Both catabolic and biosynthetic enzymes for sphingolipids have been found associated with the plasma membranes. "Signalling" sphingomyelinases are resident in or translocated to the plasma membrane, being able to convert plasma membrane sphingomyelin into ceramide [48,49]. Conversely, a plasma membrane-associated sphingomyelin synthase enzyme activity (SMS2), genetically distinct from the Golgi enzyme, has been identified [50]. Thus, the sphingomyelinase/ceramide ratio can be locally modulated possibly in response to physiological events, leading to profound consequence on the organization of sphingolipid-enriched membrane areas. In the case of GSLs, a specific membrane-bound sialidase (Neu3) has been identified and cloned [51-53]. Neu3 can be considered an ubiquitous enzyme being expressed at different levels in all the PM of tested normal and pathological human tissues such as human brain [71] normal and colon rectal carcinoma tissue, hepatic tumor and kidney carcinoma [72-76]. In addition its expression and activity were also found in normal and pathological cell lines such as erytroid and erytroleukemic cells [77-79], human fibroblasts [80], rat and mouse neurons, neuroblastoma cells [81], human breast ductal cancer T47D cells, colon carcinoma CaCo2 cells, human colorectal adenocarcinoma HT29 cells, different type of ovarian cancer cells, human cervix adenocarcinoma HeLa cells [76]. It has been demonstrated the presence of Neu3 in the lipid rafts and its co-localization with gangliosides: the non-random distribution of Neu3 at the cellular surface introduces the possibility that the biological effects of this enzyme might be due to the local reorganization of GSLs-based signaling units. Remarkably, Neu3 is able to modulate the cell surface glycolipid composition because of *trans* interactions, thus modifying the surface of neighboring cells [55].

Moreover, the presence of sialyltransferase activities at the cell surface has been also reported [57-61]. Thus, glycosylation/deglycosylation cycles might be very important mechanisms responsible for rapid and possibly transient changes of the plasma membrane GSLs composition, in analogy to that proposed for the "sphingomyelin cycle". The presence of other active glycohydrolases, β-Glucosidase, β-Galactosidase and β-Hexosaminidase [56-62], in the plasma membrane has been demonstrated, implying that local hydrolysis of GSL at the cell surface might represent a general mechanism for the control of GSL composition.

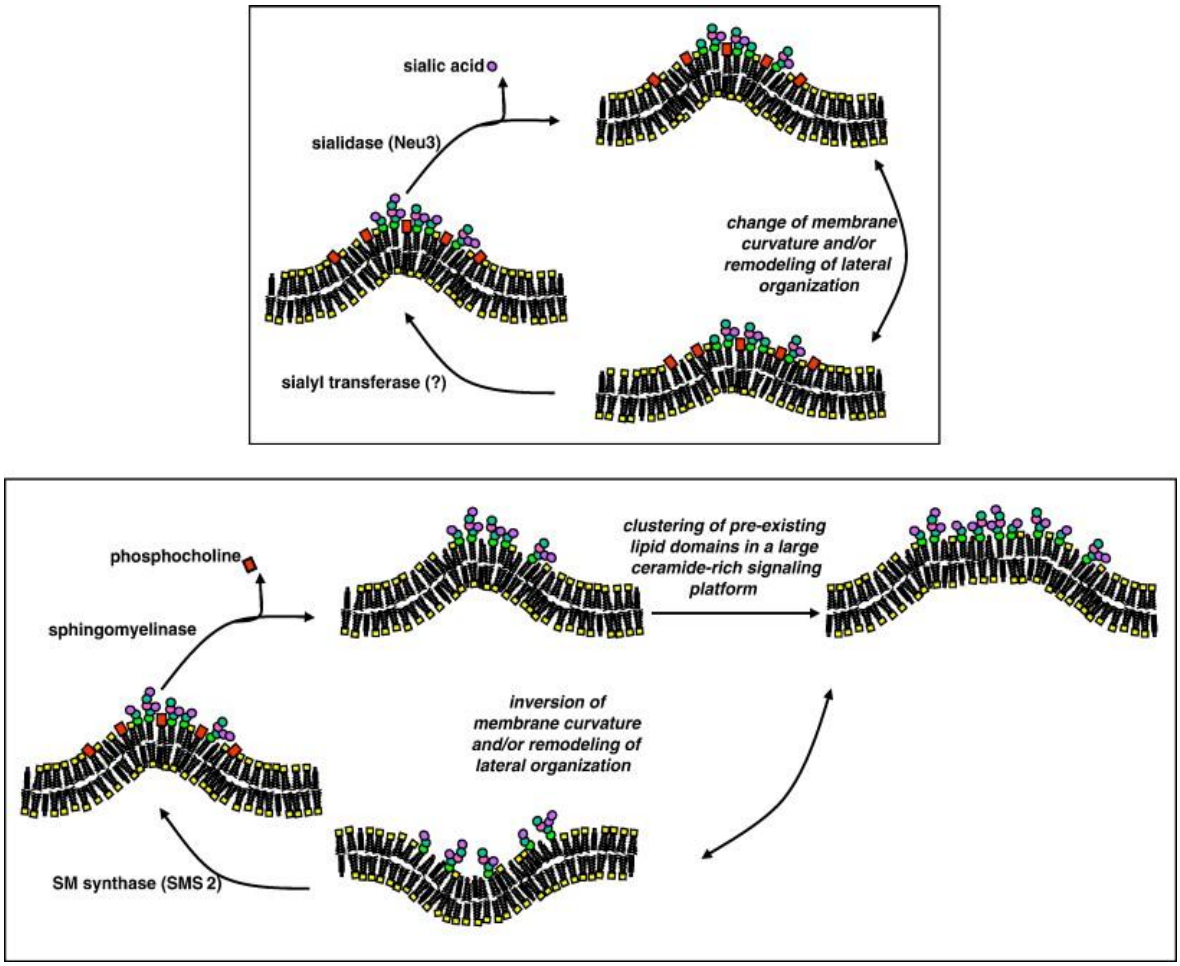

Figure 10. Regulation of sphingolipid-enriched membrane domain composition by phosphorylation/dephosphorylation ("sphingomyelin cycle") and glycosylation/ deglycosylation. The interconversion of ceramide and sphingomyelin due to the action of plasma-membrane resident sphingomyelinases and sphingomyelin synthase 2 leads to profound reorganization of the sphingolipid-enriched membrane domains. In particular, ceramide generation can lead to changes in the membrane domains into large ceramide-rich signalling platform. GSL composition can be regulated by desilylation due to the plasma membrane.associated sialidase Neu3, and probably by membrane-resident glycosyltransferase, leading to changes in the geometry and organization of GSL-rich membrane domains and in specific GSL-protein interactions.

The presence of β-Hexosaminidase A in the external leaflet of PM has been demonstrated in cultured fibroblasts [62]. Immunological and biochemical characterization of the membrane-associated β-Hex indicated that this enzyme has the same structure of that in lysosomes. PM associated β-Gal has been found in all cell lines studied for the activity of Neu3. In human fibroblasts its expression is up regulated by Neu3 [56].

On the other hand, the β-galactosidase (β-Gal) activity was measured during neuronal cell differentiation and aging, in the total cell lysate and in the PM from rat cerebellar granule cells. Both these activities resulted up regulated during cell differentiation. As expected the β-Gal activity associated to the cell PMs was less than the one found in the total cell homogenate. The total cell activity remained constant during differentiation, then increased 4 fold along aging in culture. Instead, cell surface activity increased 10 fold during differentiation, to then duplicate during the neuronal senescence [82]. β-Gal activity has been proposed as senescent marker of different cell lines [83-86]. The information on the behavior of PM associated enzyme in rat cerebellar granule cells suggests that its activity could be used as a good marker for both neuronal differentiation and neuronal aging. The identity of the protein, or proteins, responsible for the β-Gal activity present at the cell surface is still unknown, however in living human fibroblasts has been verified the presence of a β-Gal activity which displays a *trans* activity, with no necessity of detergents or activator proteins, on lactosylceramide (LacCer) immobilized on cell culture plates, suggesting that on the cell surface is present at least an enzyme having a β-galactocerebrosidase-like activity [70].

Concerning β-Glucosidases, GBA2 has been found associated to endosome vesicles or to the PM, it is insensitive to CBE whereas is specifically inhibited by N-(5-adamantane-1-yl-methoxy)pentyl)-deoxynojirimycin (AMP-DNM) [89,90]. Recently it has been described that a CBE-sensitive β-Glc activity is present in the PMs [70]. Both CBE-sensitive and CBE-insensitive β-Glc enzymes were found associated to the cell surface of rat cerebellar granule cells in culture, where they progressively increase along the differentiation and the aging process [83].

Total β-Glc activity associated to the PMs of human living fibroblasts works on natural substrates *in trans* fashion [70] and the activity is connected to Neu3 activity (like the β-Glc). In fact, in human fibroblasts over-expressing Neu3, the β-Glc activity associated to the PM was much higher of that found in normal fibroblasts. Surprisingly this is mainly due to an up-regulation of the CBE-sensitive β-glucosidase [70].

Considering the presence of lysosomal glycohydrolases at the cell surface, two aspects need to be clarified: how lysosomal deriving enzymes can reach the PM and how they can be active at the cell surface where the pH conditions are far from those of the lysosomes. It is known that a regulated fusion of lysosomes with the PM may represent a general mechanism of repairing for the PM [99], and could be responsible of the presence of lysosomal enzymes facing at the cell surface. However this enzymatic “translocation” couldn?t be accidental and the fusion of lysosomal membranes with the PM could be the way for all the lysosomal glycolipid-metabolizing enzymes to reach the cell surface where, together with specific and different membrane associated enzymes, play an active role in remodeling the glycolipid content and pattern of the external leaflet of the PM. At the cell surface the pH conditions are usually considered near to the neutrality, whereas the lysosomal pH is much more acidic. For some glycohydrolases described associated to the PM has been evaluated the optimum of pH to which they play their catalytic activity. Both the β-Hex A and Neu3 (respectively codified by the same and by a different gene with respect to the corresponding lysosomal enzyme) has been found working in acidic condition (pH 4.45 and pH 4.2 respectively). This information suggests that modulation systems, able to modify the pH conditions, even locally, could be present at the cell surface. One hypothesis for this theory may be the action of proton pumps present at the PM level for which has already been demonstrated a role in the acidification of the tumor extracellular environment [100-102].

In addition to an active in situ modification due to specific enzymatic activity a further way to modify the lipid membrane domain composition and organization

Is represented by a controlled release of GSL from the cell surface including shedding vesicle [63-65].

Glycosylation and cancer malignancy

Aberrant glycosylation, at the cell surface level, has been observed in essentially all type of human cancer. This event contributes to deep alterations in the interactions between tumor cells and the extracellular environment, which underline many of the features that defined several tumor phenotype, including self-sufficiency in growth signals, insensitivity to growth-inhibitor stimuli, evasion from programmed cell death (apoptosis), sustained angiogenesis, tissue invasion and metastasis (Figure 11) [67].

Alteration in glycan expression in cancer is usually a consequence of modification in the metabolic pathway of glycoconjugates, as a result of change in the biosynthesis, catabolism and intracellular trafficking of GSLs and glycoproteins.

Like reported above, changes of the glycoconjugate oligosaccharide structures and in particular changes of GSLs, can be obtained at the cell surface by the activities of PM-glycohydrolases. Recent study indicate that the aberrant glycosylation could be a result of initial oncogenic phenomena, as well a key event for the induction of invasion and metastasis.

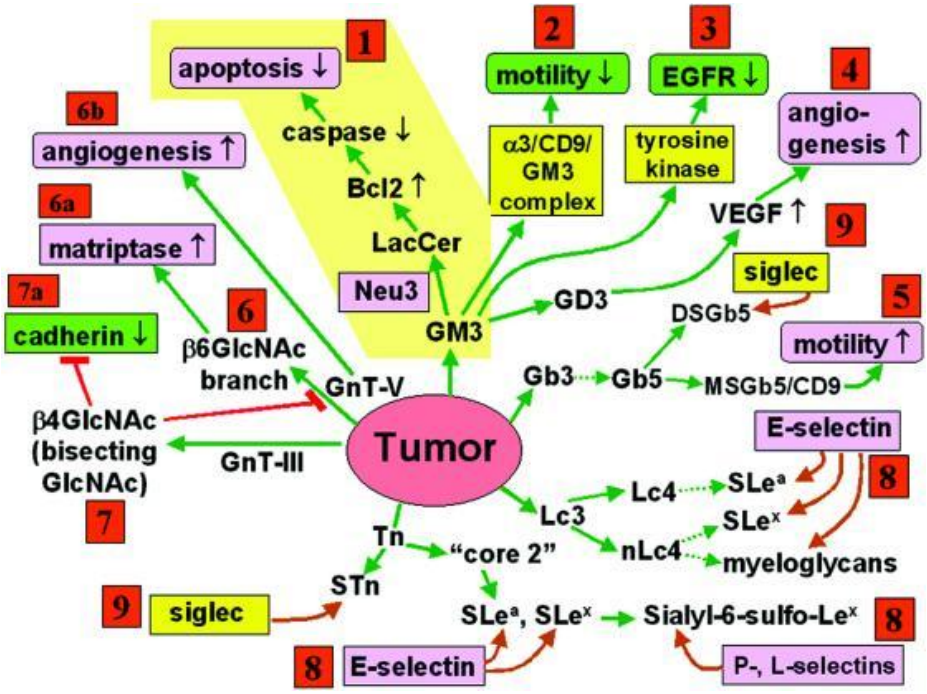

Figure 11. Glycosylation defining malignancy (invasive and metastatic phenotype of tumors) (from [67]).

Membrane lipid domains

The interest in membrane lipid domains, which is, in zones of the membrane with a peculiar lipid composition, different from that of the majority of bilayer, became very strong during the last 20 years, when many proteins assigned to cell signalling were found to be preferentially associated with an environment of lipids highly enriched in sphingolipids and cholesterol. A possible role for lipid domains in the transport of glycosylphosphatidylinositol (GPI)-anchored proteins from the Golgi apparatus to the apical plasma membrane of polarized cells was also suggested; hence, the use of the term "lipid rafts" to define this domains [103]. Biochemical studies on cell membrane lipid domains and composition, organization and biological role were carried out mainly starting from 1992, when a method capable of separating them from total cell membrane became available [102]. However, massive biophysical work on artificial membranes was carried out from the 1970s to understand the basis of the organization of aphiphilic compounds within biological membranes, leading to establishment of the existence of segregation phenomena. Today, different terms are used throughout the literature to define lipid membrane domains: every one of them implies a form of segregation of certain components within the cell membrane. Some define specific domains, as in the case of "*caveolae*", membranes invaginations containing the protein caveolin [103], or "*lipid rafts*", membrane domains that sort or transport proteins inside cells. Others define membrane portions on the basis of chemico-physical or compositional features, such as "DIM" (Detergent-Insoluble Material), "DISAM" (Detergent-Insoluble Substrate Attachment Matrix) [104], "DIG" (Detergent-Insoluble Glycolipid-enriched material) [105], "SEMF" (Sphingolipid-Enriched Membrane Fraction) [106], "GSD" (Glyco-Signalling Domains) [107], etc. To this author, DRM is a very reasonable definition, based on the operational way commonly used to obtain biochemical preparation enriched in lipid membrane domains, which is based on their relative insolubility in nonionic detergents under specific experimental conditions. The existence of lipid membrane domains in natural cell membranes was suggested by the observation that glycosphingolipids at the cell surface form clusters, which have been visualized by immune-electron microscopy using anti-glycosphingolipid antibodies [108]. Glycosphingolipid clustering in cell membranes was shown for globoside in human erythrocytes [109], polysialogangliosides in fish brain neurons [110], GM3 ganglioside in peripheral human lymphocytes, and Molt-4 lymphoid cells [111]. Several approaches, relying on more advanced technologies,

are now available allowing the detection and the study of membrane lipid domains in intact cell membranes [112,113]. These techniques are very heterogeneous and include single-particle tracking or single-fluorophore tracking microscopy [114-116], “FRAP” (Fluorescent Recovery After Photobleaching) [117], “FRET” (Fluorescence Resonance Energy Transfer) [118], and “AFM” (Atom Force Microscopy) [119], and data obtained with different approaches are sometimes conflicting. As an example, there is no agreement on their avegarge size, which ranges from 26 nm to about 2 μm [120]. In addition, from these data no information on that composes the lipid domains can be inferred. Compositional information for membrane lipid domains is largely obtained by means of the procedure published by Brown and Rose [121], based on the insolubility in aqueous nonionic detergents of those cell lipids (including cholesterol, sphingolipids and saturated PC) that in membrane models tend to segregate into a liquid-ordered phase. All the complex amphiphilic compounds that are components of cell membrane and several intrinsic membrane proteins can be solubilized by detergents, due to the formation of mixed aggregates. But, under certain experimental conditions, where low temperature, detergent concentration and detergent-to-cell ratio seem the most critical parameters, a part of the cell membrane remains insoluble in the nonionic detergent Triton X-100. Other detergents were used and claimed to be not capable of solubilizing membrane lipid domains [122-124]. After detergent treatment, the detergent-insoluble membrane fraction can be separated from the rest of the cell thanks to its relative light density (buoyancy) [125-129], using continuous or discontinuous sucrose density gradients. The low density of the detergent-insoluble material is due to the high lipid-to-protein ratio in the fraction. Low-density, detergent-insoluble fractions were isolated from a wide variety of cultured cells, including almost all normal and pathological mammalian cell types investigated so far, as well as yeast [130] and protozoans [131]. In a second time, reports on the isolation on this fraction from tissue appared [132-136]. Membrane lipid domains contain all the cell complex lipids but are highly enriched in sphingolipids and cholesterol. Nevertheless, glycerophospholipids remain the bulk components, being enriched in phosphatidylcholine that being highly enriched in the dipalmitoyl species. These results were confirmed using other procedures where the detergent is substituted by an high pH, hypertonic sodium carbonate [137], or mechanical treatments (sonication under carefully controlled conditions) [138], followed by density gradient centrifugation to recover the light fraction. The general agreement on the sphingolipid and cholesterol enrichment in the low-

density membrane fraction obtained with the above procedures, that is, under different experimental conditions, would prove that the isolated lipid membrane domains are not the result of a random rearrangement of cell components induced by the treatment but are a good mirror of an organization naturally occurring on the cell membranes. Of course, any change in the experimental conditions can yield quantitative changes of each component. Membrane lipid domains contains a small amount of proteins, in general no more than 05-2.5% of total cell proteins: however, proteins that are involved in the process of transduction of the information throughout the cell plasma membrane (including receptor and non-receptor protein tyrosine kinases, G protein coupled receptors, GTP binding proteins) result frequently enriched in the lipid domains.

Scientist are making every effort to isolate different membrane lipid domains from the DRM fraction; immunoisolation procedures allowed fractionation of the DRM fraction into sub-populations with strikingly different structure and functions. Two membrane sub-fraction were separated from DRM isolated from B16 melanoma cells by anty-GM3 ganglioside monoclonal antibody DH2 and by anti-caveolin antibody [139]. The anti-GM3 sub-fraction was enriched in GM3 and contained sphingomyelin, cholesterol and proteins c-Src and Rho A, but no caveolin, while the anti-caveolin sub fraction contained caveolin, glucosylceramide, sphingomyelin and a large amount of cholesterol, but no GM3, c-Src or Rho A. The GM3-enriched sub-fraction, but not the caveolar sub-fraction, was involved in cell adhesion-dependent signal transduction in these cells. Two sub-populations, containing two functionally different neuronal GPI-anchored proteins, Thy-1 and PrP [140], were separated from the detergent-resistant fraction isolated from mouse brain. Immunoisolation approaches based on the use of different antibodies against protein or lipid components of the lipid membrane domain fraction might thus become the method of choice for the separation of lipid membrane domains, possibly overcoming some of the negative aspect of the classical density gradient flotation method after detergent lysis and allowing attainment of novel information about the properties of functionally and structurally different sub-populations of lipid membrane domains. The use of antibodies could however be responsible for art factual clustering induced by antibody bridging or cross-linking: hence caution should be exerted also in this case.

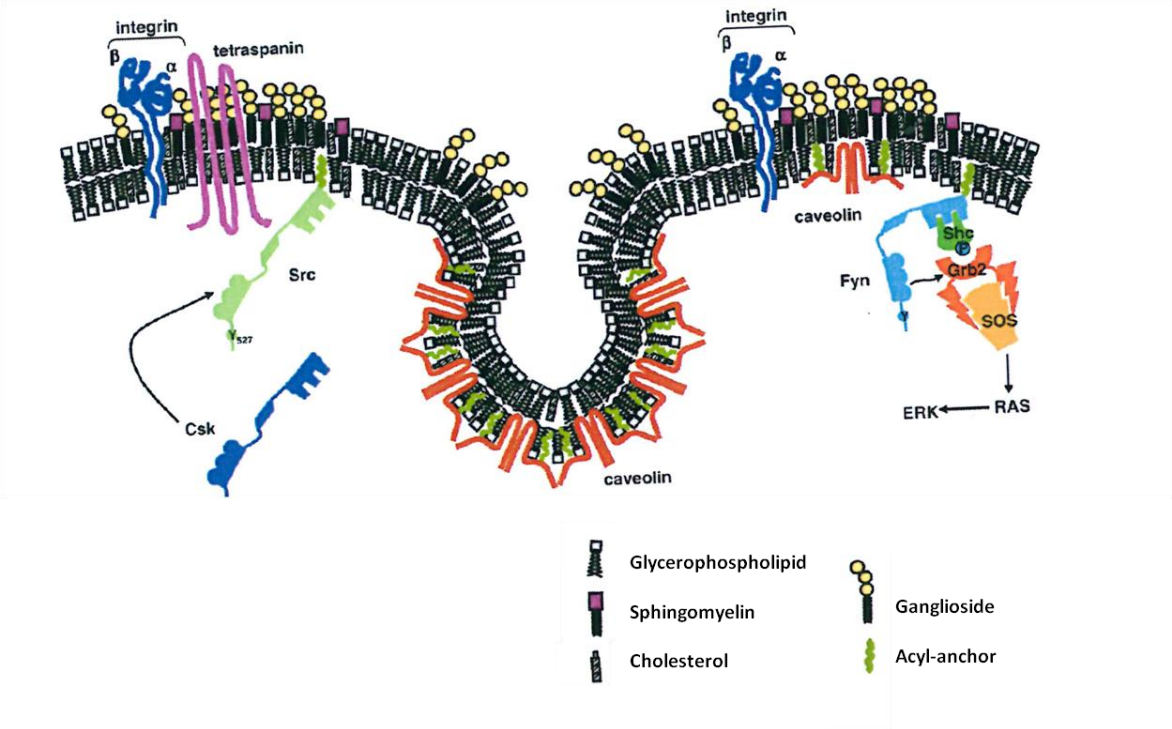

Figure 12. Membrane model containing different DRM.

References

1. Felzi T. (1985) Demonstration by monoclonal antibodies that carbohydrate structures of glycoproteins and glycolipids are onco-developmental antigens. Nature 314:53-57.

2. Carter H.E., Glick F.J., Norris W.P., and Phillips G.E. (1947) Biochemistry of the sphingolipids: III. Structure of sphingosine. J. Biol. Chem. 170:285-294.

3. Carter H.E., Rothfus J.A., Gigg R. (1961) Biochemistry of the sphingolipids: XII. Conversion of cerebrosides to ceramides and sphingosine; structure of Gaucher cerebroside. J Lipid Res 2:228-234.

4. Kolesnick R.N. (1991) Sphingomyelin and derivatives as cellular signals. Prog Lipid Res 30:1-38.

5. Hakomori S. (1990) Bifunctional role of glycosphingolipids. Modulators for transmembrane signaling and mediators for cellular interactions. J Biol Chem 265:18713-18716.

6. Yu R.K., Yanagisawa M., and Ariga T. (2007) Glycosphingolipid Structures, in Comprehensive Glycoscience (Johannis, P.K., Ed.), pp 73-122, Elsevier, Oxford.

7. Merril A.H. (2002) De novo sphingolipid biosynthesis: a necessary, but dangerous, pathways. J Biol Chem 277:25843-25846.

8. Kolter T., Proia R.L., and Sandhoff K. (2002) Combinatorial ganglioside biosynthesis. J Biol Chem 277:25859-25862.

9. Van Meer G., and Lisman Q. (2002) Sphingolipid transport: rafts and translocators. J Biol Chem 277:25855-25858.

10. Mandon E.C., Van Echten G., Birk R., Schmidt R.R., and Sandhoff K. (1991) Sphingolipid biosynthesis in cultured neurons. Down-regulation of serine palmitoyltransferase by sphingopid bases. Eur J Biochem 198:667-674.

11. Nagiec M.M., Baltisberger J.A., Wells G.B., Lester R.L., and Dickson R.C. (1994) The LCB2 gene of Saccharomyces and the related LCB1 gene encode subunits of serine palmitoyltransferase, the initial enzyme in sphingolipid synthesis. Eur J Biochem 249:239-247.

12. Weiss B., and Stoffel W. (1997) Human and murine serine-palmitoyl-CoA transferase-cloning, expression and characterization of the key enzyme in sphingolipid synthesis. Eur J Biochem 249:239-247.

13. Rother J., Van Echten G., Schwarzmann G., and Sandhoff K. (1992) Biosynthesis of sphingolipids: dihydroceramide and not sphinganine is desaturated by cultured cells. Biochem Biophys Res Commun 189:14-20.

14. Merril A.H., and Wang E. (1986) Biosynthesis of long-chain (sphingoid) bases from serine by LM cells. Evidence for introduction of the 4-trans-double bond after de novo biosynthesis of N-acylsphinganine(s). J Biol Chem 261:3764-3769.

15. Shimeno H., Soeda S., Sakamoto M., Kouchi T., Kowakame T., and Kihara T. (1998) Partial purification and characterization of sphingosine N-acyltransferase (ceramide synthase) from bovine liver mitochondrion-rich fraction. Lipids 33:601-605.

16. Geeraert L., Mannaerts G.P., and Van Velfhoven P.P. (1997) Conversion of dihydroceramide into ceramide: involvement of a desaturase. Biochem J 327:125-132.

17. Michel C., Van Echten-Deckert G., Rother J., Sandhoff K., Wang E., and Merrill A.H. Jr. (1997) Characterization of ceramide synthesis. A dihydroceramide desaturase introduces the 4,5-trans-double bond of sphingosine at the level of dihydroceramide. J Biol Chem 272:22432-22437.

18. Mikami T., Kashiwagi M., Tsuchihashi K., Akino T., and Gasa S. (1998) Substrate specificity and some other enzymatic properties of dihydroceramide desaturase (ceramide synthase) in fetal rat skin. J Biochem (Tokyo) 123:906-911.

19. Van Meer G., and Lisman Q. (2002) Sphingolipid transport: rafts and translocators. J Biol Chem 277(29):25855-25858.

20. Jeckel D., Karrenbauer A., Burger K.N., Van Meer G., and Wieland F. (1992) Glucosylceramide is synthesized at the cytosolic surface of various Golgi subfractions.

21. Warnock D.E., Lutz M.S., Blackburn W.A., Young W.W.Jr., and Baenziger J.U. (1994) Transport of newly synthesized glucosylceramide to the plasma membrane by a non-Golgi pathway.

22. Lannert H., Gorgas K., Meissner I., Wieland F.T., and Deckel D. (1998) Functional organization of the Golgi apparatus in glycosphingolipids biosynthesis. Lactsylcermaide and subsequent glycosphingolipids are formed in the lumen of the late Golgi. J Biol Chem 273:2939-2946.

23. Merril A.H. Jr. (1983) Characterization of serine palmitoyltransferase activity in Chinese hamster ovary cells. Biochim Biophys Acta 754:284-291.

24. Merril A.H. Jr., and Jones D.D. (1990) An update of the enzymology and regulation of sphingomyelin metabolism. Biochim Biophys Acta 1044:1-12.

25. Spence M.W. (1993) Sphingomyelinases. Adv Lipid Res 26, 3-23.

26. Kaufman B., Basu S., and Roseman S. (1968) Enzymatic synthesis of disialogangliosides from monosialogangliosides by sialyltransferase from embryonic chicken brain. J Biol Chem 243:5804-5807.

27. Yip M.C., and Dain J.A. (1969) The enzymic synthesis of ganglioside. 1. Brain uridine diphosphate D-galactose: N-acetyl-galactosaminyl-galactosyl-glucosyl-ceramide galactosyl transferase. Lipids 4:270-277.

28. Huwiler A., Kolter T., Pfeilshifter J., and Sandhoff K. (2000) Physiology and pathophysiology of sphingolipid metabolism and signaling. Biochim Biophys Acta 1485:63-99.

29. Wilkening G., Linke T., Uhlhorn-Dierks G., and Sandhoff K. (2000) Degradation of membrane-bound ganglioside GM1. Stimulation by bis(momoacylglycero)phosphate and the activator proteins SAP-B and GM2-AP. J Biol Chem 275:34814:35819.

30. Fingerhut R., Van Der Horst G.T., Verheijen F.W., and Conzelmann E. (1992) Degradation of gangliosides by the Lysosomal sialidase requires an activator protein. Eur J Biochem 208:623-629.

31. Zschoche A., Furst W., Sharzmann G., and Sandhoff K. (1994) Hydrolysis of Lactosylceramide by human galacvtosylceramidase and GM1-beta-galactosidase in a detergent-free system and its stimulation by sphingolipid activator proteins, sap-B and sap-C. Activator proteins stimulate Lactosylceramide hydrolysis. Eur J Biochem 222:83-90.

32. Linke T., Wilkening G., Sadeghlar F., Mozcall H., Bernardo K., Schuchman E., and Sandhoff K. (2001) Interfacial regulation of acid ceramidase activity. Stimulation of ceramide degradation by Lysosomal lipids and sphingolipid activator proteins. J Biol Chem 276:5760-5768.

33. Ito M., and Yamamgata T. (1986) A novel glycosphingolipids-degrading enzyme cleaves the linkage between the oligosaccharide and ceramide of neutral and acidic glycosphingolipids. J Biol Chem 261:14278-14282.

34. Zhou B., Li S.C., Laine R.A., Huang R.T., and Li Y.T. (1989) Isolation and characterization of ceramide glycanase from the leech Macrobdella decora. J Biol Chem 264:12272-12277.

35. Ito M., Ikegami Y., and Yamagata T. (1991) Activator proteins for glycosphingolipid hydrolysis by endoglycoceramidases. Elucidation of biological function of cell-surface glycosphingolipids in situ by endoglycoceramidases made possible using these activator proteins. J Biol Chem 266:7919-7926.

36. Basu M., Girzadas M., Dastgheib S., Baker J., Rossi F., Radin N.S., and Basu S. (1997) Ceramide glycanase from a rat mammary tissues: inhibition by PPMP(D-/L-) and its probable role in signal transduction. Indian J Biochem Biophys 34:142-149.

37. Basu M., Kelly P., Girzadas M., Li Z., and Basu S. (2000) Properties of animal ceramide glycanases. Methods Enymol 311:287-297.

38. Dastgheib S., Basu S.S., Li Z., and Basu S. (2000) Analyses of glycosphingolipids using clam, Mercenaria mercenaria, ceramide glycanase. Methods Enzymol 312:196-205.

39. Hirabayashi Y., Kimura M., Matsumoto M., Yamamoto K., Kadowaki S., and Tochikura T. (1988) A novel glycosphingolipids hydrolyzing enzyme, glycosphingolipids ceramide deacylase, which cleaves th linkage between the fatty acid and sphingosine base in glycosphingolipids. J Biochem 103:1-4

40. Furusato M., Sueyoshi N., Mitsutake S., Sakaguchi K., Kita K., Okino N., Ichinose S., Omori A., and Ito M. (2002) Molecular cloning and characterization of sphingolipid ceramide N-deacylase from marine bacterium, Shewanella alga G8. J Biol Chem 277:17300-17307.

41. Rodriguez-Lafrasse C., and Vanier M.T. (1999) Sphingosylphosphorylcholine in Niemann-Pick disease brain: accumulation in type A but not in type B. Neurochem Res 24:199-205.

42. Lombardo A., Caimi L., Marchesini S., Goi G. C., and Tettamanti G. (1980) Enzymes of lysosomal origin in human plasma and serum: assay conditions and parameters influencing the assay, *Clin Chim Acta 108*, 337-346.

43. Weng S., and Spiro R.G. (1996) Endoplasmic reticulum kifunensine-resistant alpha-mannosidase is enzymatically and immunologically related to the cytosolic alpha-mannosidase, *Arch Biochem Biophys 325*, 113-123.

44. Gopalan V., Glew R.H., Libell D.P., and DePetro J. J. (1989) The dual effects of alcohols on the kinetic properties of guinea pig liver cytosolic beta-glucosidase, *J Biol Chem 264*, 15418-15422.

45. Willemsen R., Brunken R., Sorber C.W., Hoogeveen A.T., Wisselaar H.A., Van Dongen J. M., and Reuser A. J. (1991) A quantitative immunoelectronmicroscopic study on soluble, membrane-associated and membrane-bound lysosomal enzymes in human intestinal epithelial cells, *Histochem J 23*, 467-473.

46. Venerando B., Goi G. C., Preti A., Fiorilli A., Lombardo A., and Tettamanti G. (1982) Cytosolic sialidase in developing rat forebrain, *Neurochem Int 4*, 313-320.

47. Van Meer G., Voelker D.R., Feigenson G.W. (2008) Membrane lipids: where they are and how they behave.

48. Levade T., and Jaffrezou J.P. (1999) Signalling sphingomyelinase: which, where, how and why?

49. Goni F.M., and Alonso A. (2002) Sphingomyelinase: enzymology and membrane activity.

50. Huitema K., Van Den Dikkenberg J., Brouwers J.F., and Holthuis J.C. (2004) Identification of a family of animal sphingomyelin synthases. EMBO J 23(1):33-44.

51. Hasegawa T., Yamaguchi K., Wada T., Takeda A., Itoyama Y., and Miyagi T. (2000) Molecular cloning of mouse ganglioside sialidase and its increased expression in neuro2a cell differentiation. J Biol Chem 275(11):8007-15

52. Wada T., Yoshikawa Y., Tokuyama S., Kuwabara M., Akita H., and Miyagi T. (1999) Cloning, expression and chromosomal mapping of a human ganglioside sialidase. Biochem Biophys Res Commun. 261(1):21-7.

53. Miyagi T., Wada T., Iwamatsu A., Hata K., Yoshikawa Y., Tokuyama S., and Sawada M. (1999) Molecular cloning and characterization of a plasma membrane-associated sialidase specific for gangliosides. J Biol Chem. 274(8):5004-11.

54. Kalka D., Von Reitzeinstein C., Kopitz J., and Cantz M. (2001) The plasma membrane ganglioside sialidase cofractionated with markers of lipid rafts. Biochem Biophys Res Commun 283(4):989-93.

55. Papini N., Anastasia L., Tringali C., Croci G., Bresciani R., Yamaguchi K., Miyagi T., Preti A., Prinetti A., Prioni S., Sonnino S., Tettamanti G., Venerando B., and Monti E. (2004) The plasma membrane-associated sialidase MmNEU3 modifies the ganglioside pattern of adjacent cells supporting its involvement in cell-to-cell interactions. J Biol Chem 279(17):16989-95.

56. Valaperta R., Chigorno V., Basso L., Prinetti A., Bresciani R., Preti A., Miyagi T. and Sonnino S. (2006) Plasma membrane production of ceramide from ganglioside GM3 in human fibroblasts. FASEB J 20(8):1227-9.

57. Preti A., Fiorilli A., Lombardo A., Caimi L., and Tettamanti G. (1980) Occurrence of sialyltransferase activity in the synaptosomal membranes prepared from calf brain cortex. J Neurochem 35(2):281-96.

58. Matsui Y., Lombard D., Massarelli R., Mandel P., and Dreyfus H. (1986) Surface glycosyltransferase activities during development of neuronal cell cultures. J Neurochem 46(1):144-50.

59. Durrie R., Saito M., and Rosemberg A. (1988) Endogenous glycosphingolipids acceptor specificity of sialosyltransferase system in intact Golgi membranes, synaptosomes and synaptic plasma membrane from rat brain. Biochemistry 27(10):3759-64.

60. Durrie R., and Rosemberg A. (1989) Anabolic sialosylation of gangliosides in situ in rat brain cortical slices. J Lipid Res 30(8):1259-66.

61. Iwamori M., and Iwamori Y. (2005) Changes in the glycolipid composition and characteristic activation of gm3 synthase in the thymus of mouse after administration of dexamethasone. Glycoconj J 22(3):119-26.

62. Mencarelli S., Cavalieri C., Magini A., Tancini B., Basso L., Lemansky P., Hasilik A., Li Y.T., Chigorno V., Orlacchio A., Emiliani C., and Sonnino S. (2005) Identification of plasma

membrane associated mature beta-hexosaminidase A, active towards GM2 ganglioside in human fibroblasts. FEBS Lett 579(25):5501-6.

63. Kong Y., Li R., and Ladisch S. (1998) Natural forms of shed tumor gangliosides. Biochim Biophys Acta 1394(1):43-56.

64. Deng W., Li R., and Ladisch S. (2000) Influence of cellular ganglioside depletion on tumor formation. J Natl Cancer Inst. 92(11):912-7.

65. Chigorno V., Giannotta C., Ottico E., Sciannambolo M., Mikulak J., Prinetti A., and Sonnino S. (2005) Sphingolipid uptake by cultured cells: complex aggregates of cell sphingolipids with serum proteins and lipoproteins are rapidly catabolyzed. J Biol Chem 280(4):2668-75.

66. Hakomori, S. (1996) Tumor malignancy defined by aberrant glycosylation and sphingo(glyco)lipid metabolism, *Cancer Res 56*, 5309-5318.

67. Hakomori, S. (2002) Glycosylation defining cancer malignancy: new wine in an old bottle, *Proc Natl Acad Sci U S A 99*, 10231-10233.

68. Lukong, K. E., Seyrantepe, V., Landry, K., Trudel, S., Ahmad, A., Gahl, W. A., Lefrancois, S., Morales, C. R., and Pshezhetsky, A. V. (2001) Intracellular distribution of lysosomal sialidase is controlled by the internalization signal in its cytoplasmic tail, *J Biol Chem 276*, 46172-46181.

69. Cordero, O. J., Merino, A., Paez de la Cadena, M., Bugia, B., Nogueira, M., Vinuela, J. E., Martinez-Zorzano, V. S., de Carlos, A., and Rodriguez-Berrocal, F. J. (2001) Cell surface human alpha-L-fucosidase, *Eur J Biochem 268*, 3321-3331.

70. Aureli, M., Masilamani, A. P., Illuzzi, G., Loberto, N., Scandroglio, F., Prinetti, A., Chigorno, V., and Sonnino, S. (2009) Activity of plasma membrane beta-galactosidase and beta-glucosidase, *FEBS Lett 583*, 2469-2473.

71. Kopitz, J., Sinz, K., Brossmer, R., and Cantz, M. (1997) Partial characterization and enrichment of a membrane-bound sialidase specific for gangliosides from human brain tissue, *Eur J Biochem 248*, 527-534.

72. Monti, E., Preti, A., Venerando, B., and Borsani, G. (2002) Recent development in mammalian sialidase molecular biology, *Neurochem Res 27*, 649-663.

73. Miyagi, T., Wada, T., Yamaguchi, K., Shiozaki, K., Sato, I., Kakugawa, Y., Yamanami, H., and Fujiya, T. (2008) Human sialidase as a cancer marker, *Proteomics 8*, 3303-3311.

74. Miyagi, T., Wada, T., and Yamaguchi, K. (2008) Roles of plasma membrane-associated sialidase NEU3 in human cancers, *Biochim Biophys Acta 1780*, 532-537.

75. Ueno, S., Saito, S., Wada, T., Yamaguchi, K., Satoh, M., Arai, Y., and Miyagi, T. (2006) Plasma membrane-associated sialidase is up-regulated in renal cell carcinoma and promotes interleukin-6-induced apoptosis suppression and cell motility, *J Biol Chem 281*, 7756-7764.

76. Kakugawa, Y., Wada, T., Yamaguchi, K., Yamanami, H., Ouchi, K., Sato, I., and Miyagi, T. (2002) Up-regulation of plasma membrane-associated ganglioside sialidase (Neu3) in human colon cancer and its involvement in apoptosis suppression, *Proc Natl Acad Sci U S A 99*, 10718-10723.

77. Venerando, B., Fiorilli, A., Croci, G., Tringali, C., Goi, G., Mazzanti, L., Curatola, G., Segalini, G., Massaccesi, L., Lombardo, A., and Tettamanti, G. (2002) Acidic and neutral sialidase in the erythrocyte membrane of type 2 diabetic patients, *Blood 99*, 1064-1070.

78. Tringali, C., Lupo, B., Anastasia, L., Papini, N., Monti, E., Bresciani, R., Tettamanti, G., and Venerando, B. (2007) Expression of sialidase Neu2 in leukemic K562 cells induces apoptosis by impairing Bcr-Abl/Src kinases signaling, *J Biol Chem 282*, 14364-14372.

79. Tringali, C., Anastasia, L., Papini, N., Bianchi, A., Ronzoni, L., Cappellini, M. D., Monti, E., Tettamanti, G., and Venerando, B. (2007) Modification of sialidase levels and sialoglycoconjugate pattern during erythroid and erytroleukemic cell differentiation, *Glycoconj J 24*, 67-79.

80. Chigorno, V., Cardace, G., Pitto, M., Sonnino, S., Ghidoni, R., and Tettamanti, G. (1986) A radiometric assay for ganglioside sialidase applied to the determination of the enzyme subcellular location in cultured human fibroblasts, *Anal Biochem 153*, 283-294.

81. Schengrund, C. L., and Repman, M. A. (1982) Density-dependent changes in gangliosides and sialidase activity of murine neuroblastoma cells, *J Neurochem 39*, 940-947.

82. Aureli, M., Loberto, N., Lanteri, P., Chigorno, V., Prinetti, A., and Sonnino, S. (2010) Cell surface sphingolipid glycohydrolases in neuronal differentation and aging in culture, *J Neurochem*.

83. Coates, P. J. (2002) Markers of senescence?, *J Pathol 196*, 371-373.

84. Dimri, G. P., Lee, X., Basile, G., Acosta, M., Scott, G., Roskelley, C., Medrano, E. E., Linskens, M., Rubelj, I., Pereira-Smith, O., and et al. (1995) A biomarker that identifies senescent human cells in culture and in aging skin in vivo, *Proc Natl Acad Sci U S A 92*, 9363-9367.

85. Severino, J., Allen, R. G., Balin, S., Balin, A., and Cristofalo, V. J. (2000) Is beta-galactosidase staining a marker of senescence in vitro and in vivo?, *Exp Cell Res 257*, 162-171.

86. Geng, Y. Q., Guan, J. T., Xu, X. H., and Fu, Y. C. Senescence-associated beta-galactosidase activity expression in aging hippocampal neurons, *Biochem Biophys Res Commun 396*, 866-869.

87. Neufeld, E. F. (1991) Lysosomal storage diseases, *Annu Rev Biochem 60*, 257-280.

88. Daniels, L. B., Coyle, P. J., Chiao, Y. B., Glew, R. H., and Labow, R. S. (1981) Purification and characterization of a cytosolic broad specificity beta-glucosidase from human liver, *J Biol Chem 256*, 13004-13013.

89. Boot, R. G., Verhoek, M., Donker-Koopman, W., Strijland, A., van Marle, J., Overkleeft, H. S., Wennekes, T., and Aerts, J. M. (2007) Identification of the non-lysosomal glucosylceramidase as beta-glucosidase 2, *J Biol Chem 282*, 1305-1312.

90. Overkleeft, H. S., Renkema, G. H., Neele, J., Vianello, P., Hung, I. O., Strijland, A., van der Burg, A. M., Koomen, G. J., Pandit, U. K., and Aerts, J. M. (1998) Generation of specific deoxynojirimycin-type inhibitors of the non-lysosomal glucosylceramidase, *J Biol Chem 273*, 26522-26527.

91. Clarke, C. J., Truong, T. G., and Hannun, Y. A. (2007) Role for neutral sphingomyelinase-2 in tumor necrosis factor alpha-stimulated expression of vascular cell adhesion molecule-1 (VCAM) and intercellular adhesion molecule-1 (ICAM) in lung epithelial cells: p38 MAPK is an upstream regulator of nSMase2, *J Biol Chem 282*, 1384-1396.

92. Corcoran, C. A., He, Q., Ponnusamy, S., Ogretmen, B., Huang, Y., and Sheikh, M. S. (2008) Neutral sphingomyelinase-3 is a DNA damage and nongenotoxic stress-regulated gene that is deregulated in human malignancies, *Mol Cancer Res 6*, 795-807.

93. Krut, O., Wiegmann, K., Kashkar, H., Yazdanpanah, B., and Kronke, M. (2006) Novel tumor necrosis factor-responsive mammalian neutral sphingomyelinase-3 is a C-tail-anchored protein, *J Biol Chem 281*, 13784-13793.

94. Stoffel, W., Jenke, B., Block, B., Zumbansen, M., and Koebke, J. (2005) Neutral sphingomyelinase 2 (smpd3) in the control of postnatal growth and development, *Proc Natl Acad Sci U S A 102*, 4554-4559.

95. Kim, W. J., Okimoto, R. A., Purton, L. E., Goodwin, M., Haserlat, S. M., Dayyani, F., Sweetser, D. A., McClatchey, A. I., Bernard, O. A., Look, A. T., Bell, D. W., Scadden, D. T., and Haber, D. A. (2008) Mutations in the neutral sphingomyelinase gene SMPD3 implicate the ceramide pathway in human leukemias, *Blood 111*, 4716-4722.

96. Karakashian, A. A., Giltiay, N. V., Smith, G. M., and Nikolova-Karakashian, M. N. (2004) Expression of neutral sphingomyelinase-2 (NSMase-2) in primary rat hepatocytes modulates IL-beta-induced JNK activation, *FASEB J 18*, 968-970.

97. Marchesini, N., and Hannun, Y. A. (2004) Acid and neutral sphingomyelinases: roles and mechanisms of regulation, *Biochem Cell Biol 82*, 27-44.

98. Tani, M., and Hannun, Y. A. (2007) Neutral sphingomyelinase 2 is palmitoylated on multiple cysteine residues. Role of palmitoylation in subcellular localization, *J Biol Chem 282*, 10047-10056.

99. Reddy, A., Caler, E. V., and Andrews, N. W. (2001) Plasma membrane repair is mediated by Ca(2+)-regulated exocytosis of lysosomes, *Cell 106*, 157-169.

100. Cardone, R. A., Casavola, V., and Reshkin, S. J. (2005) The role of disturbed pH dynamics and the Na+/H+ exchanger in metastasis, *Nat Rev Cancer 5*, 786-795.

101. Chiche, J., Ilc, K., Laferriere, J., Trottier, E., Dayan, F., Mazure, N. M., Brahimi-Horn, M. C., and Pouyssegur, J. (2009) Hypoxia-inducible carbonic anhydrase IX and XII promote tumor cell growth by counteracting acidosis through the regulation of the intracellular pH, *Cancer Res 69*, 358-368.

102. Casey, J. R., Grinstein, S., and Orlowski, J. (2010) Sensors and regulators of intracellular pH, *Nat Rev Mol Cell Biol 11*, 50-61.

103. Simons K., and Ikonen E. (1997) Functional rafts in cell membranes. Nature 387(6633):569-72.

104. Brown D.A., and Rose J.K. (1992) Sorting of GPI-anchored proteins to glycolipid-enriched membrane subdomains during transport to the apical cell surface. Cell 68(3):533-44.

105. Kurzchalia T.V., and Parton R.G. (1999) Membranes microdomains and caveolae. Curr Opin Cell Biol 11(4):424-31.

106. Okada Y., Mugnai G., Bremer E.G., and Hakomori S. (1984) Glycosphingolipids in detergent-insoluble substrate attachment matrix (DISAM) prepared from substrate attachment material (SAM). Their possible role in regulating cell adhesion. Exp Cell Res 155(2):448-56.

107. Harder T., and Simons K. (1997) Caveolae, digs, and the dynamics of sphingolipid-cholesterol microdomain. Curr Opin Cell Biol 9(4):534-42.

108. Prinetti A., Chighorno V., Tettamanti G., and Sonnino S. (2000) Sphingolipid-enriched membrane domains from rat cerebellar granule cells differentiated in colture. J Biol Chem 275(16):11658-65.

109. Hakomori S.I. (2000) Cell adhesion/recognition and signal transduction through glycosphingolipids function. Glycoconj J 17(3 -4):143-51.

110. Hakomori S.I., Handa K., Iwabuchi K., Yamamura S., and Prinetti A. (1998) New insights in glycosphingolipids function: “glycosignaling domain”, a cell surface assembly of

glycosphingolipids with signal transducer molecules involved in cell adhesion coupled with signaling. Glycobiology 8(10):xi-xix.

111. Tillack T.W., Allietta M., Moran R.E., and Young W.W. Jr. (1983) Localization of globoside and Forssman glycolipids on erythrocyte membranes. Biochim Biophys Acta 733(1):15-24.

112. Rahmann H., Rosner H., Kortje K.H., Beitinger H., and Seybold V. (1994) Ca(2+)-ganglioside-interaction in neuronal differentiation and development. Prog Brain Res 101:127-45.

113. Sorice M., Parolini I., Sansolini T., Garofalo T., Dolo V., Sargiacomo M., Tai T., Peschle C., Torrisi M.R., and Pavan A. (1997) Evidence for the existence of ganglioside-enriched plasma membrane domains in human peripheral lymphocytes. J Lipid Res 38(5):969-80.

114. Ishitsuka R., Sato S.B., and Kobayashi T. (2005) Imaging lipid rafts. J Biochem 137(3):249-54.

115. Lagerholm B.C., Weinreb G.E., Jacobson K., and Thompson N.L. (2005) Detecting microdomains in intact cell membranes. Annu Rev Phys Chem 56:309-36.

116. Saxton M.J. (1997) Single particle tracking : the distribution of diffusion coefficients. Biophys J 72(4):1744-53.

117. Jacobsin K., Sheets E.D., and Simson R. (1995) Revisiting the fluid mosaic model of membranes. Science 268(5216):1441-2.

118. Sheets E.D., Lee G.M., Simson R., and Jacobson K. (1997) Transient confinement of a glycosylphosphatidylinositol-anchored protein in the plasma membrane. Biochemistry 36(41):12449-58.

119. Varma R., and Mayor S. (1998) GPI-anchored proteins are organized in submicron domains at the cell surface. Nature 394(6695):798-801.

120. Pralle A., Keller P., Florin E.L., Simons K., and Horber J.K. (2000) Sphingolipid-cholesterol rafts diffuse as small entities in the plasma membrane of mammalian cells. J Cell Biol 148(5):997-1008.

121. Poole K., Meder D., Simons K., and Muller D. (2004) The effect of raft lipid depletion on microvilli formation in MDKC cells, visualized by atomic force microscopy. FEBS Lett 565(1-3):53-8.

122. Shutz G.J., Kada G., Pastushenko V.P., and Schindler H. (2000) Properties of lipid microdomains in a muscle cell membrane visualized by single molecule microscopy. EMBO J 19(5):892-901.

123. Brown D.A., and Rose J.K. (1992) Sorting of GPI-anchored proteins to glycolipid-enriched membrane subdomains during transport to the apical cell surface. Cell 68(3):533-44.

124. Taylor C.M., Kada G., Pastushenko V.P,. and Schindler H. (2000) Properties of lipid microdomains in a muscle cell membrane visualized by single molecule microscopy. EMBO J 19(5):892-901.

125. Simons M., Kramer E.M., Thiele C., Stoffel W., and Trotter J. (2000) Assembly of myelin by association of proteolipid protein with cholesterol- and galactosylceramide-rich membrane domains. J Cell Biol 151(1):143-54.

126. Roper K., Corbeil D., and Huttner W.B. (2000) Retention of prominin in microvilli reveals distinct cholesterol-based lipid micro-domains in the apical plasma membrane. Nat Cell Biol 2(9):582-92.

127. Sargiacomo M., Sudol M., Tang Z., and Lisanti M.P. (1993) Signal transducing molecules and glycosyl-phosphatidylinositol-linked proteins form a caveolin-rich insoluble complex in MDCK cells. J Cell Biol 122(4):789-807.

128. Zurzolo C., Van't Hof W., Van Meer G., and Rodriguez-Boulan E. (1994) VIP21/caveolin, glycosphingolipids clusters and the sorting of glycosylphosphatidylinositol.anchoered proteins in epithelial cells. EMBO J 13(1):42-53.

129. Iwabuchi K., and Nagaoka I. (2002) Lactosylceramide-enriched glycosphingolipids signaling domain mediates superoxide generation from human neutrophils. Blood 100(4):1454-64.

130. Prinetti A., Iwabuchi K., and Hakomori S. (1999) Glycosphingolipid-enriched signaling domain in moise neuroblastoma Neuro2a cells. Mechanism of ganglioside-dependent neuritogenesis. J Biol Chem 274(30):20916-24.

131. Parton R.G. (1994) Ultrastructural localization of gangliosides; GM1 is concentrated in caveolae. J Histochem Cytochem 42(2):155-66.

132. Kubler E., Dohlman H.G., and Lisanti M.P. (1996) Identification of Triton X-100 insoluble membrane domains in the yeast saccharomyces cerevisiae. Lipid requirements for targeting of heterotrimeric G-protein subunits. J Biol Chem 271(51):32975-80.

133. Zhang X., and Thompson G.A. Jr. (1997) An apparent association between glycosylphosphatidylinositol-anchored proteins and a sphingolipid in tetrahymena member. Biochem J 323(Pt 1):197-206.

134. Chang W.J., Ying Y.S., Rothberg K.G., Hooper N.M., Turner A.J., Gambliel H.A., De Gunzburg J., Mumby S.M., Gilman A.G., and Anderson R.G. (1994) Purification and characterization of smooth muscle cell caveolae. J Cell Biol 126(1):127-38.

135. Kasahara K., Watanabe Y., Yamamoto T., and Sanai Y. (1997) Association of Src family tyrosine kinase Lyn with ganglioside GD3 in rat brain. Possible regulation of Lyn by glycosphingolipids in caveolae-like domains. J Biol Chem 272(47):29947-53.

136. Madore N., Smith K.L., Graham C.H., Jen A., Brady K., Hall S., and Morris R. (1999) Functionally different GPI proteins are organized in different domains on the neuronal surface. EMBO J 18(24):6917-26.

137. Parkin E.T., Turner A.J., and Hooper N.M. (1999) Amyloid precursor protein, although partially detergent-insoluble in mouse cerebral cortex, behaves as an atypical lipid raft protein. Biochem J 344 (Pt 1):23-30.

138. Kawabuchi M., Satomi Y., Takao T., Shimonishi Y., Nada S., Nagai K., Tarakhovsky A., and Okada M. (2000) Transmembrane phosphoprotein Cbp regulates the activities of Src-family tyrosine kinases. Nature 404(6781):999-1003.

139. Song K.S., Li S., Okamoto T., Quilliam L.A., Sargiacomo M., and Lisanti M.P. (1996) Co-purification and direct interaction of Ras with caveolin, an integral membrane protein of caveolae microdomains. Detergent-free purification of caveolae microdomains. J Biol Chem 271(16):9690-7.

140. Smart E.J., Ying Y.S., Mineo C., and Anderson R.G. (1995) A detergent-free method for purifying caveolae membrane from tissue culture cells. Proc Natl Acad Sci USA 92(22):10104-8.

141. Madore N., Smith K.L., Graham C.H., Jen A., Brady K., Hall S., and Morris R. (1999) Functionally different GPI proteins are organized in different domains on the neuronal surface. EMBO J 18(24):6917-26.

142. Iwabuchi K., Handa K., and Hakomori S. (1998) Separation of “glycosphingolipid signaling domain” from caveolin-containing membrane fraction in mouse melanoma B16 cells and its role in cell adhesion coupled with signaling. J Biol Chem 273(50):33766-73.

143. Miklavcic J.J, Schabl K.L., Mazurak V.C., Thomson A.B.R., and Clandinin M.T. (2012) Dietary ganglioside reduce proinflammatory signaling. J Nutr Metab 2012:280286.

Theme I

Exploring the link between ceramide, abiraterone and ionizing radiation in prostate cancer cell death

Introduction

Prostate cancer

Prostate cancer (PC) is one of the most commonly diagnosed malignant tumors: in the United States, PC is the second leading cause of cancer-related death in men, and it is a growing problem worldwide [1]. The disease is very heterogeneous in terms of grade, genetics, ploidy, and oncogene/tumor suppressor gene expression, and its biological, hormonal, and molecular characteristics are extremely complex. Growth of early PC requires 5α-dihydrotestosterone (DHT) produced from testosterone by the 5α-reductase enzyme system: such prostate cells are described as androgen-dependent (AD). Because prostate cancer exerts androgen-dependent growth, androgen ablation or anti-androgen therapies are very effective [2-4]. Androgen receptor (AR) antagonists including bicalutamide or flutamide are used as monotherapy or in combination with castration to block androgen action [5-8]. Afterwards, the prostate cancer cells may respond to androgen but do not require it for growth: these cells are androgen sensitive (AS). This leads to periods of remission from disease, but almost invariably, the PC recurs, by which time the PC cells have become androgen-independent (AI)[9,10]. In the past year, several molecular mechanisms for progression to hormone refractoriness have been proposed based on observations of experimental or clinical PC [11-14]. Five possible mechanisms of development of AR-independent PC have been proposed:

1) *The Hypersensitive pathway:* more AR is produced (usually by gene amplification), or AR has enhanced sensitivity to compensate for low levels of androgen, or more testosterone is converted to the more potent androgen, dihydrotestosterone (DHT), by 5α-reductase.
2) *The promiscuuos pathway:* selection of mutations in the AR that confers broader ligand specificity (flutamide/bicalutamide itself, corticosteroid hormones or other similar molecules);
3) *The outlaw pathway:* up-regulation of crosstalk signal transduction pathways that activate AR in a ligand-independent manner. For example receptor tyrosine kinases (RTKs) are activated, and the AR is phosphorylated by either the AKT (protein kinase B) or the mitogen-activated protein kinase (MAPK) pathway, producing a ligand-independent AR
4) *The bypass pathway:* alternative mechanisms of cell survival, for example activating the anti-apoptotic protein BCL2.

5) *The lurker cell pathway:* androgen-independent cancer cells that are present all the time in the prostate, possibly epithelial stem cells, might be selected by therapy.

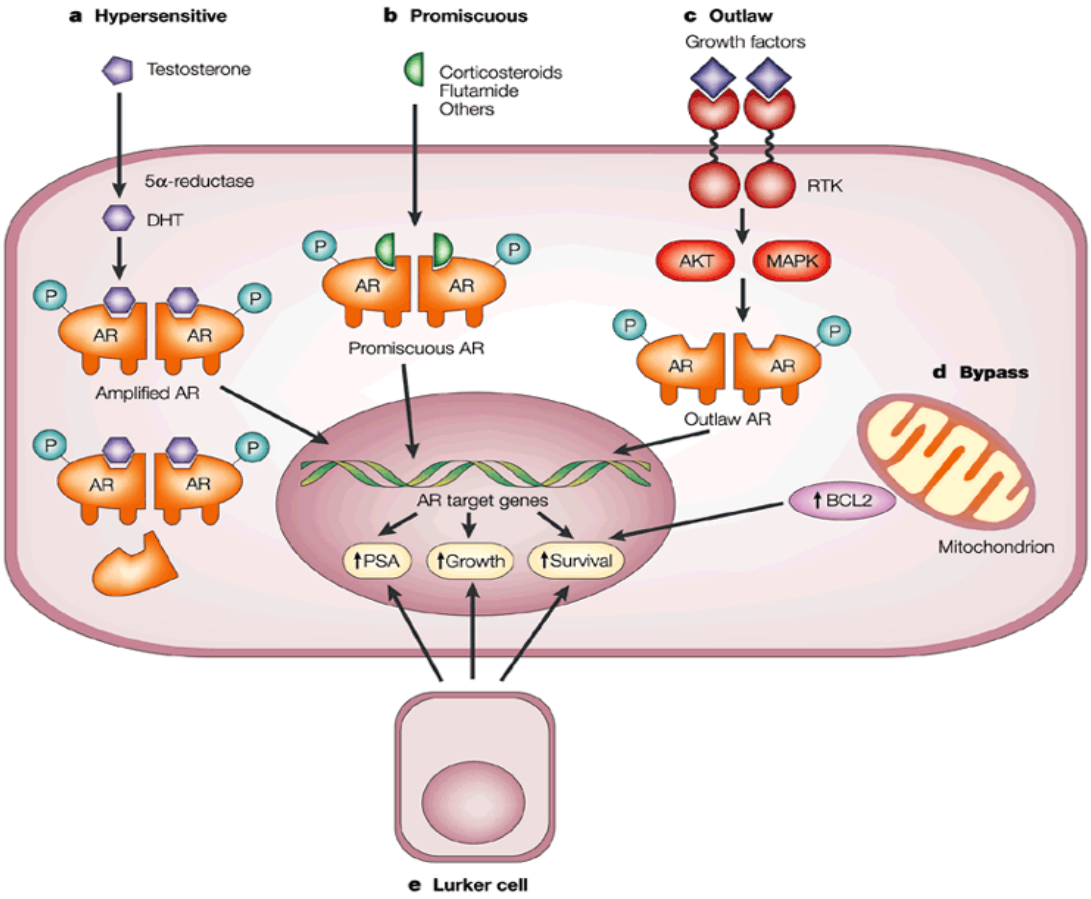

Figure 1. Possible mechanisms of development of androgen-indipendent PC (from [15]).

In addition, AR can function through a suppressor element to repress its own expression and the expression of additional genes, including those that mediate androgen synthesis (Figure 2). This negative feedback loop suppresses AR signaling at high androgen levels but allows increased AR and androgen synthesis in castration-resistant prostate cancer (CRPC). Activation (or repression) of target genes leads to biological responses including growth, survival and the production of prostate-specific antigen (PSA).

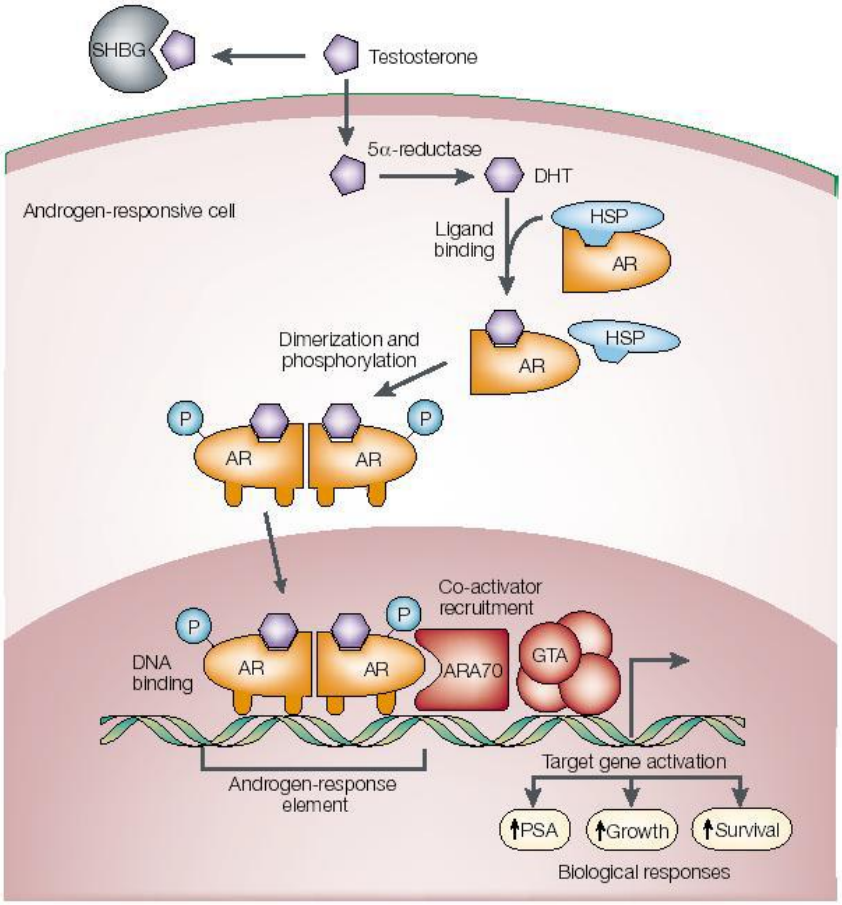

Figure 2. Androgen action. Testosterone circulates in the blood bound to albumin (not shown) and sex-hormone-binding globulin (SHBG), and exchanges with free testosterone. Free testosterone enters prostate cells and is converted to dihydrotestosterone (DHT) by the enzyme 5α-reductase. Binding of DHT to the androgen receptor (AR) induces dissociation from heat-shock proteins (HSPs) and receptor phosphorylation. The AR dimerizes and can bind to androgen-response elements in the promoter regions of target genes. Co-activators (such as ARA70) and corepressors (not shown) also bind the AR complex, facilitating or preventing, respectively, its interaction with the general transcription apparatus (GTA). Activation (or repression) of target genes leads to biological responses including growth, survival and the production of prostate-specific antigen (PSA).

Organ-confined PC is treated with surgery (radical prostectomy) or radiation therapy, and an increase in PSA level usually represents the first sign of recurrence [16]. Moreover, PC most commonly metastasizes to the bones, lymph nodes, and may invade rectum, bladder and lower ureters after local progression. The route of metastasis to bone is thought to be venous as the prostatic venous plexus draining the prostate connects with the vertebral veins. Eradication of advanced PC still represents an unsolved clinical problem, making the development of alternative treatment approaches desirable.

Ionizing radiation and prostate cancer

Radiotherapy represents the therapeutic strategy for the treatment of an increasing number of tumors, included PC. Recently, various schemes of radical radiation therapy, based on the excellent results of phase I-II studies using the hypofractionation in different cancer diseases, have been developed. Thanks to the application of conformal/intensity-modulated techniques in combination with precise image-guided localization of the target, radiotherapy dose escalation has been shown to improve disease control. Therefore, it should be possible to use a larger dose per fraction without increasing the risk of serious late injury to the normal tissues. In the last years, studies of radiobiology focused to provide rationale for evaluating proteins known to play an important role in the control of the apoptotic pathway as potential biomarkers. Despite some limitations, such as time-consuming procedures, low resolution due to heterogeneity of proteins and post-translational modifications, proteomic approach could be used to study molecular biomarkers to predict and follow the radiotherapy response.

Irradiation of cancer cells leads to cell death by different mechanisms as summarized in Figure 3 (extracted from [17]):

1) *DNA damage*: irradiation may induce irreparable DNA damage causing brakes in DNA strands or leading to replicational and transcriptional errors. In both cases DNA damage initiates apoptosis via p53-dependent mechanisms;
2) *Mitochondrial damage*;
3) *Oxidative stress*: irradiation leads to reactive oxygen species formation, bringing mainly to necrosis;
4) *Plasma membrane modifications*: it has been demonstrated that Cer is involved in cell death after irradiation via induction of apoptosis. In fact, several lines of evidence demonstrated, cell irradiation results in the activation of cell surface SMase leading to ectopic ceramide formation with the consequent activation of Cer-dependent-apoptosis [18].

So far, no data on the effect of ionizing radiations on the activities of PM-associated glycosidases are available, even if some lines of evidence suggested that these enzymes could contribute to the formation of pro-apoptotic Cer under some circumstances.

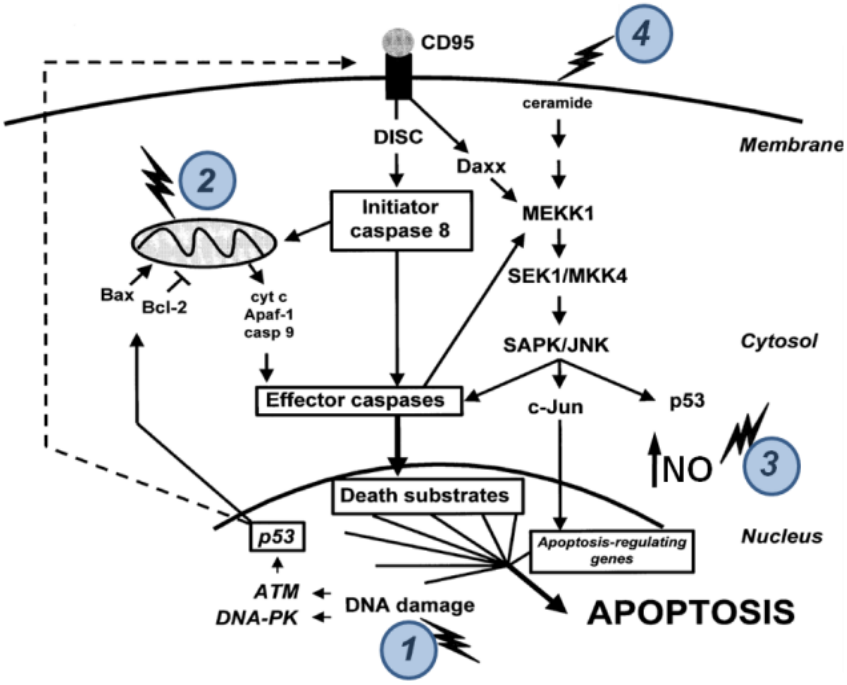

Figure 3. Irradiation-induced cell death pathways. DNA damage (1), mitochondrial damage (2) and superoxide production (3) bring mainly to necrosis, Cer is involved in irradiation-induced apoptosis (4).

It has been demonstrated that in human fibroblasts the over-expression of Neu3, which is parallel by the increase in the expression/activity of β-Gal and β-Gluc, causes the onset of apoptosis due to increased Cer production at the PM level [19,20]. Activation of glycosidases by ionizing radiations could change the ratio between apoptotic Cer and antiapoptotic/proliferative LacCer (Figure 4). For example Cer produced by SM or glycolipid hydrolysis forms large Cer-enriched membrane platforms, instrumental to the modulation of cell signaling processes. This could explain why some tumors are more responsive to irradiation than others, such as the prostate cancer, characterized by high level of radio resistance. For this reason big efforts are employed to develop new drugs, which alone or in combination with radiotherapy are able to rescue or at least to reduce the resistance phenomenon.

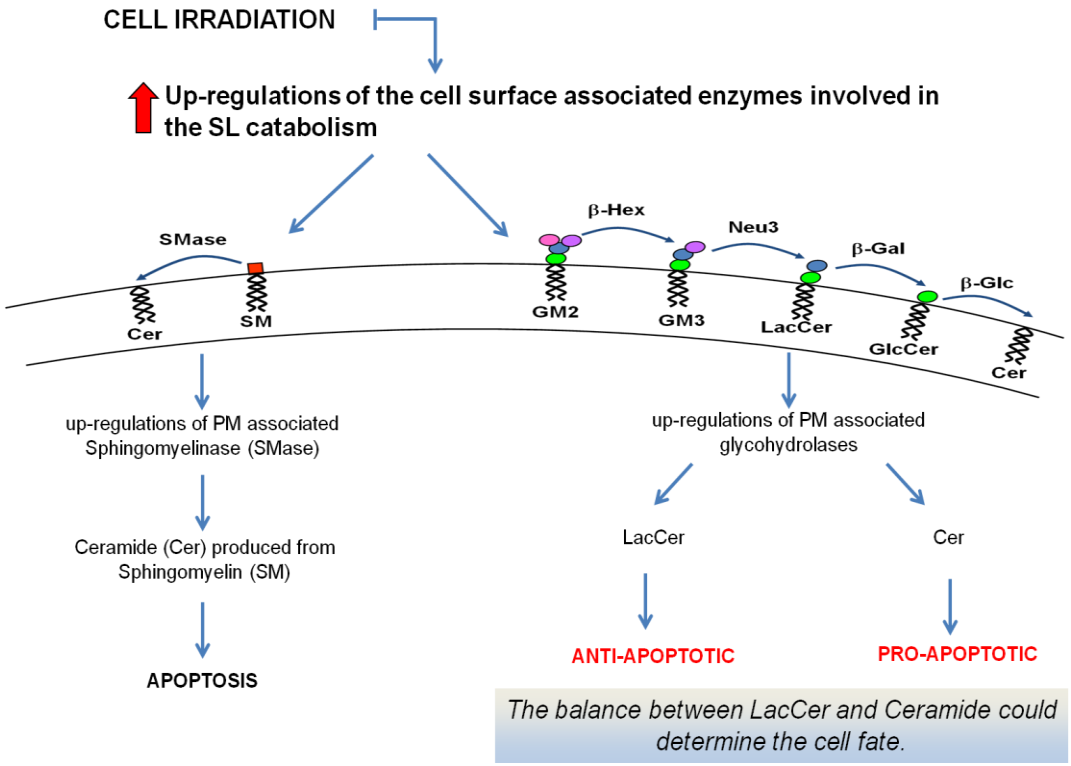

Figure 4. Up-regulation of cell surface-associated enzymes involved in SL-catabolism after cell irradiation.

Abiraterone: new drug for PC treatment

The development and progression of CRPC is dependent on intratumoral steroidogenesis, resulting in androgen synthesis and activation of the androgen receptor. Compared with primary prostate tumors, metastatic CRPC display alterations in the genes encoding steroidogenic enzymes, including the up-regulated expression of Cytocrome P450 17α-hydroxylase/17,20-lyase (CYP17A1) [24]. In addition, much evidence indicates that CRPC can synthesize androgen from cholesterol [23]. Abiraterone acetate is a potent inhibitor of CYP17A1, a key enzyme in the androgen biosynthesis pathway, which is active in the testis and adrenal glands where it catalyzes the conversion of pregnenolone and progesterone into the weak androgens dehydroepiandrosterone and androstenedione, respectively [21,22] (Figure 5). Early clinical trials demonstrated that abiraterone acetate has a significant and sustained antitumor activity in CRPC even if its molecular mechanism that could be independent from the CYP17A1 inhibition is still unknown.

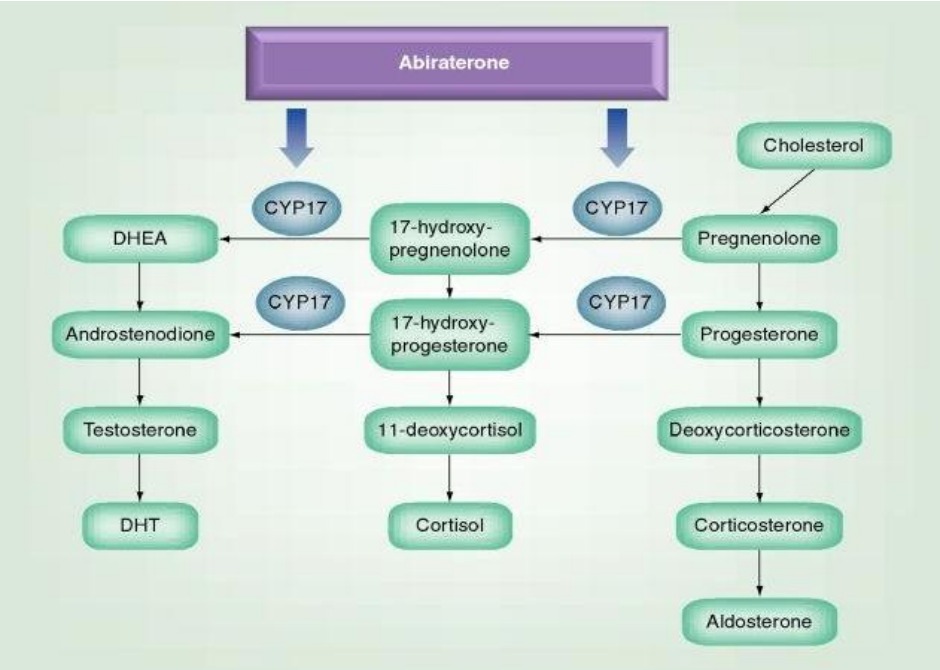

Figure 5. Mechanism of action of abiraterone acetate.

Aim

Prostate cancer is one of the main leading cause of cancer-related death in men because of the development of resistance to radiotherapy and androgen ablation. Interestingly, recent lines of evidence on the possible involvement of changes in the PM sphingolipid composition due to the activation of the PM-associated glycohydrolases in the onset of cell death, open a new possible scenario also for PC. For this reason, the main aim of this thesis is to study the possible effect of abiraterone and ionizing radiation on the activity of the PM-associated glycohydrolases in the production of Cer.

Material and Methods

Materials

Commercial chemicals were of the highest purity available, common solvents were distilled before use and water was doubly distilled in a glass apparatus. Trypsin, EDTA, Trypan blue, HEPES buffer solution, sodium pyruvate, aprotinine, PMSF, Glycine, reagents for cell culture and RPMI-1640 medium were from Sigma Chemical Co. (St Louis, MO, USA).

Fetal bovine serum (FBS), penicillin/streptomycin and glutamine were purchased from EuroClone (Leeds, UK); AM-calcein, DMEM-F12 were from Invitrogen (Carlsbad, CA, USA).

6-hexadecanoylamino-4-methylumbelliferone (H-MUB), 4-methylumbelliferone (MUB), 4-methylumbelliferyl-β-D-galactopyranoside (MUB-Gal), 4-methylumbelliferil-β-N-acetylglucosaminide (MUG) and 4-methylumbelliferyl-β-D-glucopyranoside (MUB-Glc) were from Glycosynth (Warrington, UK).

6-hexadecanoylamino-4-methylumbelliferyl-phosphorylcholine (H-MUB-PC) was from Moscerdam Substrates (Oegstgeest, Netherland). High-performance silica gel thin-layer plates (HPTLC Kieselgel 60) were from Merck GmbH (Milan, Italy).

The preparation of isotopically labeled [1-^{3}H]sphingosine (specific radioactivity, 2.2 Ci/mmole) has been described in detail [25].

Abiraterone acetate was from Janssen-Cilag International.

METHODS

Cell Cultures

LNCaP, PC3 and DU145 prostate cancer cells were cultured and propagated in RPMI-1640. Medium were supplemented with 10% FCS (heat-inactivated), 1% glutamine, 1% penicillin/streptomycin, 1% sodium pyruvate and 1% HEPES. The cells were cultivated as monolayer in a humidified atmosphere at 37°C and 5% CO_2.

Abiraterone treatment

After a pivotal study aimed to establish the cytostatic but non cytotoxic concentration of the drug, the androgen-sensitive LNCaP cells were subjected to a single treatment with 10 μM abiraterone while the androgen-insensitive PC3 and DU145 cells with 25 μM abiraterone. When the different cell lines were subjected to the combined treatment with abiraterone and ionizing radiation, cells were pre-treated with the drug for 24 hours before irradiation.

Irradiation of cells

The most widely used technique for mathematically modeling the effect of radiation on cancer cell survival, is linear quadratic (LQ) formalism. The core formula involved is an expression which correlate the probability of survival, S, of a population of mammalian cells following exposure to an individual radiation dose, d, as follows:

$$S = \exp[-\alpha D-\beta D2]$$

where α and β are tumor- or normal tissue-specific parameters. Rearrangement of the equation to account for the total impact of n individual fractions of radiation exposure yields another common expression for the biologically effective dose (BED):

$$BED = nd(1+/\alpha/\beta)$$

The units of BED are Gray (Gy), the standard unit of radiation dose. The BED is a convenient metric for comparing the relative impact of a given schedule of radiation dose on a given tumor or tissue, as long as the α/β ratio is known or closely estimated. I irradiated the cell lines with 6 Mev photons (direct field) with a linear accelerator, at a single dose of 9 Gy.

Determination of cell viability

At the end of the enzyme assays and at different times after irradiation and pharmacological treatment, cell viability was assessed by calcein staining and by Trypan blue exclusion test [26]. For the calcein staining, cells were washed with PBS, the plate was then put on ice and 200 µl of a calcein-AM solution (6.25 µg/ml in PBS) were added to each well. Cells were incubated for 15 minutes at 37°C, 5% CO_2. Calcein-AM was then removed and 100 µl of PBS and 50 µl of 1% Triton X-100 were added to each well. Plate was stirred at RT for 15 minutes and then the fluorescence was detected by a microplate reader (Victor, Perkin-Elmer).

The number of living and dead cells after treatment with different abiraterone concentrations, has been determined by counting cells after Trypan blue staining, as previously described [27].

Plasma Membrane (PM) associated glycohydrolase assays

We recently described a simple method that allows to measure the activity of several glycohydrolases associated with the PMs in living cells. This method is based on the observation that the fluorigenic substrates commonly used for the *in vitro* assay of glycohydrolase activities are not taken up by living cells [26]. In fact, under the appropriate experimental conditions, we did not observe any fluorescence associated with the cells. Moreover, the artificial substrates were not subjected to spontaneous, non-enzymatic hydrolysis nor hydrolyzed by secreted enzymes. Thus, their hydrolysis under these experimental conditions is due exclusively to the PM-associated enzymatic activities [20,26]. PM associated β-Galactosidase (β-Gal), conduritol B epoxide (CBE)-sensitive β-Glucosidase GBA1, β-Glucosidase GBA2, β-Hexosaminidase (β-Hex) and SMase activities were determined in control or differently treated living cells plated in 96-well microplate at different density (depending on the cell lines and on the treatment), by a high throughput assay (HTA). For GBA1 and GBA2 assays, cells were pre-incubated for 30 minutes at room temperature with 5 nM AMP-dNM (adamantane-pentyl-dNM; N-(5-adamantane-1-yl-methoxy-pentyl) deoxynojirimycin) [28] and 1 mM CBE (Sigma) in DMEM-F12, respectively. β-Gal, β-Hex and β-Glc activities were assayed using the artificial substrates MUB-Gal, MUG and MUB-Glc solubilized in DMEM-F12 without phenol red at pH 6 at the final concentrations of 250 µM, 2 mM and 6 mM respectively. SMase activity was assayed using the artificial substrates H-MUB-PC

solubilized in the same DMEM-F12 reported for the other enzymes at the final concentration of 100 µM. At different times (from 2 to 6 hours) aliquots of the medium were analyzed by fluorimetry in a microplate reader (MUB: λ_{ex}: 355 nm /λ_{em}: 460nm ; H-MUB: λ_{ex}:405 nm /λ_{em}:460nm) after adding 15 volumes of 0.25 M glycine (containing 0,3% Triton X-100 for SMase assay), pH 10.7. Standards free MUB and H-MUB were used to establish the calibration curves in order to quantify the substrates hydrolysis.

Enzymatic activities in total cell lysates

The enzymatic activities of β-Galactosidase, β-Glucosidase GBA1 and GBA2, β-Hexosaminidase and sialidase Neu3 in the total cell lysates were determined using fluorigenic substrates as previously described [26] with some modifications. Briefly, cells were washed twice with PBS, harvested, and resuspended in water in the presence of a protease inhibitor. Aliquots of cell homogenates were transferred to a 96-well microplate and were performed with three-fold in replicate. MUB substrates were solubilized in McIlvaine buffer at the same final concentrations and the same pH values used for the in vivo assay. The reaction mixtures were incubated at 37°C with gentle shaking. The developed fluorescence was detected at various times by a Victor microplate reader (Perkin Elmer) after transferring 10 µl of the reaction mixtures to a 96 well microplate and adding 190 µl of 0.25 M glycine, pH 10.7.

Cell treatments with tritiated lipids

Treatment of cell cultures with [1-^{3}H]sphingosine. [1-^{3}H]sphingosine was administered to pharmacologically treated, 9 Gy irradiated and control cells in order to metabolically label all SLs as previously described [29]. [1-^{3}H]sphingosine dissolved in methanol was transferred into a sterile glass tube, and dried under a nitrogen stream; the residue was then solubilized in an appropriate volume of pre-warmed (37°C) cell medium to obtain the desired final concentration ($3x10^{-9}$ M). After a 2 hours incubation (pulse), the medium was removed, cells were washed and incubated up to 72 hr (chase) with medium not containing the radioactive precursor. After chase, cells were collected and radioactive lipids were analyzed as described below.

Preparation of SL-enriched membrane domains by sucrose gradient centrifugation

After incubation (pulse) with [1-^{3}H]sphingosine and 72 hr (chase) with the different treatments, cells were collected in PBS (containing 0.4 mM Na_3VO_4). After centrifugation at 270xg for 10 minutes, cell pellet was lysed in the 1-1.5 ml lysis buffer (1% Triton X-100, 10 mM Tris-HCl pH 7.5, 150 mM NaCl, 5 mM EDTA, 1 mM Na_3VO_4, 1 mM PMSF and 10 µM/ml aprotinin) at 4°C for 20 minutes. After Dounce homogenization (11 strokes), each cell lysate was centrifuged at 1300xg for 5 minutes to remove nuclei and cellular debris, and the Post Nuclear Supernatant (PNS) was removed and transferred in a new tubes.

The PNS fraction was mixed with an equal volume of 85% of sucrose (w/v) in 10 mM Tris Buffer HCl pH 7.5, 150 mM NaCl, 5 mM EDTA and 1 mM Na_3VO_4, placed at the bottom of a discontinuous sucrose concentration gradient (30-5%) in the same buffer, and centrifuged 17 hr at 200,000xg at 4°C. After ultracentrifugation, eleven fraction were collected starting from the top of the tube. The light-scattering band, corresponding to the DRM fraction, was located at the interface between 5% and 30% sucrose and corresponding to fraction 5 or 6. The entire procedure was performed in ice immersion. After that, the fractions were dialyzed , lyophilized and subjected to lipid extraction and SL analysis.

Radioactive lipid analyses

Cells were lyophilized and subjected to lipid extraction and SL analyses. Total lipids from lyophilized cells were extracted with chloroform/methanol/water 20:10:1 by vol, followed by chloroform/methanol 2:1 by vol. The total lipid extracts were subjected to a two-phase partitioning by adding 20% water to the lipid extract; the total lipid extract, the aqueous and organic phases were analyzed by HPTLC. [^{3}H]SLs of total extracts and organic phases were separated using the solvent system chloroform-methanol-water 110:40:6 by vol, and those of aqueous phases with chloroform-methanol-0.2% aqueous $CaCl_2$, 50:42:11 by vol. For the specific determination of Cer content, radioactive lipids of the organic phases were separated using the solvent system hexane-chloroform-acetone-acetic acid 20:70:20:2 by vol. [^{3}H]SLs were identified by referring to the position of standards in the chromatogram and quantified by radioimaging after 48 hours of acquisition (β-Imager 2000, Biospace, Paris, France).

Statistics

All the experiments have been performed threefold in replicate and repeated three times. Data are presented as the mean values ± standard deviations and were tested for significance employing ONE or Two way ANOVA with Bonferroni post-test analysis, as specified in figure legends. The level of significance was set at $p<0.05$.

Other analytical methods

The radioactivity associated with lipid extracts was determined by liquid scintillation counting. The protein assays were carried out using the DC Protein Assay kit (Biorad).

Results

Effect of abiraterone on prostate cancer cell viability

As previously described, abiraterone is a new potential drug for prostate cancer treatment; this drug inhibits the androgen biosynthesis by potently blocking the cytochrome P450 c17, the key enzyme in testosterone synthesis. This drug is also able to down regulate AR expression, and to inhibit its nuclear translocation, resulting in a further block of androgen-receptor signalling pathway. In addition, recent lines of evidence suggest other molecular mechanism of action of abiraterone, even if their clarification needs to be investigated. For this reason, I first tested the efficacy of this drug on both the androgen-sensitive prostate cancer cell lines LNCaP, and the androgen-insensitive PC3 and DU145 cells.

In figure 6 is reported the effect of different concentrations of abiraterone (ranging from 0.1 to 50 µM) on LNCaP cells viability. As shown, the decreased number of living cells is followed by a strong increase in death cells in a time- and dose-dependent manner.

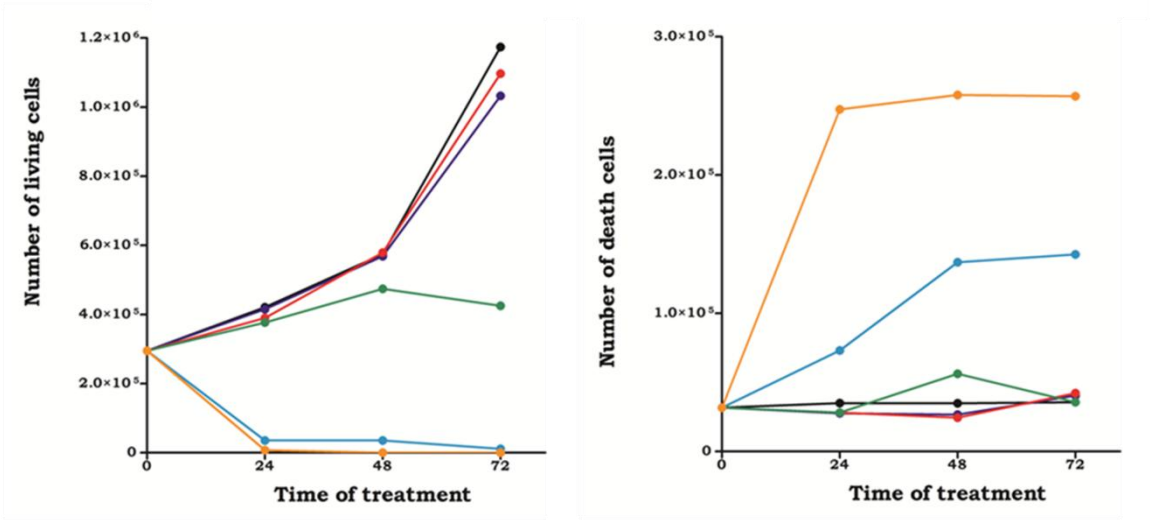

Figure 6. Effect of different concentrations of abiraterone on LNCaP cell viability. The number of living and death cells were evaluated by Trypan Blue exclusion test. The tested concentrations were: 0.1 µM ( ), 1 µM ( ), 10 µM ( ), 25 µM ( ) and 50 µM ( ) respect to control cells ( ). Each value is the mean of three independent experiments performed in triplicate.

These results indicate that abiraterone exerts an important cytotoxic effect also at low concentration showing a cytostatic effect at 10 µM.

In the same experimental conditions I evaluated the effect of abiraterone on the androgen-insensitive PC3 and DU145 cells. Surprisingly, as shown in Figure 7 and 8, I obtained very similar results also in these cell lines. As expected, the

androgen-insensitive cells are more resistant with respect to the androgen-sensitive LNCaP cells, showing a cytostatic effect at 25 µM.

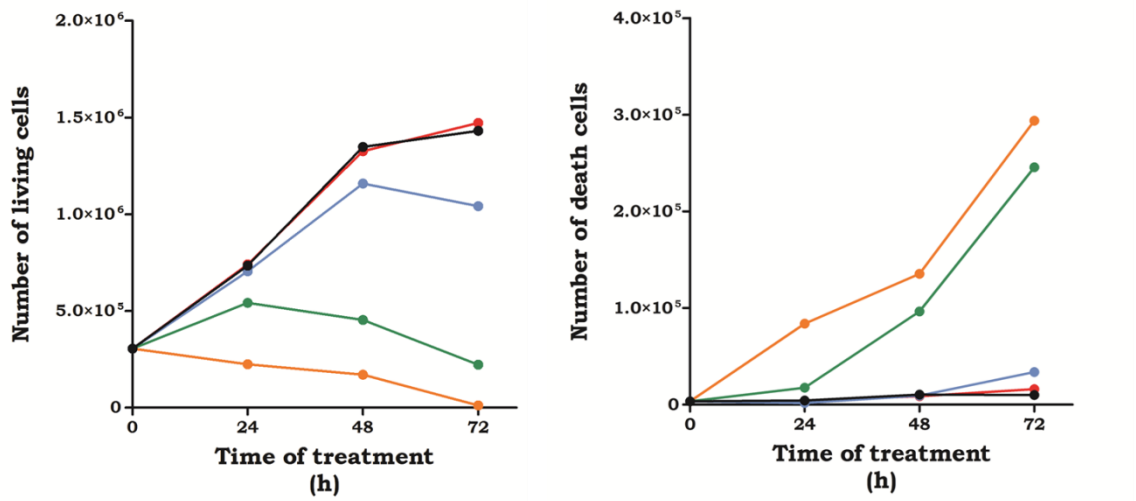

Figure 7. Effect of different concentrations of abiraterone on PC3 cell viability. The number of living and death cells were evaluated by Trypan Blue exclusion test. The tested concentrations were: 10 µM ( ), 25 µM ( ), 50 µM ( ) and 100 µM ( ) respect to control cells ( ). Each value is the mean of three independent experiments performed in triplicate.

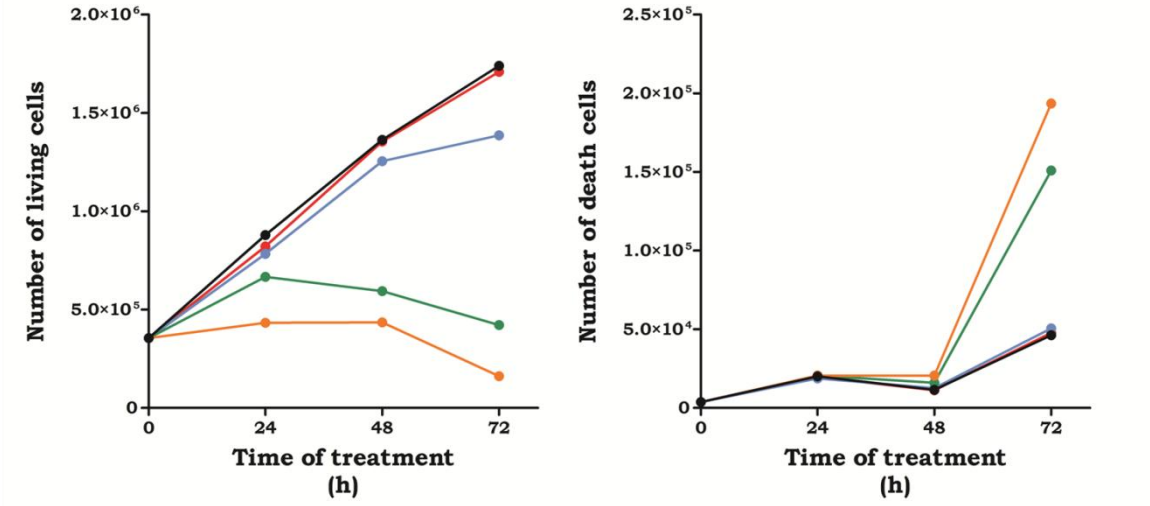

Figure 8. Effect of different concentration of abiraterone on DU145 cell viability. The number of the living and death cells were evaluated with Trypan Blue exclusion test. The testing concentrations were: 10 µM ( ), 25 µM ( ), 50 µM ( ) and 100 µM ( ) respect to the control cells ( ). Each value is the mean of three independent experiments performed in triplicate.

These results indicate that abiraterone treatment causes cell growth arrest and death independently by the androgen pathway.

Effect of abiraterone and ionizing radiation treatments on prostate cancer cell viability

Prostate cancer cell lines LNCaP, PC3 and DU145 are characterized by high level of radio-resistance; for this reason I wondered if abiraterone could sensitize these cells to ionizing radiation. To this purpose, after 24 hours of pre-treatment with abiraterone, cells were irradiated with 9 Gy and cell viability was evaluated at different time points.

In Figure 9 is shown the effect of the single treatment with 10 µM abiraterone, and that one of ionizing radiation (9Gy) or the effect of the combined treatment on LNCaP cell viability. These results indicate that the single treatment produces a cytostatic effect in LNCaP cells, while the combined treatment causes a strong increase in the number of death cells compared to each single treatment.

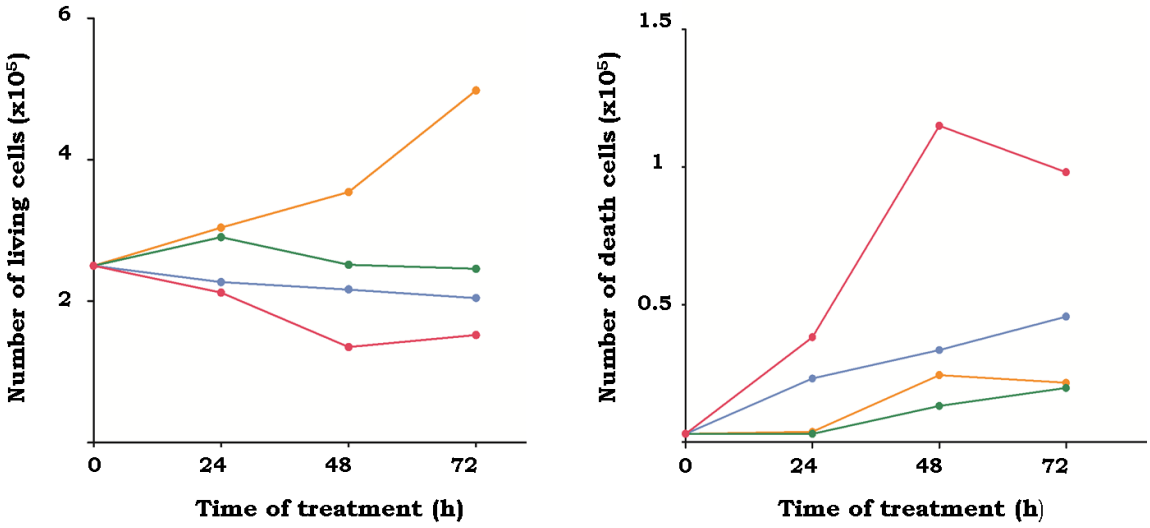

Figure 9. Effect of single treatment with abiraterone or ionizing radiation and of their combined treatment on LNCaP cell viability. The treatment with abiraterone always started 24 hours before the irradiation and all the results are expressed as hours after the cell irradiation. The number of living and death cells were evaluated by Trypan Blue exclusion test. Each value is the mean of three independent experiments performed in triplicate.

( ) Ctrl cells; ( ) 10µM abiraterone; ( ) 9Gy Ray and ( ) 10µM abiraterone + 9Gy Ray.

I then evaluated the effect of the same treatments on both PC3 and DU145 cells: as shown in Figure 10, I obtained very similar results, especially after the combined treatment with 25 µM abiraterone and 9 Gy ionizing radiation.

Indeed, in both experiments, after 72 hours of combined treatment, almost 90% reduction in cell proliferation is observed.

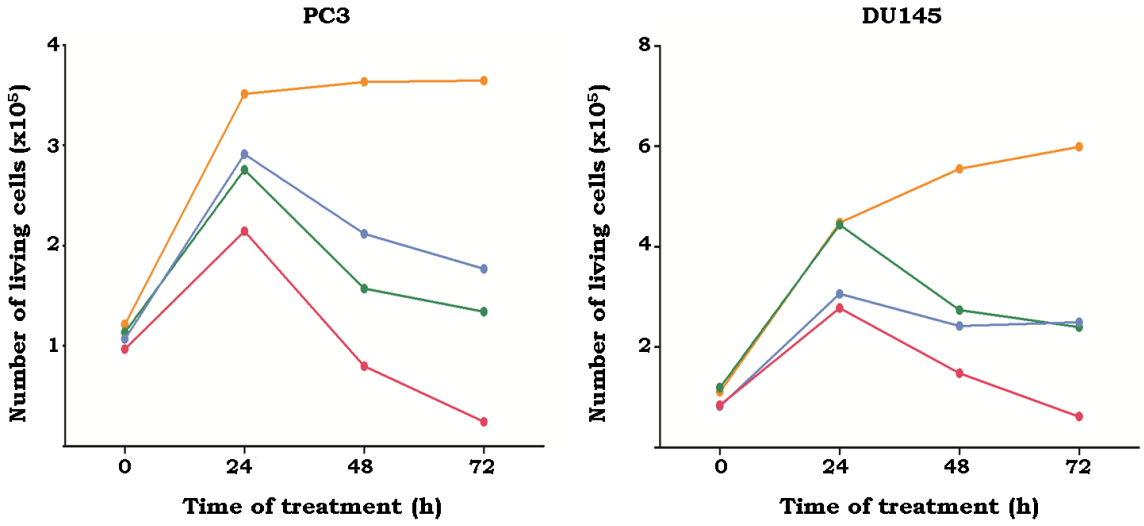

Figure 10. Effect of single treatment with abiraterone or ionizing radiation and of their combined treatment on the viability of androgen-insensitive cell lines. The treatment with abiraterone always started 24 hours before the irradiation and all the results are expressed as hours after the cell irradiation. The number of living cells was evaluated by Calcein staining. Each value is the mean of three independent experiments performed in triplicate.

( ) Ctrl cells; ( ) 25μM abiraterone; ( ) 9Gy Ray and ( ) 25μM abiraterone + 9Gy Ray.

These results indicate that abiraterone sensitizes prostate cancer cells to ionizing radiation independently from the androgen pathway. To investigate the possible molecular mechanism I focused the study on the possible involvement of the ectopic ceramide production triggered directly at the cell plasma membrane level. In fact, Aureli et al recently reported the first detailed information on the activation of several cell surface glycohydrolases in healthy and pathological cells subjected to ionizing radiation: this event is followed by the production of PM ceramide and the onset of apoptotic cell death [41]. On the basis of these findings I evaluated the activity of different glycohydrolases, both lysosomal and plasma-membrane associated, at different time-points after each single or combined treatment.

To this regard, all prostate cancer cell lines were treated with abiraterone alone or ionizing radiation and with the combined treatment; then, at different time-points cells were subjected to the evaluation of the cell surface associated glycohydrolases activity, in particular GBA1, GBA2, β-Galactosidase and β-Hexosaminidase. Interestingly, as reported in Tables 1-12 the different

treatments cause a time dependent increase of the activity of these enzymes in comparison to untreated cells. In particular, in androgen-sensitive LNCaP cells treated with abiraterone alone or in combination with ionizing radiation, the activity of the PM-associated GBA1 increases after 48 hr reaching the highest value after 72 hr. The effects of yhe single treatment with ionizing radiation is different: indeed, in Figure 11, is shown a peak and through trend.

Similar results were obtained by the analysis of GBA2, β-Galactosidase and β-Hexosaminidase activities. In particular, all cell treatments resulted in increased activity of GBA2, is i (from 2 to 2.8 fold compared tocontrol cells) (Figure 12). Conversely, the activity of β-Galactosidase and β-Hexosaminidase shows the highest peak only when cells are subjected to the combined treatment with abiraterone and ionizing radiation (Figure 14). I also evaluated the SMase activity but no difference between treated and control cells are observed (not shown data), thus suggesting that Cer does not derive from sphingomyeline breakdown, as previously described by Kolesnick et al. [18]. Collectively , these results indicate that in LNCaP cells all cell treatments cause an effect on the activity of plasma-membrane associated glycohydrolases.

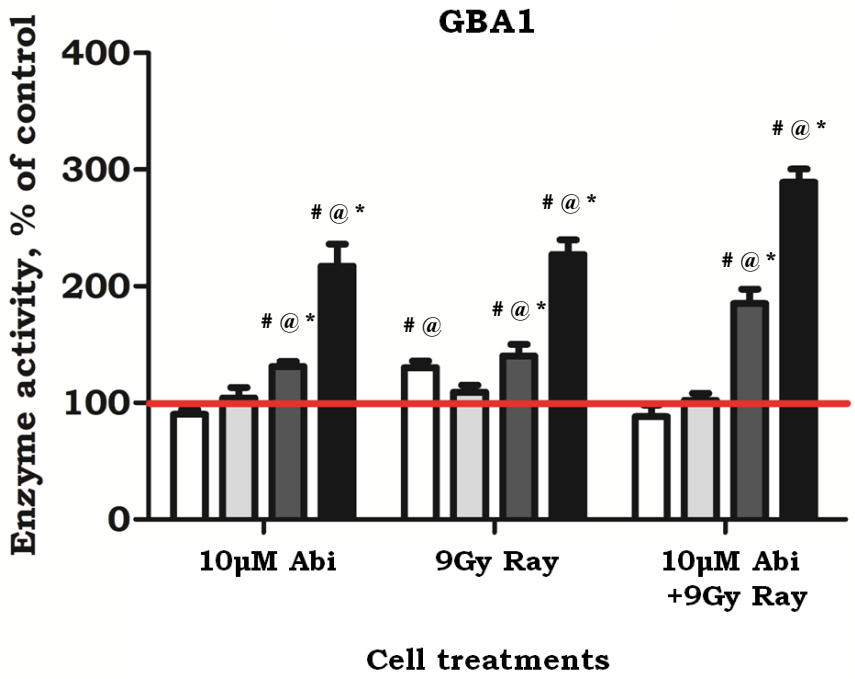

Figure 11. Cell surface associated β-Glucosidase GBA1 activity in androgen-sensitive LNCaP cells treated with 10 µM abiraterone, 9 Gy ionizing radiation and the combined treatment. The activity was determined in living cells treated or not for 2 (▭), 24 (▭), 48 (▬) and 72 (■) hours from irradiation. The data are the average of three experiments performed in triplicate for each cell treatment, expressed as percentage relative to the value of control cells (red line). Two Way ANOVA followed by Bonferroni post-tests #p<0.05 versus control cells, @ p<0.05 vs different treatments, *p<0.05 vs different times for the same treatment.

Plasma membrane associated GBA1 (pmoles/10⁶ cells/hr)				
Type of treatment	Time after cell irradiation			
	2hr	24hr	48hr	72hr
Ctrl	3463 ± 193	3109 ± 127	4504 ± 263	3054 ± 314
10 µM Abi	2662 ± 163	2813 ± 363	2268 ± 235	2126 ± 134
9 Gy Ray	2055 ± 115	2695 ± 92	2500 ± 315	2443 ± 322
10 µM Abi + 9 Gy Ray	2726 ± 157	5470 ± 481	5958 ± 336	9715 ± 388

Table 1. GBA1 activity determined in LNCaP cells treated with 10 µM abiraterone, 9 Gy ionizing radiation and the combined treatment. The activity was determined in living LNCaP cells treated or not (Ctrl) for 2, 24, 48 and 72 hours from irradiation. Each value is the mean of three independent experiments performed in three-fold replicate ± SD. The data are expressed as picomoles per million cells per hours.

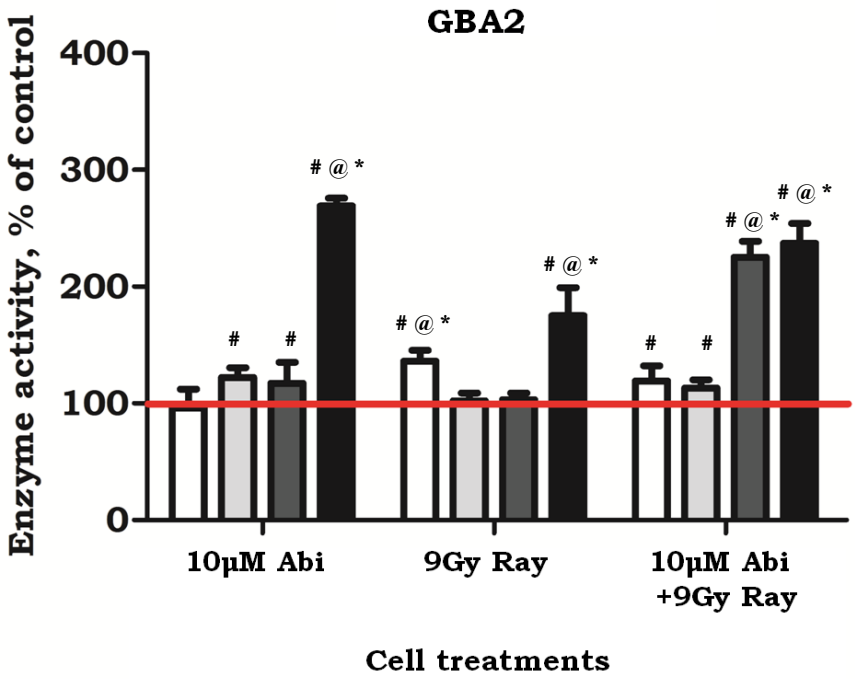

Figure 12. Cell surface associated β-Glucosidase GBA2 activity in androgen-sensitive LNCaP cells treated with 10 µM abiraterone, 9 Gy ionizing radiation and the combined treatment. The activity was determined in living cells treated or not for 2 (▭), 24 (▭), 48 (▬) and 72 (■) hours from irradiation. The data are the average of three experiments performed in triplicate for each cell treatment, expressed as percentage relative to the value of control cells (red line). Two Way ANOVA followed by Bonferroni post-tests #p<0.05 versus control cells, @ p<0.05 vs different treatments, *p<0.05 vs different times for the same treatment.

Plasma membrane associated GBA2 (pmoles/10^6 cells/hr)				
Type of treatment	Time after cell irradiation			
	2hr	24hr	48hr	72hr
Ctrl	1184 ± 146	1131 ± 183	1613 ± 151	1403 ± 183
10 µM Abi	793 ± 51	1092 ± 140	702 ± 49	697 ± 62
9 Gy Ray	434 ± 75	378 ± 71	497 ± 28	832 ± 157
10 µM Abi + 9 Gy Ray	804 ± 76	2688 ± 67	1139 ± 158	2091 ± 153

Table 2. GBA2 activity determined in LNCaP cells treated with 10 µM abiraterone, 9 Gy ionizing radiation and the combined treatment. The activity was determined in living LNCaP cells treated or not (Ctrl) for 2, 24, 48 and 72 hours from irradiation. Each value is the mean of three independent experiments performed in three-fold replicate ± SD. The data are expressed as picomoles per million of cell per hours.

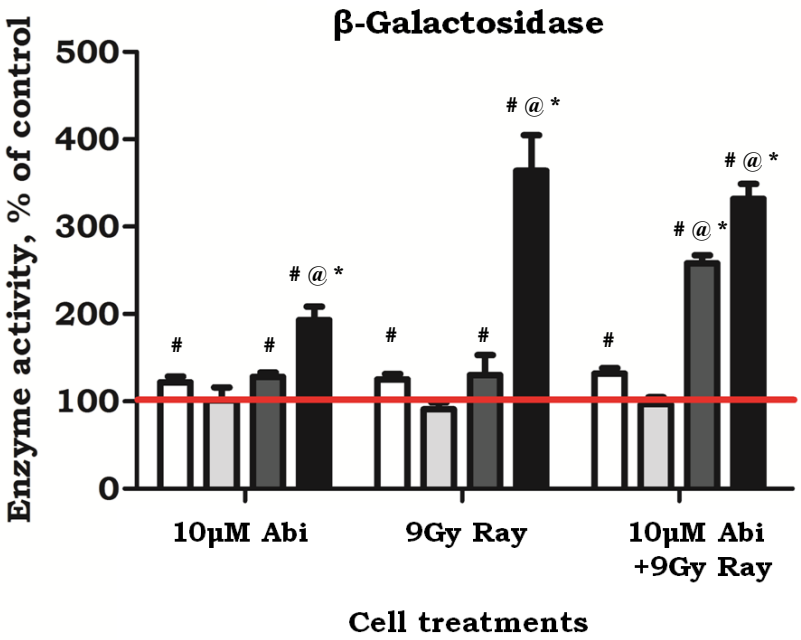

Figure 13. Cell surface associated β-Galactosidase activity in androgen-sensitive LNCaP cells treated with 10 μM abiraterone, 9 Gy ionizing radiation and the combined treatment. The activity was determined in living cells treated or not for 2 (▭), 24 (▭), 48 (▭) and 72 (■) hours from irradiation. The data are the average of three experiments performed in triplicate for each cell treatment, expressed as percentage relative to the value ofcontrol cells (red line). Two Way ANOVA followed by Bonferroni post-tests #p<0.05 versus control cells, @ p<0.05 vs different treatments, *p<0.05 vs different times for the same treatment.

Plasma membrane associated β-Galactosidase (pmoles/10^6 cells/hr)				
Type of treatment	Time after cell irradiation			
	2hr	24hr	48hr	72hr
Ctrl	620 ± 101	755 ± 49	820 ± 167.5	425 ± 63.6
10 μM Abi	375 ± 37	368 ± 33	357 ± 52.9	304 ± 23.3
9 Gy Ray	345 ± 23	513 ± 58	539 ± 41.2	990 ± 330.0
10 μM Abi + 9 Gy Ray	447 ± 8	813 ± 65	2892 ± 324	2411 ± 124

Table 3. β-Galactosidase activity determined in LNCaP cells treated with 10 μM abiraterone, 9 Gy ionizing radiation and the combined treatment. The activity was determined in living LNCaP cells treated or not for 2, 24, 48 and 72 hours from irradiation. Each value is the mean of three independent experiments performed three-fold in replicate ± SD. The data are expressed as picomoles per million cells per hours.

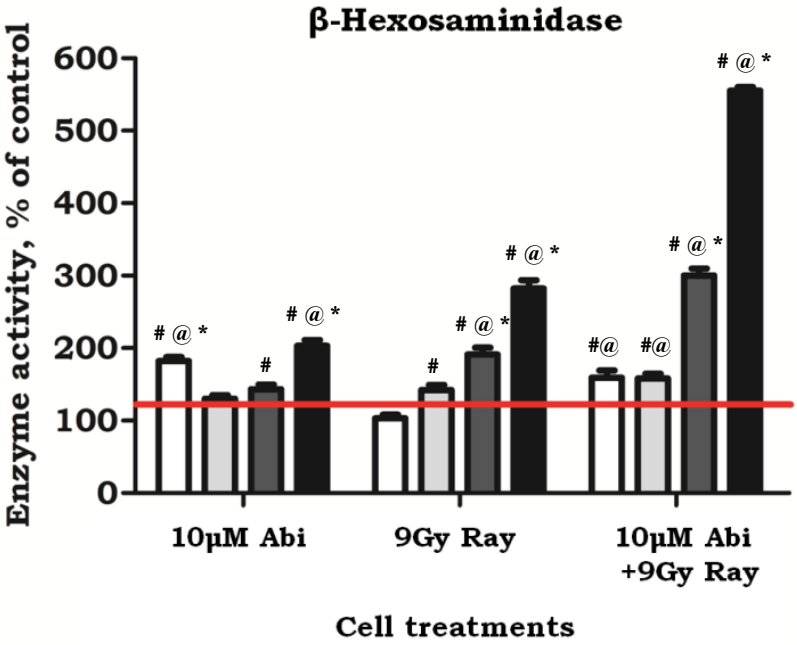

Figure 14. Cell surface associated β-Hexosaminidase activity in androgen-sensitive LNCaP cells treated with 10 μM abiraterone, 9 Gy ionizing radiation and the combined treatment. The activity was determined in living cells treated or not for 2 (▭), 24 (▭), 48 (▬) and 72 (■) hours from e irradiation. The data are the average of three experiments performed in triplicate for each cell treatment, expressed as percentage relative to the value of control cells (red line). Two Way ANOVA followed by Bonferroni post-tests #$p<0.05$ versus control cells, @ $p<0.05$ vs different treatments, *$p<0.05$ vs different times for the same treatment.

Plasma membrane associated β-Hexosaminidase (pmoles/10^6 cells/hr)				
Type of treatment	Time after cell irradiation			
	2hr	24hr	48hr	72hr
Ctrl	10340 ± 902	18816 ± 1114	10676 ± 574	16482 ± 1698
10 μM Abi	13442 ± 593	18588 ± 1078	18130 ± 1346	24179 ± 652
9 Gy Ray	7781 ± 771	14317 ± 1325	14441 ± 1306	25673 ± 3732
10 μM Abi + 9 Gy Ray	10521 ± 385	26407 ± 1051	50810 ± 2097	196616 ± 1882

Table 4. β-Hexosaminidase activity determined in LNCaP cells treated with 10 μM abiraterone, 9 Gy ionizing radiation and the combined treatment. The activity was determined in living LNCaP cells treated or not (Ctrl) for 2, 24, 48 and 72 hours from irradiation. Each value is the mean of three independent experiments performed in three-fold replicate ± SD. The data are expressed as picomoles per million cells per hours.

Different results were obtained in androgen-insensitive PC3 cells. In fact, in these cells the single treatment with 25 μM abiraterone does nott induce any variation in the PM-associated activity of GBA1, GBA2, β-Galactosidase and β-Hexosaminidase. Conversely, as shown in Figure 15, in PC3 cells the single treatment with ionizing radiation induces an higher increase in the activity of the PM-associated GBA1 after 2 hr followed by a reduction at 24 hr and increase again at 72 hr. In addition, the combined treatment induces an increase in the GBA1 activity starting at 48 hr and reaching the highest value after 72 hours.

The same trend is also found for the activity of GBA2 (Figure 16), β-Galactosidase (Figure 17) and β-Hexosaminidase (Figure 18), where the single treatment with ionizing radiation determines an higher increase after 2 hr and the combined treatment causes the highest increase after 72 hours from the irradiation. All these data suggest that in androgen-insensitive PC3 cells, ionizing radiation treatment cause firstly a change on plasma-membrane glycohydrolases activities which is notably more evident when the cells are subjected to the combined treatment.

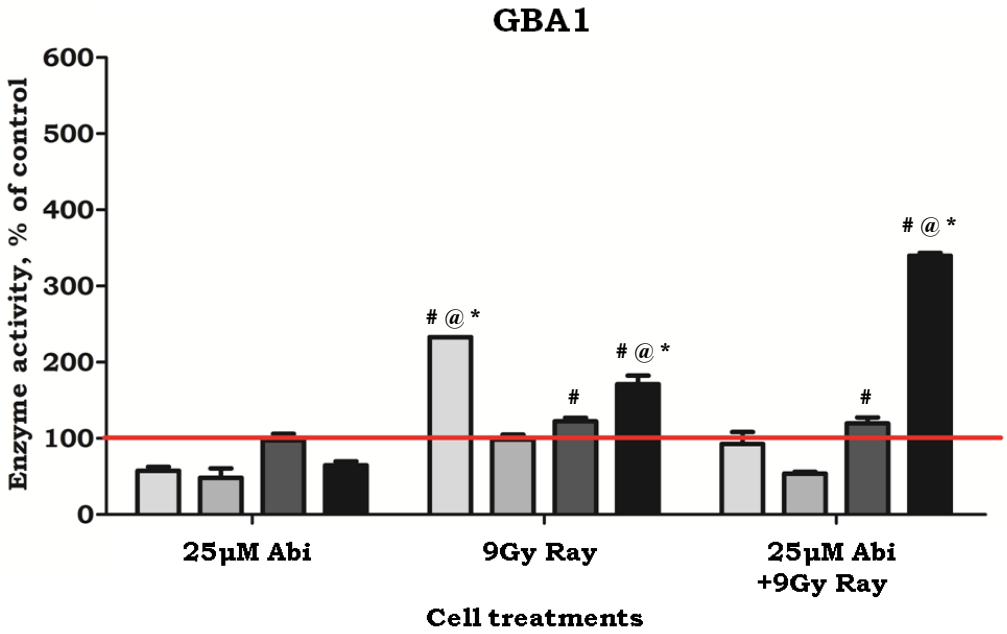

Figure 15. Cell surface associated β-Glucosidase GBA1 activity in androgen-insensitive PC3 cells treated with 25 µM abiraterone, 9 Gy ionizing radiation and the combined treatment. The activity was determined in living cells treated or not for 2 ( ), 24 ( ), 48 ( ) and 72 ( ) hours from irradiation. The data are the average of three experiments performed in triplicate for each cell treatment, expressed as percentage relative to the valueof control cells (red line). Two Way ANOVA followed by Bonferroni post-tests #p<0.05 versus control cells, @ p<0.05 vs different treatments, *p<0.05 vs different times for the same treatment.

Plasma membrane associated GBA1 (pmoles/10^6 cells/hr)				
Type of treatment	Time after cell irradiation			
	2hr	24hr	48hr	72hr
Ctrl	390 ± 58.4	224 ± 11.7	910 ± 0.4	361 ± 5.7
25 µM Abi	381 ± 17.7	184 ± 22.4	375 ± 24.4	205 ± 4.8
9 Gy Ray	612 ± 46.7	627 ± 52.4	748 ± 37.3	732 ± 58.1
25 µM Abi + 9 Gy Ray	834 ± 31.6	539 ± 28.4	1428 ± 158.5	2832 ± 113.1

Table 5. GBA1 activity determined in PC3 cells treated with 25 µM abiraterone, 9 Gy ionizing radiation and the combined treatment. The activity was determined in living PC3 cells treated or not (Ctrl) for 2, 24, 48 and 72 hours from irradiation. Each value is the mean of three independent experiments performed in three-fold replicate ± SD. The data are expressed as picomoles per million cells per hours.

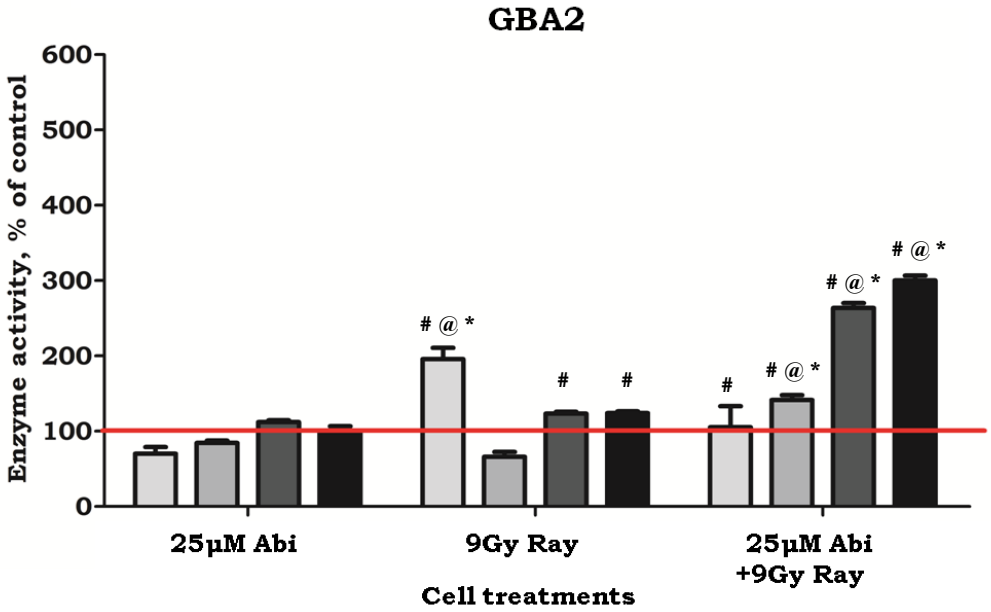

Figure 16. Cell surface associated β-Glucosidase GBA2 activity in androgen-insensitive PC3 cells treated with 25 µM abiraterone, 9 Gy ionizing radiation and the combined treatment. The activity was determined in living PC3 cells treated or not for 2 ( ), 24 ( ), 48 ( ) and 72 ( ) hours from irradiation. The data are the average of three experiments performed in triplicate for each cell treatment, expressed as percentage relative to the value of control cells (red line). Two Way ANOVA followed by Bonferroni post-tests #p<0.05 versus control cells, @ p<0.05 vs different treatments, *p<0.05 vs different times for the same treatment.

Plasma membrane associated GBA2 (pmoles/10^6 cells/hr)				
Type of treatment	Time after cell irradiation			
	2hr	24hr	48hr	72hr
Ctrl	118 ± 8.4	83 ± 7.2	231 ± 35.1	112 ± 31.1
25 µM Abi	206 ± 10.7	174 ± 5.5	136 ± 8.7	291 ± 19.6
9 Gy Ray	282 ± 31.3	316 ± 7.6	348 ± 7.7	744 ± 48.1
25 µM Abi + 9 Gy Ray	685 ± 33.1	675 ± 55.9	849 ± 20.2	2057 ± 127.3

Table 6. GBA2 activity determined in PC3 cells treated with 25 µM abiraterone, 9 Gy ionizing radiation and the combined treatment. The activity was determined in living PC3 cells treated or not (Ctrl) for 2, 24, 48 and 72 hours from irradiation. Each value is the mean of three independent experiments performed in three-fold replicate ± SD. The data are expressed as picomoles per million cells per hours.

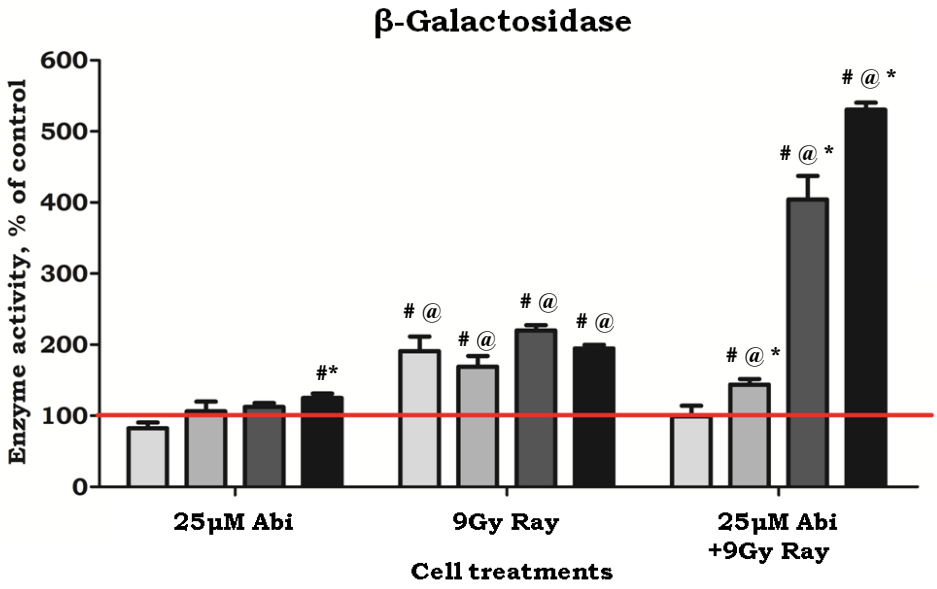

Figure 17. Cell surface associated β-Galactosidase activity in androgen-insensitive PC3 cells treated with 25 μM abiraterone, 9 Gy ionizing radiation and the combined treatment. The activity was determined in PC3 living cells treated or not for 2 ( ), 24 ( ), 48 ( ) and 72 ( ) hours from irradiation. The data are the average of three experiments performed in triplicate for each cell treatment, expressed as percentage relative to the value of control cells (red line). Two Way ANOVA followed by Bonferroni post-tests #$p<0.05$ versus control cells, @ $p<0.05$ vs different treatments, *$p<0.05$ vs different times for the same treatment.

Plasma membrane associated β-Galactosidase (pmoles/10^6 cells/hr)				
Type of treatment	Time after cell irradiation			
	2hr	24hr	48hr	72hr
Ctrl	429 ± 70.9	353 ± 29.4	820 ± 167.5	425 ± 63.6
25 μM Abi	211 ± 36.2	224 ± 31.1	357 ± 52.9	304 ± 23.3
9 Gy Ray	245 ± 20.0	275 ± 15.1	539 ± 41.2	990 ± 330.0
25 μM Abi + 9 Gy Ray	591 ± 41.1	739 ± 44.8	1151 ± 58.3	3135 ± 310.0

Table 7. β-Galactosidase activity determined in PC3 cells treated with 25 μM abiraterone, 9 Gy ionizing radiation and the combined treatment. The activity was determined in living PC3 cells treated or not (Ctrl) for 2, 24, 48 and 72 hours from irradiation. Each value is the mean of three independent experiments performed in three-fold replicate ± SD. The data are expressed as picomoles per million cells per hours.

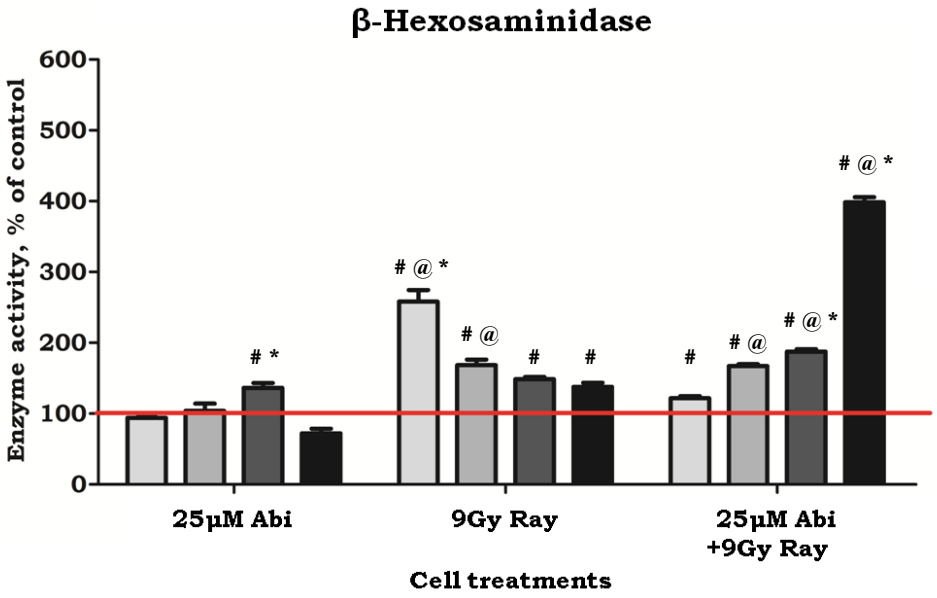

Figure 18. Cell surface associated β-Hexosaminidase activity in androgen-insensitive PC3 cells treated with 25 µM abiraterone, 9 Gy ionizing radiation and the combined treatment. The activity was determined in PC3 living cells treated or not for 2 ( ), 24 ( ), 48 ( ) and 72 ( ) hours from irradiation. The data are averages of three experiments performed in triplicate for each cell treatment, expressed as percentage relative to the value of control cells (red line). Two Way ANOVA followed by Bonferroni post-tests #p<0.05 versus control cells, @ p<0.05 vs different treatments, *p<0.05 vs different times for the same treatment.

Plasma membrane associated β-Hexosaminidase (pmoles/10^6 cells/hr)				
Type of treatment	Time after cell irradiation			
	2hr	24hr	48hr	72hr
Ctrl	23963 ± 1124	22553 ± 1320	61908 ± 10076	29148 ± 921
25 µM Abi	13037 ± 2013	13560 ± 1398	21983 ± 1695	21781 ± 593
9 Gy Ray	18669 ± 869	25430 ± 1780	27758 ± 806	35001 ± 1244
25 µM Abi + 9 Gy Ray	29961 ± 1493	21644 ± 1363	41265 ± 2429	119413 ± 8403

Table 8. β-Hexosaminidase activity determined in PC3 cells treated with 25 µM abiraterone, 9 Gy ionizing radiation and the combined treatment. The activity was determined in living PC3 cells treated or not (Ctrl)for 2, 24, 48 and 72 hours from irradiation. Each value is the mean of three independent experiments performed in three-fold replicate ± SD. The data are expressed as picomoles per million cells per hours.

The same experiments were performed in androgen-insensitive DU145 cells. As shown in Figure 19, the activity of PM-associated GBA1 increases 2.5 times after 2 hours from cell irradiation. Also in this case, the major effect is exerted by the combined treatment that induces 2 and 4 fold increase in the GBA1 activity after 48 and 72 hours respectively. Differently, the activity of the PM-associated GBA2 (Figure 20), increases 3 fold after 48 and 72 hours from the single treatment with abiraterone, while no changes are observed after irradiation. Finally, after 48 and 72 hours from the combined treatment, GBA2 activity increases respectively 6 and 7 fold respect to control cells.

As shown in Figure 21, the activity of β-Galactosidase increases after 48 and 72 hours after all the different cell treatments reaching the highest activity after the combined treatment. Similar results were obtained also for β-Hexosaminidase activity as shown in Figure 22.

All these results indicate that in androgen-insensitive DU145 cells, all the treatment cause an increase in plasma-membrane associated glycohydrolases activities; in particular, the combined treatment with abiraterone and ionizing radiation is most effective.

In summary all the cell lines tested show that the combined treatment induces a major cytotoxic effect which is accompanied by the highest increase in the PM-associated hydrolases activity.

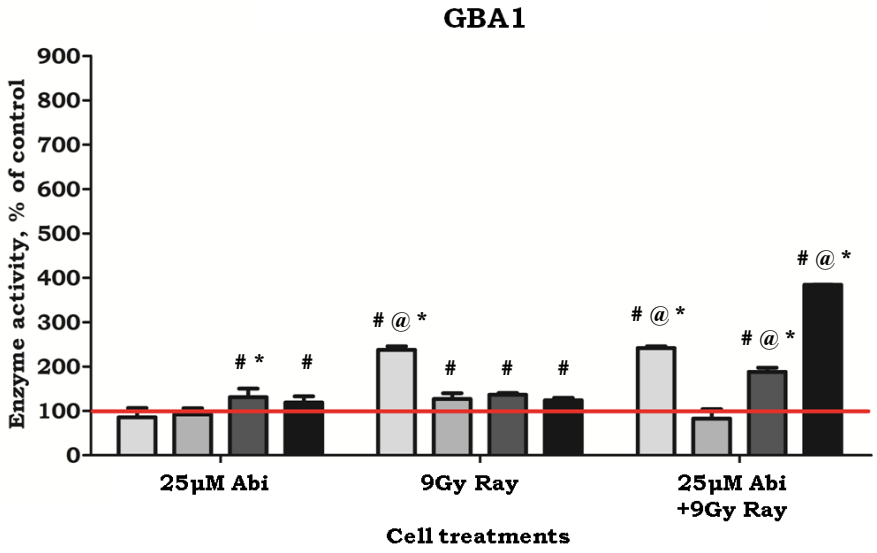

Figure 19. Cell surface associated β-Glucosidase GBA1 activity in androgen-insensitive DU145 cells treated with 25 µM abiraterone, 9 Gy ionizing radiation and the combined treatment. The activity was determined in living cells treated or not for 2 ( ), 24 ( ), 48 ( ) and 72 ( ) hours from irradiation. The data are the average of three experiments performed in triplicate for each cell treatment, expressed as percentage relative to the value of control cells (red line). Two Way ANOVA followed by Bonferroni post-tests #p<0.05 versus control cells, @ p<0.05 vs different treatments, *p<0.05 vs different times for the same treatment.

Plasma membrane associated GBA1 (pmoles/10^6 cells/hr)				
Type of treatment	Time after cell irradiation			
	2hr	24hr	48hr	72hr
Ctrl	227 ± 26.2	194 ± 40.3	540 ± 40.8	548 ± 22.0
25 µM Abi	138 ± 9.8	127 ± 18.1	175 ± 22.6	114 ± 24.5
9 Gy Ray	189 ± 21.3	247 ± 48.5	258 ± 9.7	355 ± 34.3
25 µM Abi + 9 Gy Ray	287 ± 13.8	342 ± 47.2	356 ± 18.7	1102 ± 5.7

Table 9. GBA1 activity determined in DU145 cells treated with 25 µM abiraterone, 9 Gy ionizing radiation and the combined treatment. The activity was determined in living DU145 cells treated or not (Ctrl) for 2, 24, 48 and 72 hours from irradiation. Each value is the mean of three independent experiments performed in three-fold replicate ± SD. The data are expressed as picomoles per million cells per hours.

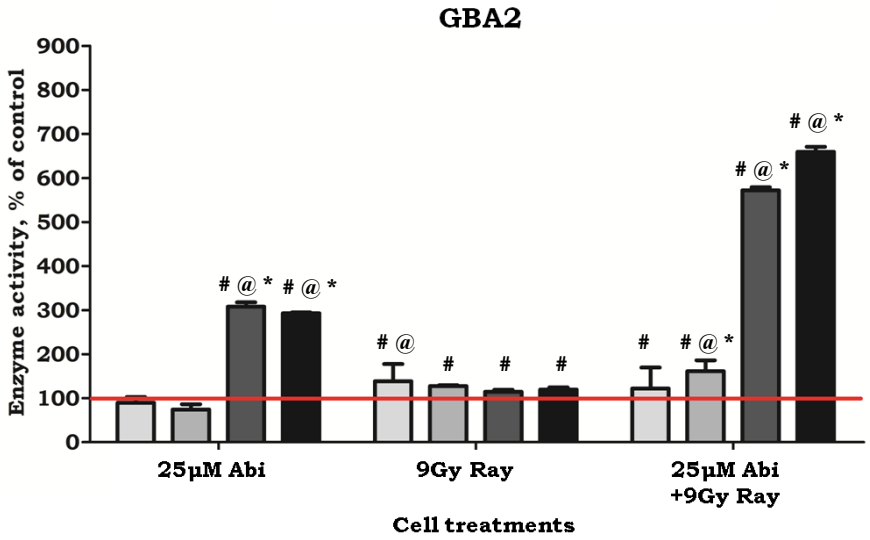

Figure 20. Cell surface associated β-Glucosidase GBA2 activity in androgen-insensitive DU145 cells treated with 25 µM abiraterone, 9 Gy ionizing radiation and the combined treatment. The activity was determined in living cells treated or not for 2 ( ), 24 ( ), 48 ( ) and 72 ( ) hours from irradiation. The data are the average of three experiments performed in triplicate for each cell treatment, expressed as percentage relative to the value of control cells (red line). Two Way ANOVA followed by Bonferroni post-tests #$p<0.05$ versus control cells, @ $p<0.05$ vs different treatments, *$p<0.05$ vs different times for the same treatment.

Plasma membrane associated GBA2 (pmoles/10^6 cells/hr)				
Type of treatment	Time after cell irradiation			
	2hr	24hr	48hr	72hr
Ctrl	105 ± 25.6	94 ± 12.2	145 ± 57.8	128 ± 58.6
25 µM Abi	70 ± 9.4	52 ± 6.2	89 ± 2.1	113 ± 28.0
9 Gy Ray	79 ± 5	243 ± 23.8	88 ± 4.2	452 ± 30.8
25 µM Abi + 9 Gy Ray	168 ± 27.3	492 ± 9.0	201 ± 9.2	1108 ± 123.3

Table 10. GBA2 activity determined in DU145 cells treated with 25 µM abiraterone, 9 Gy ionizing radiation and the combined treatment. The activity was determined in living DU145 cells treated or not (Ctrl) for 2, 24, 48 and 72 hours from irradiation. Each value is the mean of three independent experiments performed in three-fold replicate ± SD. The data are expressed as picomoles per million cells per hours.

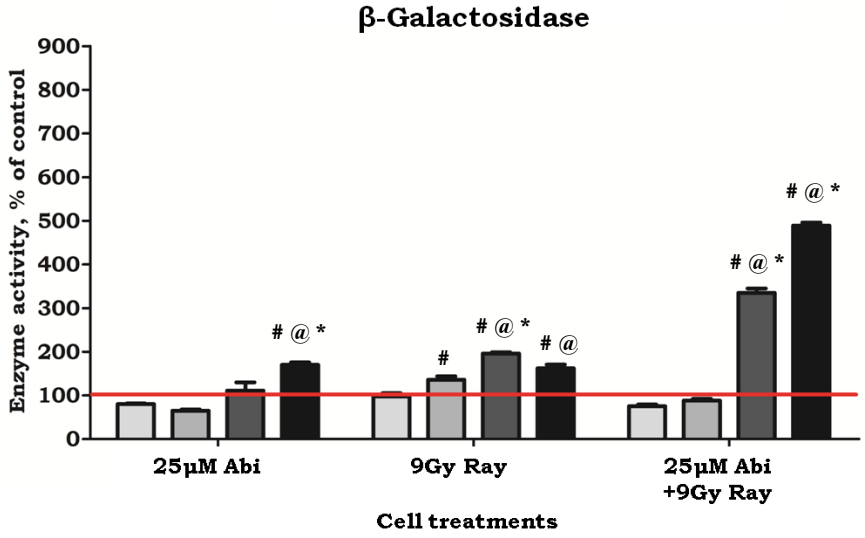

Figure 21. Cell surface associated β-Galactosidase activity in androgen-insensitive DU145 cells treated with 25 μM abiraterone, 9 Gy ionizing radiation and the combined treatment. The activity was determined in living cells treated or not for 2 ( ), 24 ( ), 48 ( ) and 72 ( ) hours from the irradiation. The data are the average of three experiments performed in triplicate for each cell treatment, expressed as percentage relative to the value of control cells (red line). Two Way ANOVA followed by Bonferroni post-tests #p<0.05 versus control cells, @ p<0.05 vs different treatments, *p<0.05 vs different times for the same treatment.

Plasma membrane associated β-Galactosidase (pmoles/10^6 cells/hr)				
Type of treatment	Time after cell irradiation			
	2hr	24hr	48hr	72hr
Ctrl	471 ± 27.9	378 ± 5.9	459 ± 34.3	353 ± 15.6
25 μM Abi	209 ± 11.5	135 ± 4.3	284 ± 22.7	184 ± 7.8
9 Gy Ray	219 ± 20.4	243 ± 45.8	429 ± 12.9	734 ± 72.4
25 μM Abi + 9 Gy Ray	329 ± 20.1	559 ± 32.1	534 ± 44.5	1604 ± 111.7

Table 11. β-Galactosidase activity determined in DU145 cells treated with 25 μM abiraterone, 9 Gy ionizing radiation and the combined treatment. The activity was determined in living DU145 cells treated or not (Ctrl) for 2, 24, 48 and 72 hours from irradiation. Each value is the mean of three independent experiments performed in three-fold replicate ± SD. The data are expressed as picomoles per million cells per hours.

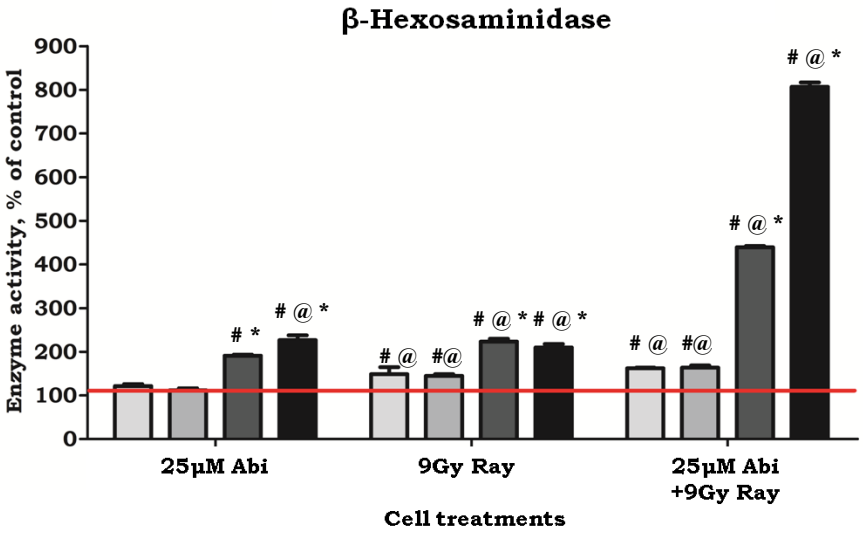

Figure 22. Cell surface associated β-Hexosaminidase activity in androgen-insensitive DU145 cells treated with 25 µM abiraterone, 9 Gy ionizing radiation and the combined treatment. The activity was determined in living cells treated or not for 2 ( ), 24 ( ), 48 ( ) and 72 ( ) hours from irradiation. The data are the average of three experiments performed in triplicate for each cell treatment, expressed as percentage relative to the value of control cells (red line). Two Way ANOVA followed by Bonferroni post-tests #p<0.05 versus control cells, @ p<0.05 vs different treatments, *p<0.05 vs different times for the same treatment.

Plasma membrane associated β-Hexosaminidase (pmoles/10^6 cells/hr)				
Type of treatment	Time after cell irradiation			
	2hr	24hr	48hr	72hr
Ctrl	20721 ± 1842	25197 ± 1046	30814 ± 4881	33617 ± 557
25 µM Abi	8907 ± 76	9992 ± 405	12892 ± 524	14580 ± 725
9 Gy Ray	8234 ± 405	15731 ± 426	18413 ± 1109	36212 ± 980
25 µM Abi + 9 Gy Ray	8303 ± 191	18842 ± 2014	17420 ± 1362	66995 ± 6750

Table 12. β-Hexosaminidase activity determined in DU145 cells treated with 25 µM abiraterone, 9 Gy ionizing radiation and the combined treatment. The activity was determined in living DU145 cells treated or not (Ctrl) for 2, 24, 48 and 72 hours from irradiation. Each value is the mean of three independent experiments performed in three-fold replicate ± SD. The data are expressed as picomoles per million cells per hours.

Effect of abiraterone and ionizing radiation treatments on glycohydrolase activities associated with the total cell lysate in androgen sensitive and insensitive-prostate cancer cell lines

Most of Glycohydrolases, whose activity is can be measured at the plasma membrane level, are mainly intracellular enzymes. For this reason, the activity of GBA1, non-lysosomal β-Glucosidase GBA2, β-Galactosidase and β-Hexosaminidase were also measured in the total cell lysate of the different PC cell lines subjected to single treatment with abiraterone or ionizing radiation and both.

In LNCaP cells the treatment with abiraterone induces a mild increase only of GBA2 and β-Galactosidase activity (figures 24-25). Instead, the combined treatment induces an increase on the activity of GBA1, β-Galactosidase and β-Hexosaminidase (Figures 23-25-26).

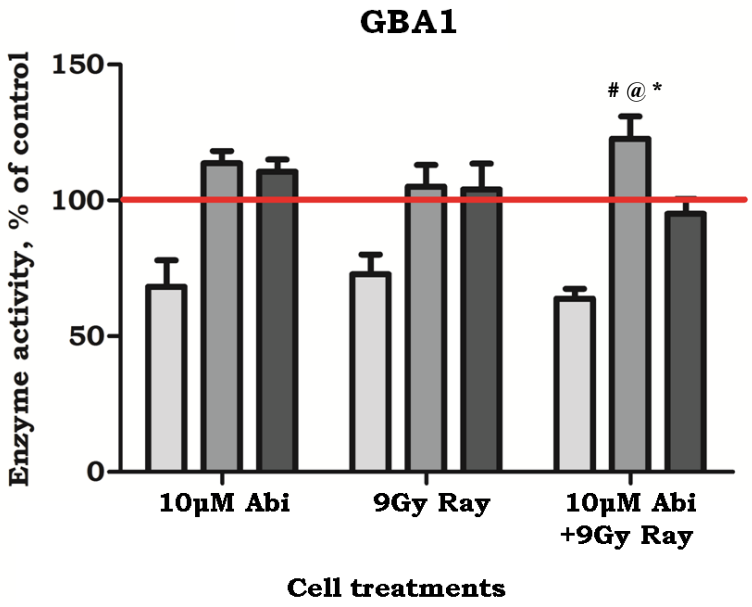

Figure 23. Activity of CBE-sensitive β-Glucosidase GBA1 in androgen-sensitive LNCaP cells treated with 10 μM abiraterone, 9 Gy ionizing radiation and the combined treatment. The activity was determined in total cell lysate of LNCaP cells treated or not for 2 ( ), 24 ( ) and 48 ( ) hours from irradiation, and was evaluated in the presence of the specific inhibitor of GBA2, the AMP-dNM. The data are the average of three experiments performed in triplicate for each cell treatment, expressed as percentage relative to the value of control cells (red line). Two Way ANOVA followed by Bonferroni post-tests #$p<0.05$ versus control cells, @ $p<0.05$ vs different treatments, *$p<0.05$ vs different times for the same treatment.

Activity of GBA1 in total cell lysate (pmoles/mg protein/hr)			
Type of treatment	Time after cell irradiation		
	2hr	24hr	48hr
Ctrl	8068 ± 267	8892 ± 241	10281 ± 151
10 μM Abi	5500 ± 536	10107 ± 460	11364 ± 511
9 Gy Ray	5874 ± 426	9348 ± 739	10706 ± 1008
10 μM Abi + 9 Gy Ray	5150 ± 186	10914 ± 897	9762 ± 536

Table 13. GBA1 activity determined in LNCaP cells treated with 10 μM abiraterone, 9 Gy ionizing radiation and the combined treatment. The activity was determined in cell lysate of LNCaP cells treated or not (Ctrl) for 2, 24 and 48 hours from irradiation. Each value is the mean of three independent experiments performed in three-fold replicate ± SD. The data are expressed as picomoles per milligram cell proteins per hours.

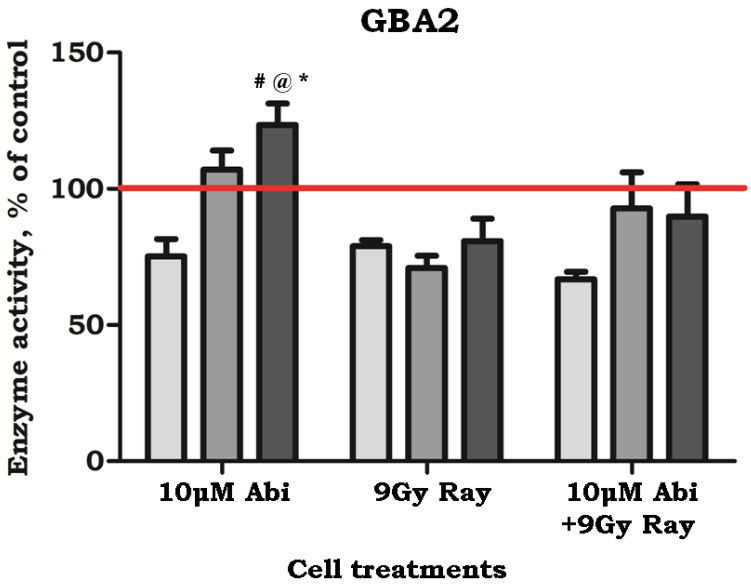

Figure 24. Activity of AMP-dNM-sensitive β-Glucosidase GBA2 in androgen-sensitive LNCaP cells treated with 10 µM abiraterone, 9 Gy ionizing radiation and the combined treatment. The activity was determined in total cell lysate of LNCaP cells treated or not for 2 ( ), 24 ( ) and 48 ( ) hours from irradiation, and was evaluated in the presence of the specific inhibitor of GBA1, CBE. The data are the average of three experiments performed in triplicate for each cell treatment, expressed as percentage relative to the value of control cells (red line). Two Way ANOVA followed by Bonferroni post-tests #p<0.05 versus control cells, @ p<0.05 vs different treatments, *p<0.05 vs different times for the same treatment.

Activity of GBA2 in total cell lysate (pmoles/mg protein/hr)			
Type of treatment	Time after cell irradiation		
	2hr	24hr	48hr
Ctrl	3836 ± 185	3899 ± 529	3381 ± 412
10 µM Abi	2885 ± 184	4170 ± 294	4172 ± 123.4
9 Gy Ray	3026 ± 70	2765 ± 123	2731 ± 227
10 µM Abi + 9 Gy Ray	2561 ± 72	3619 ± 479	3036 ± 360

Table 14. GBA2 activity determined in LNCaP cells treated with 10 µM abiraterone, 9 Gy ionizing radiation and the combined treatment. The activity was determined in cell lysate of LNCaP cells treated or not (Ctrl) for 2, 24 and 48 hours from irradiation. Each value is the mean of three independent experiments performed in three-fold replicate ± SD. The data are expressed as picomoles per milligram cell proteins per hours.

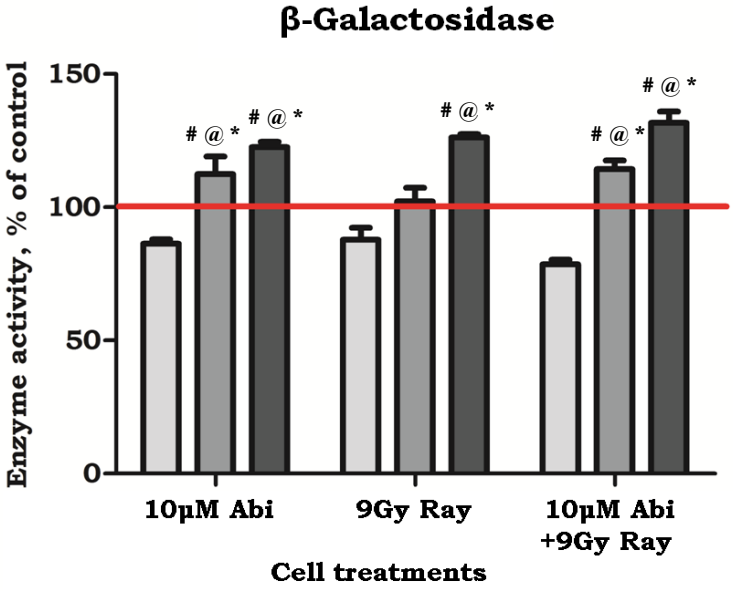

Figure 25. Activity of β-Galactosidase in androgen-sensitive LNCaP cells treated with 10 μM abiraterone, 9 Gy ionizing radiation and the combined treatment. The activity was determined in total cell lysate of LNCaP cells treated or not for 2 ( ), 24 ( ) and 48 ( ) hours from irradiation. The data are the average of three experiments performed in triplicate for each cell treatment, expressed as percentage relative to the value of control cells (red line). Two Way ANOVA followed by Bonferroni post-tests #$p<0.05$ versus control cells, @ $p<0.05$ vs different treatments, *$p<0.05$ vs different times for the same treatment.

Activity of β-Galactosidase in total cell lysate (nmoles/mg protein/hr)			
Type of treatment	Time after cell irradiation		
	2hr	24hr	48hr
Ctrl	68.8 ± 2.2	97.1 ± 5.6	88.7 ± 3.8
10 μM Abi	59.4 ± 0.9	108.2 ± 7.1	108.6 ± 2.1
9 Gy Ray	60.4 ± 2.7	99.3 ± 5.1	111.9 ± 1.4
10 μM Abi + 9 Gy Ray	54.1 ± 0.9	111 ± 3.7	116.8 ± 4.9

Table 15. β-Galactosidase activity determined in LNCaP cells treated with 10 μM abiraterone, 9 Gy ionizing radiation and the combined treatment. The activity was determined in cell lysate of LNCaP cells treated or not (Ctrl) for 2, 24 and 48 hours from irradiation. Each value is the mean of three independent experiments performed in three-fold replicate ± SD. The data are expressed as nanomoles per milligram cell proteins per hours.

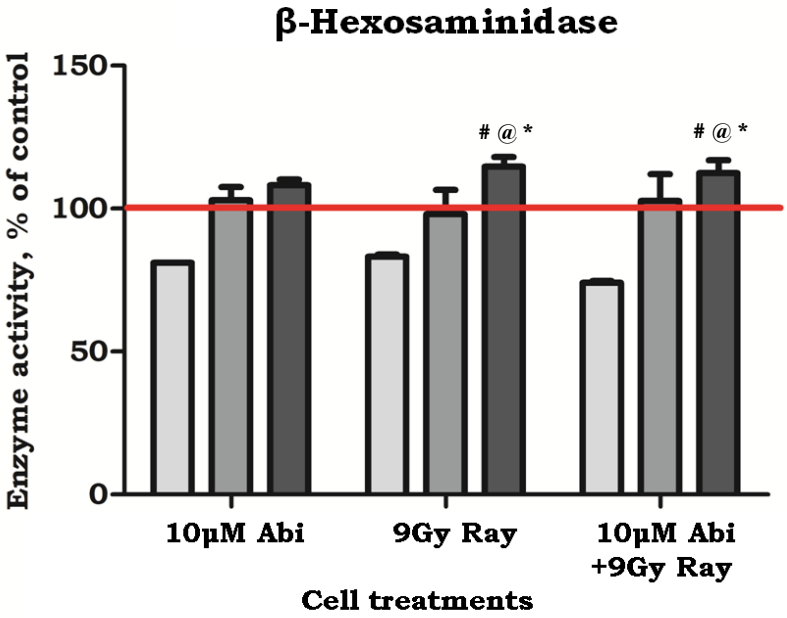

Figure 26. Activity of β-Hexosaminidase in androgen-sensitive LNCaP cells treated with 10 μM abiraterone, 9 Gy ionizing radiation and the combined treatment. The activity was determined in total cell lysate of LNCaP cells treated or not for 2 ( ), 24 ( ) and 48 ( ) hours from irradiation. The data are the average of three experiments performed in triplicate for each cell treatment, expressed as percentage relative to the value of control cells (red line). Two Way ANOVA followed by Bonferroni post-tests #$p<0.05$ versus control cells, @ $p<0.05$ vs different treatments, *$p<0.05$ vs different times for the same treatment.

Activity of β-Hexosaminidase in total cell lysate (nmoles/mg protein/hr)			
Type of treatment	Time after cell irradiation		
	2hr	24hr	48hr
Ctrl	1802 ± 7.3	2312 ± 77.8	2190 ± 114.4
10 μM Abi	1462 ± 0.8	2378 ± 110.7	2369 ± 47.0
9 Gy Ray	1499 ± 9.5	2269 ± 191.3	2513 ± 82.7
10 μM Abi + 9 Gy Ray	1334 ± 10.3	2375 ± 222.9	2463 ± 110

Table 16. β-Hexosaminidase activity determined in LNCaP cells treated with 10 μM abiraterone, 9 Gy ionizing radiation and the combined treatment. The activity was determined in cell lysate of LNCaP cells treated or not (Ctrl) for 2, 24 and 48 hours from irradiation. Each value is the mean of three independent experiments performed in three-fold replicate ± SD. The data are expressed as nanomoles per milligram cell proteins per hours.

In androgen-insensitive PC3 cells the activities of GBA1 (Figure 27), GBA2 (Figure 28) and β-Galactosidase (Figures 29) increase after all the cell treatment, especially after the single treatment with abiraterone and after the combined one. Differently, the activity of the β-Hexosaminidase does not show any change (Figure 30).

This trend is also maintained by GBA1 (Figure 31), β-Galactosidase (Figure 33) and β-Hexosaminidase (Figure 34) activities in DU145 cells, while the activity of GBA2 increases after 48 hours with the single treatment of abiraterone or in combination with irradiation (Figure 32).

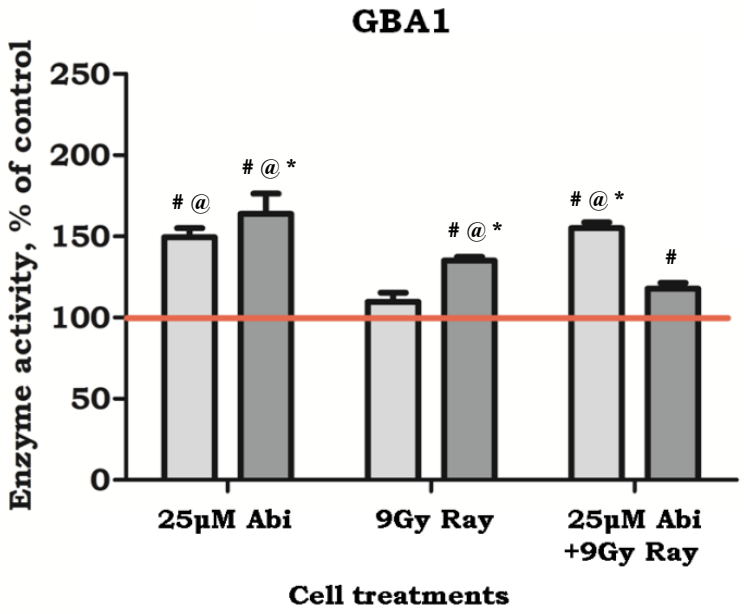

Figure 27. Activity of CBE-sensitive β-Glucosidase GBA1 in androgen-insensitive PC3 cells treated with 25 µM abiraterone, 9 Gy ionizing radiation and the combined treatment. The activity was determined in total cell lysate of LNCaP cells treated or not for 2 (▭) and 48 (▭) hours from the irradiation. The data are the averageof three experiments performed in triplicate for each cell treatment, expressed as percentage relative to the value of control cells (red line). Two Way ANOVA followed by Bonferroni post-tests #p<0.05 versus control cells, @ p<0.05 vs different treatments, *p<0.05 vs different times for the same treatment.

Activity of GBA1 in total cell lysate (pmoles/mg protein/hr)		
Type of treatment	Time after cell irradiation	
	2hr	48hr
Ctrl	568 ± 33	545 ± 69
25 µM Abi	848 ± 75	893 ± 47
9 Gy Ray	622 ± 36	736 ± 17
25 µM Abi + 9 Gy Ray	881 ± 30	642 ± 23

Table 17. GBA1 activity determined in PC3 cells treated with 25 µM abiraterone, 9 Gy ionizing radiation and the combined treatment. The activity was determined in cell lysate of PC3 cells treated or not (Ctrl) for 2 and 48 hours from irradiation. Each value is the mean of three independent experiments performed in three-fold replicate ± SD. The data are expressed as picomoles per milligram cell proteins per hours

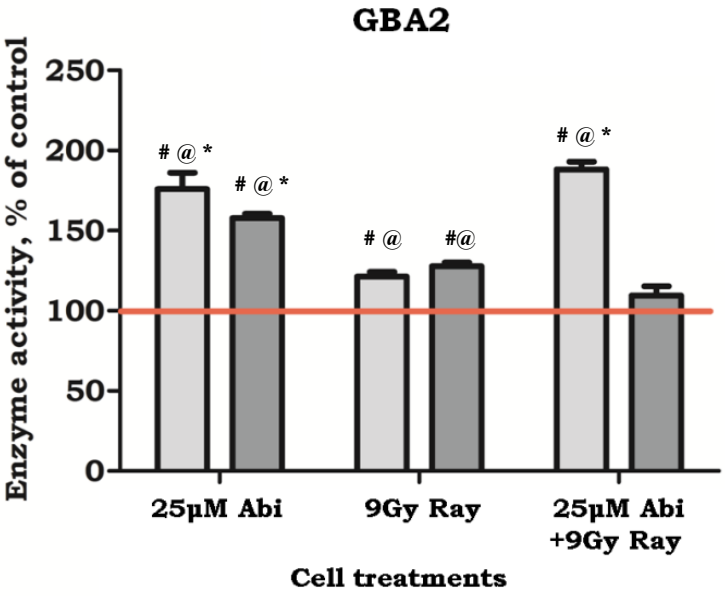

Figure 28. Activity of AMP-dNM-sensitive β-Glucosidase GBA2 in androgen-insensitive PC3 cells treated with 25 µM abiraterone, 9 Gy ionizing radiation and the combined treatment. The activity was determined in total cell lysate of PC3 cells treated or not for 2 (▭) and 48 (▭) hours from irradiation. The data are the average of three experiments performed in triplicate for each cell treatment, expressed as percentage relative to the value of control cells (red line). Two Way ANOVA followed by Bonferroni post-tests #p<0.05 versus control cells, @ p<0.05 vs different treatments, *p<0.05 vs different times for the same treatment.

Activity of GBA2 in total cell lysate (pmoles/mg protein/hr)		
Type of treatment	Time after cell irradiation	
	2hr	48hr
Ctrl	388 ± 40	462 ± 12
25 µM Abi	682 ± 64	730 ± 11
9 Gy Ray	471 ± 14	591 ± 14
25 µM Abi + 9 Gy Ray	731 ± 34	506 ± 30

Table 18. GBA2 activity determined in PC3 cells treated with 25 µM abiraterone, 9 Gy ionizing radiation and the combined treatment. The activity was determined in cell lysate of PC3 cells treated or not (Ctrl) for 2 and 48 hours from irradiation. Each value is the mean of three independent experiments performed in three-fold replicate ± SD. The data are expressed as picomoles per milligram cell proteins per hours.

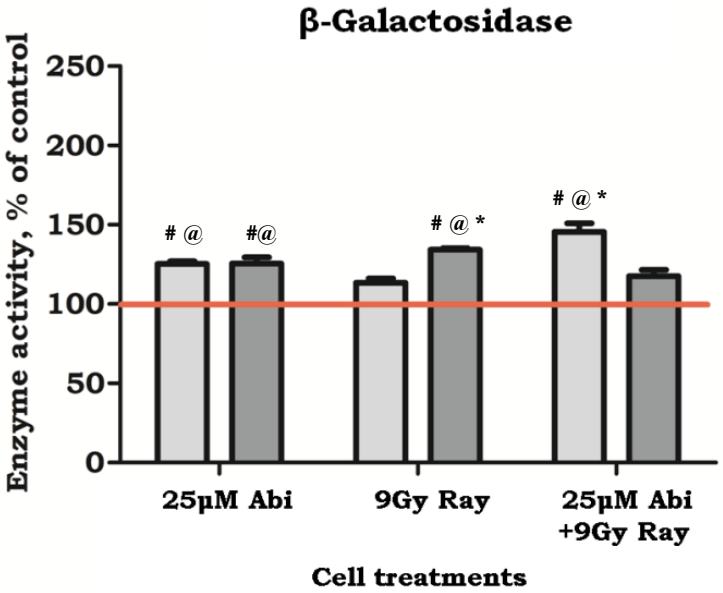

Figure 29. Activity of β-Galactosidase in androgen-insensitive PC3 cells treated with 25 μM abiraterone, 9 Gy ionizing radiation and the combined treatment. The activity was determined in total cell lysate of PC3 cells treated or not for 2 (▭) and 48 (▭) hours from irradiation. The data are averages of three experiments performed in triplicate for each cell treatment, expressed as percentage relative to the value of control cells (red line). Two Way ANOVA followed by Bonferroni post-tests #$p<0.05$ versus control cells, @ $p<0.05$ vs different treatments, *$p<0.05$ vs different times for the same treatment.

Activity of β-Galactosidase in total cell lysate (nmoles/mg protein/hr)		
Type of treatment	Time after cell irradiation	
	2hr	48hr
Ctrl	33.4 ±0.6	27.5 ± 1.1
25 μM Abi	41.9 ± 2.1	34.5 ± 1.9
9 Gy Ray	38.0 ± 1.0	36.9 ± 0.4
25 μM Abi + 9 Gy Ray	48.7 ± 2.6	32.4 ± 1.3

Table 19. β-Galactosidase activity determined in PC3 cells treated with 25 μM abiraterone, 9 Gy ionizing radiation and the combined treatment. The activity was determined in cell lysate of PC3 cells treated or not (Ctrl) for 2 and 48 hours from irradiation. Each value is the mean of three independent experiments performed in three-fold replicate ± SD. The data are expressed as nanomoles per milligram cell proteins per hours.

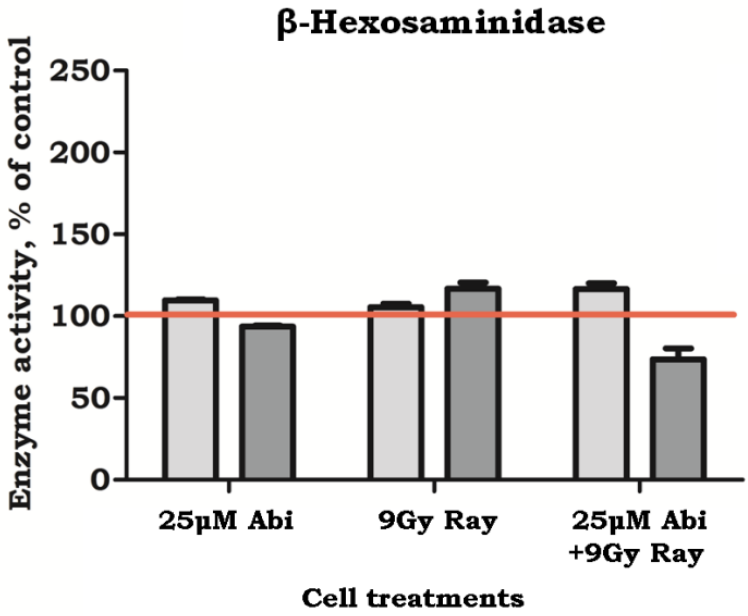

Figure 30. Activity of β-Hexosaminidase in androgen-insensitive PC3 cells treated with 25 μM abiraterone, 9 Gy ionizing radiation and the combined treatment. The activity was determined in total cell lysate of PC3 cells treated or not for 2 (▭) and 48 (▭) hours from irradiation. The data are the average of three experiments performed in triplicate for each cell treatment, expressed as percentage relative to the value of control cells (red line). Two Way ANOVA followed by Bonferroni post-tests #p<0.05 versus control cells.

Activity of β-Hexosaminidase in total cell lysate (nmoles/mg protein/hr)		
Type of treatment	Time after cell irradiation	
	2hr	48hr
Ctrl	550 ± 3.6	476 ± 2.3
25 μM Abi	603 ± 16.6	446 ± 5.1
9 Gy Ray	580 ± 11.9	556 ± 21.3
25 μM Abi + 9 Gy Ray	640 ± 22.6	350 ± 23.5

Table 20. β-Hexosaminidase activity determined in PC3 cells treated with 25 μM abiraterone, 9 Gy ionizing radiation and the combined treatment. The activity was determined in cell lysate of PC3 cells treated or not (Ctrl) for 2 and 48 hours from irradiation. Each value is the mean of three independent experiments performed in three-fold replicate ± SD. The data are expressed as nanomoles per milligram cell proteins per hours.

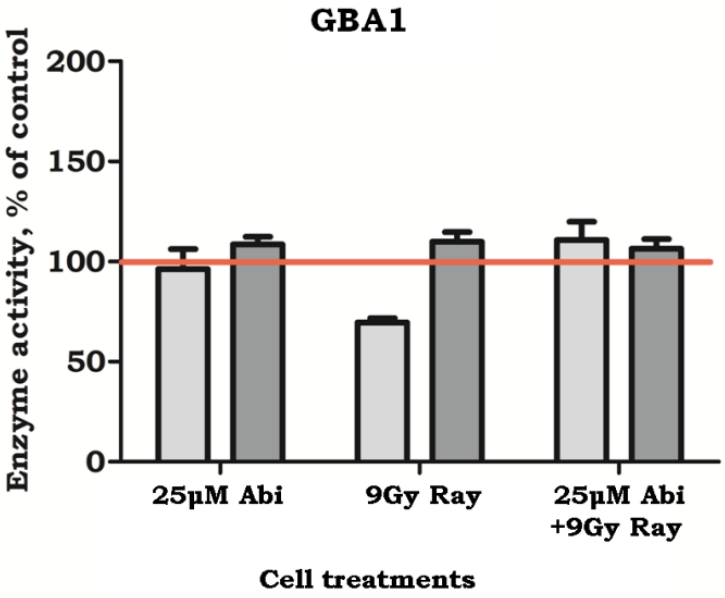

Figure 31. GBA1 activity determined in androgen-insensitive DU145 cells treated with 25 µM abiraterone, 9 Gy ionizing radiation and the combined treatment. The activity was determined in cell lysate of DU145 cells treated or not for 2 ( ) to 48 ( ) hours from irradiation. The data are expressed as enzyme activity respect to the control cells (red line).

Activity of GBA1 in total cell lysate (pmoles/mg protein/hr)		
Type of treatment	Time after cell irradiation	
	2hr	48hr
Ctrl	938 ± 79	751 ± 29
25 µM Abi	902 ± 90	815 ± 31
9 Gy Ray	653 ± 14	825 ± 40
25 µM Abi + 9 Gy Ray	1039 ± 34	800 ± 38

Table 21. GBA1 activity determined in androgen-insensitive DU145 cells treated with 25 µM abiraterone, 9 Gy ionizing radiation and the combined treatment.
The activity was determined in cell lysate of DU145 cells treated or not (Ctrl) for 2 to 48 hours from the irradiation. Each value is the mean of three independent experiments performed in three-fold replicate ± SD. The data are expressed as picomoles per milligram cell proteins per hours.

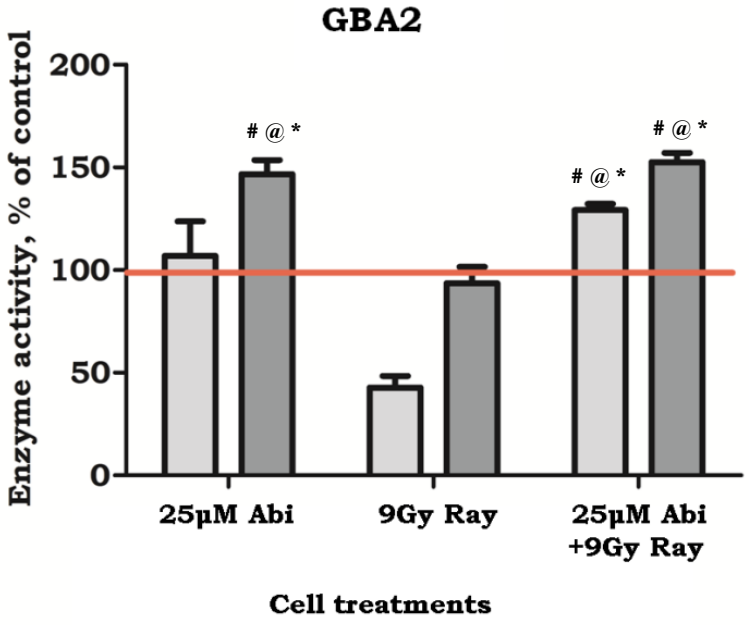

Figure 32. Activity of AMP-dNM-sensitive β-Glucosidase GBA2 in androgen-insensitive DU145 cells treated with 25 µM abiraterone, 9 Gy ionizing radiation and the combined treatment. The activity was determined in total cell lysate of DU145 cells treated or not for 2 (▭) and 48 (▭) hours from the irradiation. The data are the average of three experiments performed in triplicate for each cell treatment, expressed as percentage relative to the value of control cells (red line). Two Way ANOVA followed by Bonferroni post-tests #p<0.05 versus control cells, @ p<0.05 vs different treatments, *p<0.05 vs different times for the same treatment.

Activity of GBA2 in total cell lysate (pmoles/mg protein/hr)		
Type of treatment	Time after cell irradiation	
	2hr	48hr
Ctrl	449 ± 38	389 ± 14
25 µM Abi	480 ± 81	570 ± 39
9 Gy Ray	192 ± 11	364 ± 29
25 µM Abi + 9 Gy Ray	581 ± 17	593 ± 26

Table 22. GBA2 activity determined in DU145 cells treated with 25 µM abiraterone, 9 Gy ionizing radiation and the combined treatment. The activity was determined in cell lysate of DU145 cells treated or not (Ctrl) for 2 and 48 hours from irradiation. Each value is the mean of three independent experiments performed in three-fold replicate ± SD. The data are expressed as picomoles per milligram cell proteins per hours.

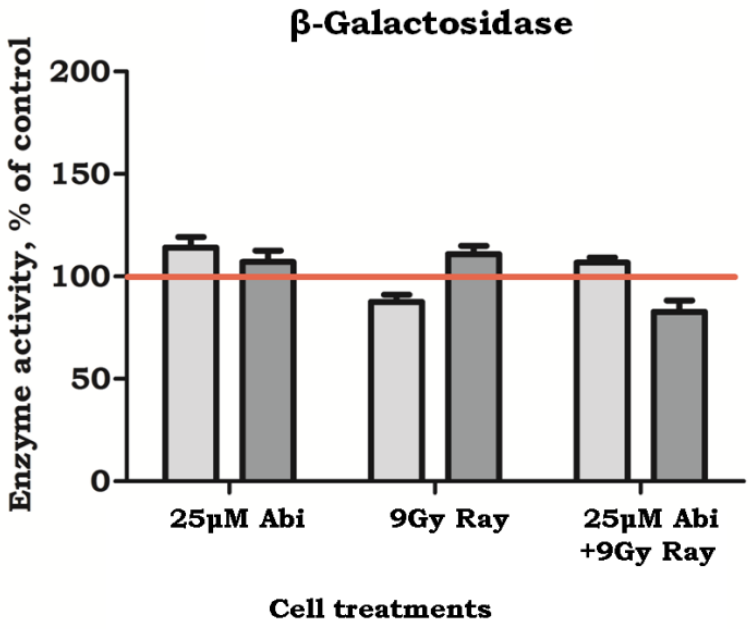

Figure 33. Activity of β-Galactosidase in androgen-insensitive DU145 cells treated with 25 μM abiraterone, 9 Gy ionizing radiation and the combined treatment. The activity was determined in total cell lysate of DU145 cells treated or not for 2 (▭) and 48 (▭) hours from the irradiation. The data are the average of three experiments performed in triplicate for each cell treatment, expressed as percentage relative to the value of control cells (red line).

Activity of β-Galactosidase in total cell lysate (nmoles/mg protein/hr)		
Type of treatment	Time after cell irradiation	
	2hr	48hr
Ctrl	58 ± 3.1	31 ± 1.9
25 μM Abi	66 ± 3.5	33 ± 1.8
9 Gy Ray	51 ± 1.8	34 ± 1.4
25 μM Abi + 9 Gy Ray	62 ± 1.5	25 ± 1.4

Table 23. β-Galactosidase activity determined in DU145 cells treated with 25 μM abiraterone, 9 Gy ionizing radiation and the combined treatment. The activity was determined in cell lysate of DU145 cells treated or not (Ctrl) for 2 and 48 hours from irradiation. Each value is the mean of three independent experiments performed in three-fold replicate ± SD. The data are expressed as nanomoles per milligram cell proteins per hours.

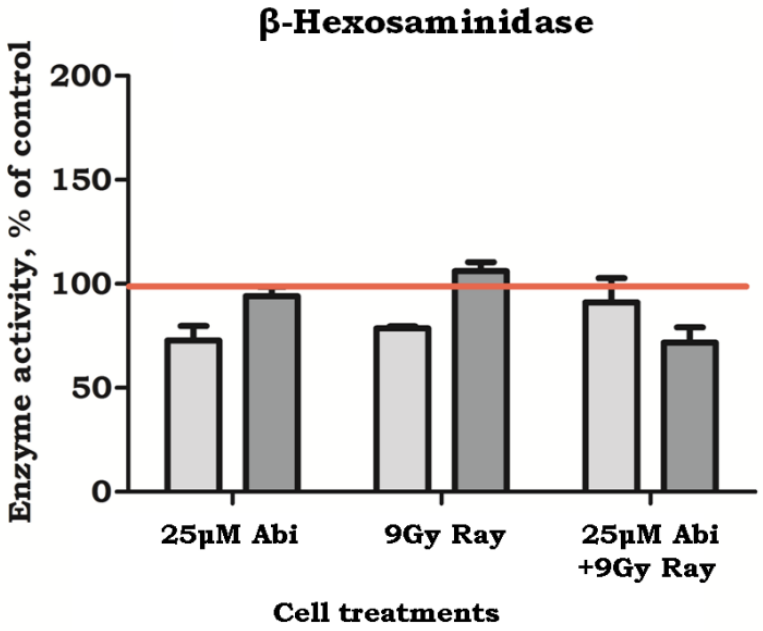

Figure 34. Activity of β-Hexosaminidase in androgen-insensitive DU145 cells treated with 25 μM abiraterone, 9 Gy ionizing radiation and the combined treatment. The activity was determined in total cell lysate of DU145 cells treated or not for 2 (▭) and 48 (▭) hours from irradiation. The data are the average of three experiments performed in triplicate for each cell treatment, expressed as percentage relative to the value of control cells (red line)..

Activity of β-Hexosaminidase in total cell lysate (nmoles/mg protein/hr)		
Type of treatment	Time after cell irradiation	
	2hr	48hr
Ctrl	837 ± 88	506 ± 15
25 μM Abi	609 ± 43	476 ± 22
9 Gy Ray	658 ± 67	537 ± 23
25 μM Abi + 9 Gy Ray	762 ± 88	363 ± 26

Table 24. β-Hexosaminidase activity determined in DU145 cells treated with 25 μM abiraterone, 9 Gy ionizing radiation and the combined treatment. The activity was determined in cell lysate of DU145 cells treated or not (Ctrl) for 2 and 48 hours from irradiation. Each value is the mean of three independent experiments performed in three-fold replicate ± SD. The data are expressed as nanomoles per milligram cell proteins per hours.

Effect of different treatments on ceramide production

All the results obtained on the enzymatic activities indicate that the most significant variation occurs at the PM level. It is of common knowledge that the increased activity of these enzyme in response to different stimuli (such as chemo- and radiotherapy), could rapidly activate the hydrolysis of complex glycosphingolipids, leading to the ectopic production of ceramide and the onset of cell apoptosis. To this purpose, the analysis of sphingolipid pattern and composition after the different cell treatments has been performed:, cells were first treated with abiraterone and/or irradiation, and then SLs were metabolically radiolabeled at the steady state with [1-^{3}H]sphingosine. As shown in Figure 35 and Table 25, in LNCaP cells all the different treatments induce an increase in ceramide content. In particular, the treatment with 10 μM abiraterone, 9 Gy ionizing radiation and the combined one, induces a 2, 2.5 and 3.3 fold increase in ceramide level respectively.

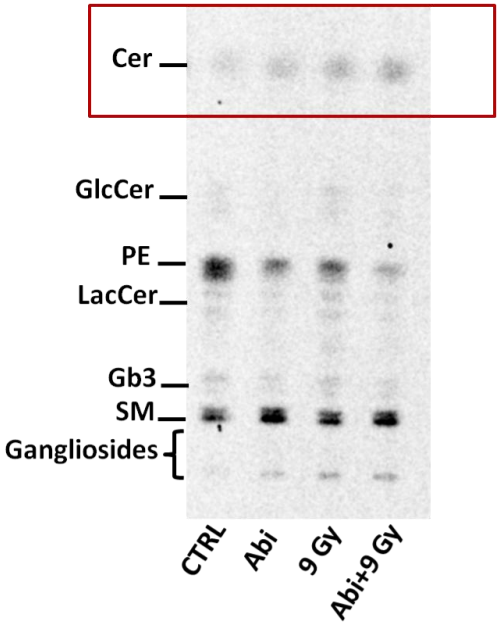

Figure 35. HPTLC separation of total radioactive lipids extracted from LNCaP cells subjected to different treatments. Extraction was performed 72 hr from cell irradiation. Total lipid extract was separated on HPTLC silica gel 100 plates using the solvent system chloroform-methanol-water 110:40:6 by volume. 700 dpm were applied in each line and after separation HPTLC were submitted to 3 days counting by digital radio-imaging.

	Ctrl	*10 µM Abi*	*9 Gy Ray*	*10 µM Abi + 9 Gy Ray*
Cer	4.9 %	9.4 %	11.8 %	16.4 %
GlcCer	3.3 %	2.4 %	6.7 %	4.2 %
PE	52.8 %	25.7 %	29.4 %	15.0 %
LacCer	6.2 %	4.1 %	9.0 %	5.8 %
Gb3	4.7 %	4.5 %	6.5 %	5.8 %
SM	26.1 %	49.6 %	29.7 %	44.4 %
Ganglioside	1.9 %	4.4 %	6.9 %	8.4 %

Table 25. **Radioactivity quantification of sphingolipids after HPTLC separation as reported in Figure 35 (24 hr)** data are expressed as percentage relative of single species respect to total sphingolipid amount. Data represent the mean ± SD, n = 2 independent experiments, 3 replicates for each experiment.

Comparable results were observed also for the androgen-insensitive PC3 and DU145 cell lines (Figure 36-37, Table 26-27): in particular, after the single treatment with 25 μM abiraterone and the combined one in PC3 cells, Cer rose up respectively 1.7 and 2.2 fold respect to control cells, while the single treatment with ionizing radiation does not cause a significant increase in Cer level. Moreover, in DU145 cells Cer rose up respectively 1.7, 1.8 and 2.1 fold respect to control cells.

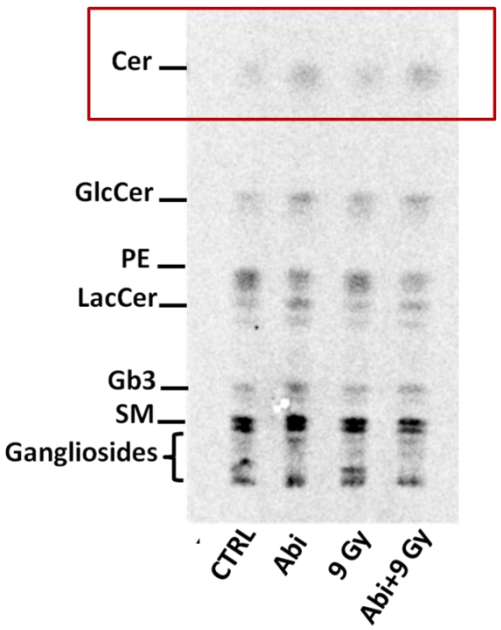

Figure 36. HPTLC separation of total radioactive lipids extracted from PC3 cells subjected to the different treatments. Extraction was performed 72 hr from the cell irradiation. Total extract was separated on HPTLC silica gel 100 plates using the solvent system chloroform-methanol-water 110:40:6 by volume. 700 dpm were applied in each line and after separation, HPTLC were submitted to 3 day counting by digital radio-imaging.

	Ctrl	*25 μM Abi*	*9 Gy Ray*	*25 μM Abi + 9 Gy Ray*
Cer	4.1 %	6.8 %	4.7 %	9.0 %
GlcCer	5.9 %	8.9 %	8.7 %	10.3 %
PE	17.5 %	9.5 %	15.0 %	10.2 %
LacCer	8.8 %	10.2 %	7.9 %	10.1 %
Gb3	8.6 %	12.2 %	7.6 %	9.6 %
SM	27.0 %	27.9 %	27.7 %	26.5 %
Ganglioside	28.1 %	24.5 %	28.5 %	24.2 %

Table 26. Radioactivity quantification of sphingolipids separated by HPTLC as reported in Figure 36 (24 hr); data are expressed as percentage relative of single species respect to the total sphingolipid amount. Data represent the mean ± SD, n = 2 independent experiments, 3 replicates for each experiment.

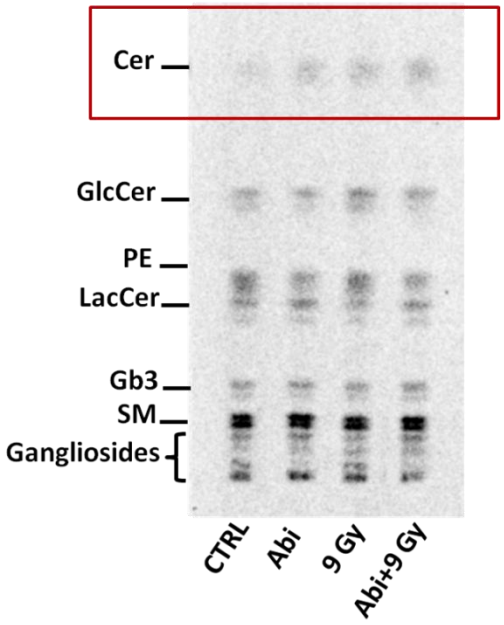

Figure 37. HPTLC separation of total radioactive lipids extracted from DU145 cells subjected to different treatments. Extraction was performed 72 hr from the cell irradiation. Total extract was separated on HPTLC silica gel 100 plates using the solvent system chloroform-methanol-water 110:40:6 by volume. 700 dpm were applied in each line and after separation, HPTLC were submitted to 3 day counting by digital radio-imaging.

	Ctrl	*25μM Abi*	*9 Gy Ray*	*25μM Abi + 9 Gy Ray*
Cer	3.4 %	5.8 %	6.2 %	7.3 %
GlcCer	10.5 %	8.8 %	13.4 %	9.7 %
PE	17.4 %	10.8 %	16.0 %	9.5 %
LacCer	12.2 %	12.4 %	9.7 %	10.7 %
Gb3	9.1 %	9.7 %	8.7 %	9.7 %
SM	23.7 %	26.1 %	23.4 %	26.7 %
Ganglioside	23.6 %	26.5 %	22.6 %	26.3 %

Table 27. **Radioactivity quantification of sphingolipids separated by HPTLC as reported in Figure 37 (24 hr);** data are expressed as percentage relative of single species respect to the total sphingolipid amount. Data represent the mean ± SD, n = 2 independent experiments, 3 replicates for each experiment.

All these results suggest that in PC cells the different treatments cause significant changes in the cell sphingolipid content and pattern; this should be followed by changes in the plasma membrane cell structure. It is of common knowledge that sphingolipids segregate within cholesterol leading to the creation of membrane domains called Sphingolipid Enriched Membrane Domains (SEMD). These domains are also enriched in selected proteins involved in the control of signal transduction. Indeed, it has been demonstrated that the SEMD are involved in the regulation of several cellular processes including cell death. For this reason, in order to evaluate the possible molecular mechanism involved in the cell death I purified SEMD by using a method based on the separation on a sucrose gradient, followed by ultracentrifugation in order to obtain detergent insoluble low-density membrane fractions. The SEMD were prepared for all the prostate cancer cell lines subjected to the treatments described before: only vehicle, abiraterone, ionizing radiation and both the treatments. After feeding experiments with radioactive sphingosine (in conditions to radiolabel cell sphingolipids at the steady state), cells were harvested, lysed and centrifuged to obtain the Post Nuclear Supernatant (PNS). PNS were loaded on a discontinuous sucrose gradient, ultracentrifuged and eleven fractions (#) were collected from the top of each tube. The radioactivity associated with each fraction was determinate by liquid scintillation counting, and as shown in Figures 38-40-42, cell-radioactivity, mainly due to SLs, was largely associated with fractions 5-6, corresponding to the low density fractions (DRM) that are resistant to detergent solubilization. Moreover, some radioactivity was also associated with fractions 10-11, corresponding to the high density fractions (HD fraction) that contain membrane solubilized by detergent and the higher quantity of cell proteins. Interestingly, the DRM fractions prepared from all the cell lines tested, show an increase in ceramide level after all the cell treatments respect to control cells.

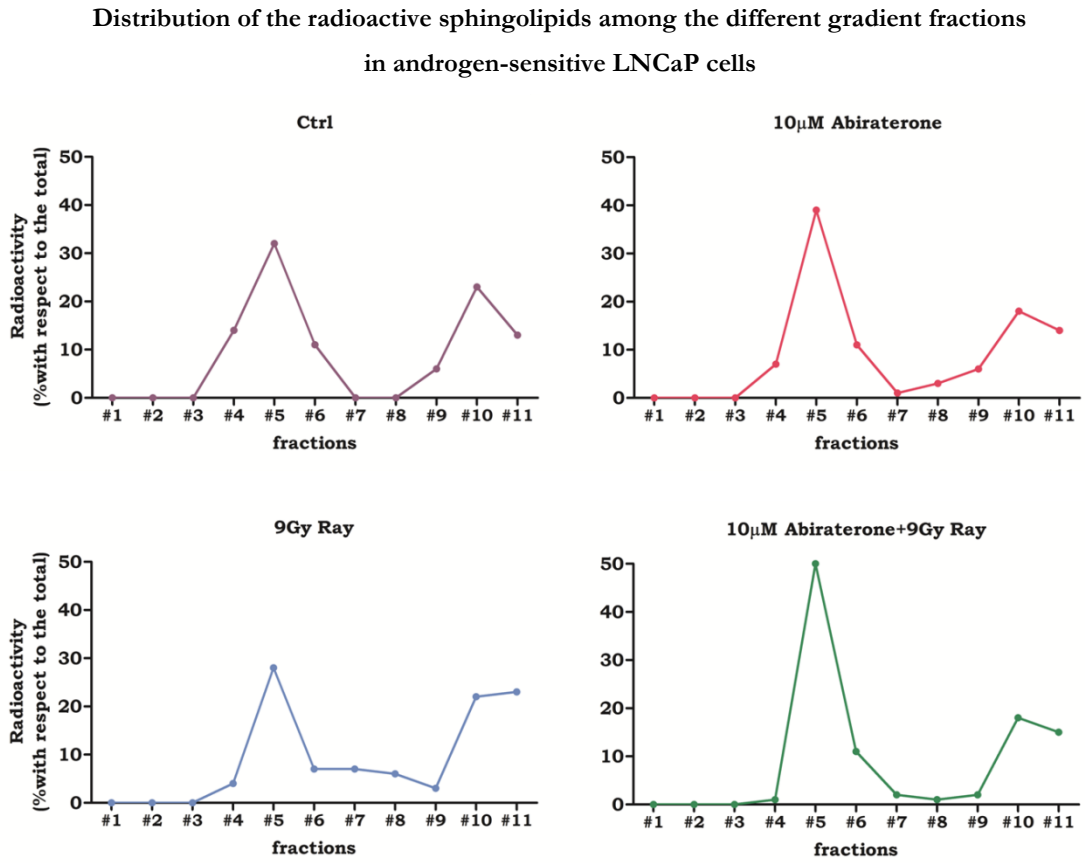

Figure 38. LNCaP gradient fractions analysis. Distribution of total radioactivity in sucrose density fractions from control (Ctrl) and treated cells. The data as percentage relative of single fraction radioactivity with respect to total radioactivity.

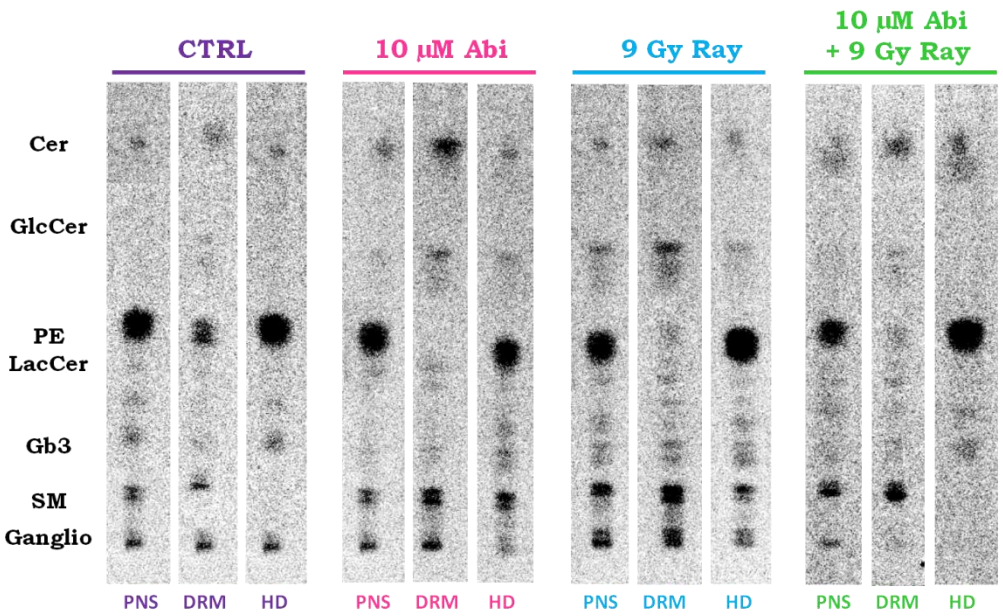

Figure 39. HPTLC separation of radioactive total lipid extract obtained from DRM fractions prepared from control and treated LNCaP cells. A total of 800 dpm of lipid extract were applied on a 4 mm line. HPTLC was run in the solvent system chloroform-methanol-water, 110:40:6 by volume. Digital autoradiography was performed with a Biospace β-imager instrument for 48 hours.

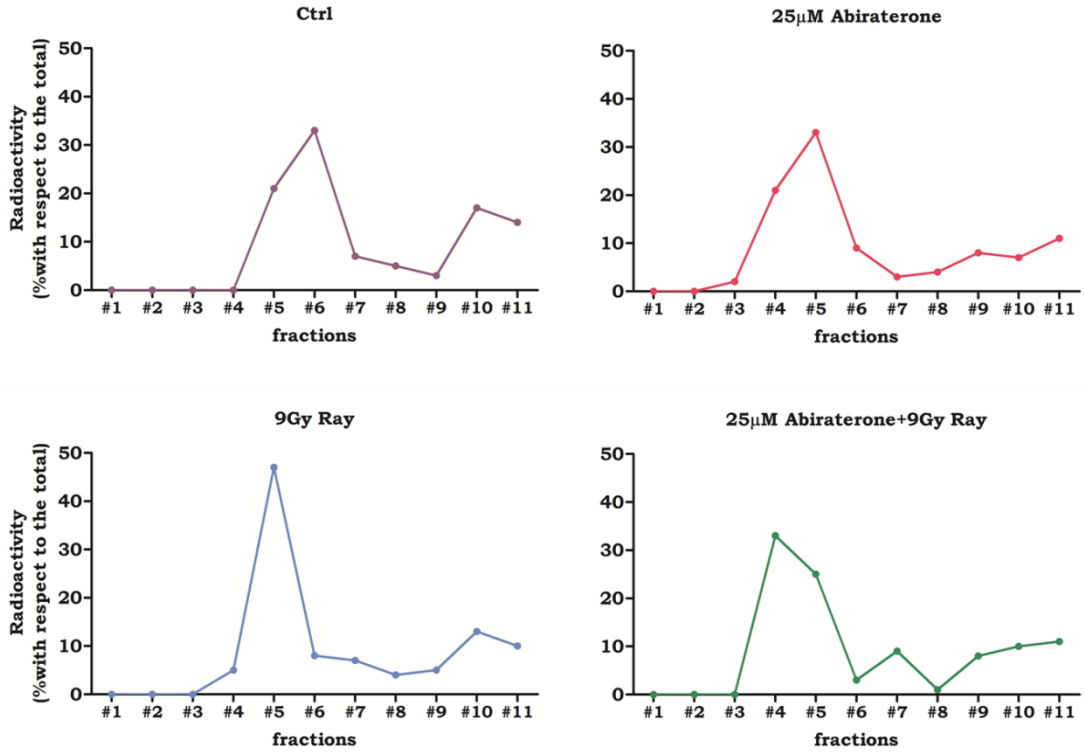

Figure 40. PC3 gradient fraction analysis. Distribution of total radioactivity in sucrose density fractions from control (Ctrl) and treated cells. The data as percentage relative of single fraction radioactivity with respect to total radioactivity.

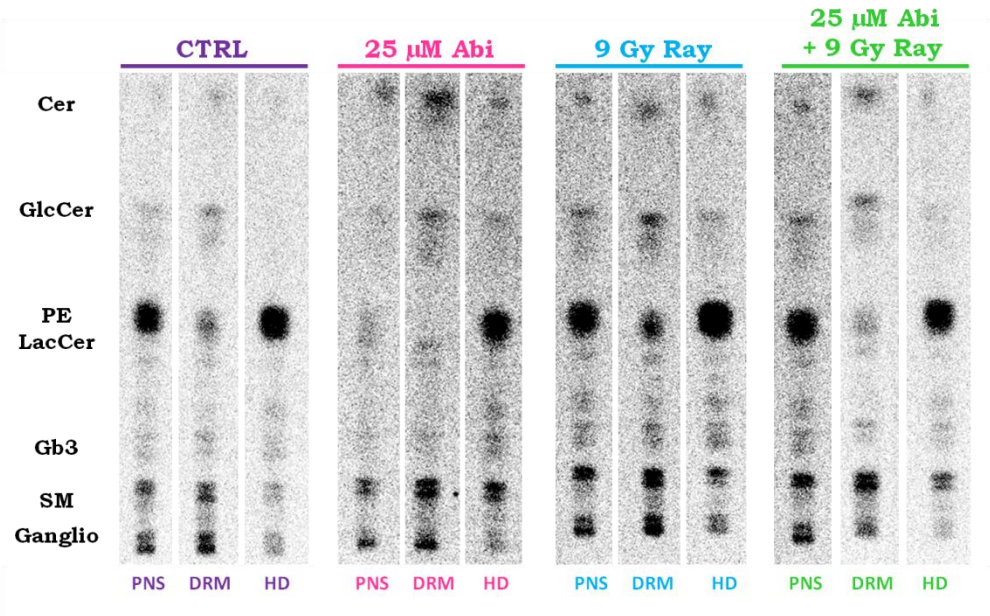

Figure 41. HPTLC separation of radioactive total lipid extract obtained from DRM fractions prepared from control and treated PC3 cells. A total of 800 dpm of lipid extract were applied on a 4 mm line. HPTLC was run in the solvent system chloroform-methanol-water, 110:40:6 by volume. Digital autoradiography was performed with a Biospace β-imager instrument for 48 hours.

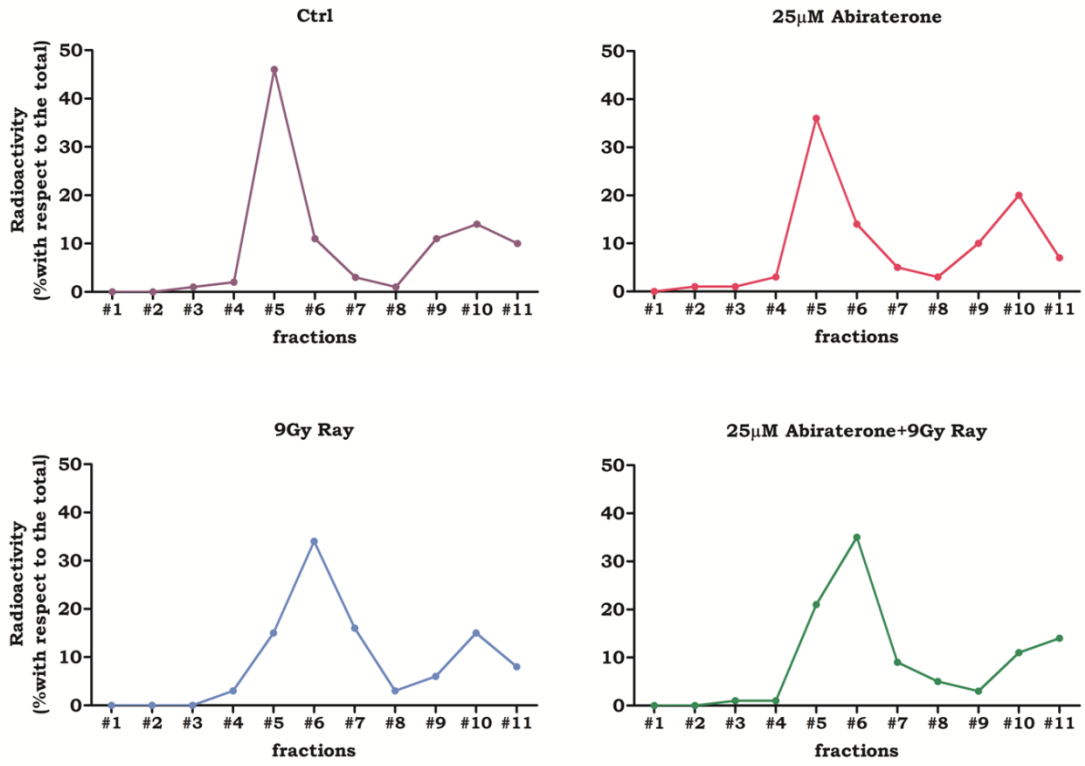

Figure 42. DU145 gradient fraction analysis. Distribution of total radioactivity in sucrose density fractions from control (Ctrl) and treated cells. The data as percentage relative of single fraction radioactivity with respect to the total amount of radioactivity.

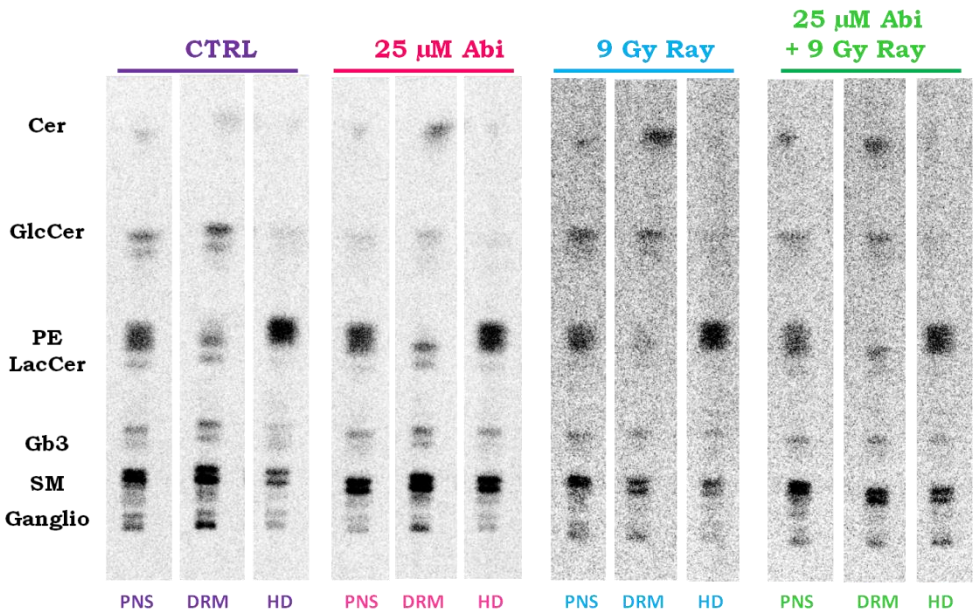

Figure 43. HPTLC separation of radioactive total lipid extract obtained from DRM fractions prepared from control and treated DU145 cells. A total of 800 dpm of lipid extract were applied on a 4 mm line. HPTLC was run in the solvent system chloroform-methanol-water, 110:40:6 by volume. Digital autoradiography was performed with a Biospace β-imager instrument for 48 hours.

Discussion

SL glycohydrolases have been known from long time as lysosomal catabolic enzymes necessary to remove the hydrophilic head from SLs to obtain ceramide. Cer is then hydrolyzed by ceramidase to sphingosine that can be recycled or completely catabolyzed, outside of lysosomes, to water and carbon dioxide [30].
Recently, more specific information suggests the presence of some SL hydrolases at the plasma membrane [31]. The availability of a simple methodology able to selectively detect the enzyme activities associated with PM on living cells, without the interference of the enzymatic lysosomal activities, allowed to better understand the behavior of these enzymes [26].
Some of them are localized at plasma membrane as a consequence of fusion processes between lysosomes and PM, whereas other ones are resident PM-enzymes with structures and properties different from the lysosomal enzymes, such as the β-glucocerebrosidase GBA2, sialidase Neu3 and probably the neutral SMase [31]. The action of these enzymes, which modifies the SL structure has been considered a system able to change the PM organization and properties, mainly related to cell signaling processes [32]. An increase in the activity of PM SMase is claimed to be responsible for the formation of large Cer-rich platforms necessary for the cell signaling [33]. Activation of SMase by TNF-α leads to the Cer dependent phosphorylation cascade resulting in cell apoptosis [34]. The activation of the plasma membrane SMase after ionizing radio-treatment used on radiotherapy is well known to have a central role in cell death and tumor reduction, through cell apoptosis caused by an increase of PM Cer [36,36]. Previously, it has been shown that in human fibroblasts an increased expression of sialidase Neu3 was associated with a rise of β-Glucosidase and β-Galactosidase activity, followed by a further increase on PM ceramide content leading to apoptotic cell death [19].
In this thesis I show some results on the plasma-membrane glycohydrolase activity. obtained in different PC cell lines after the treatment with the anti-androgen drug abiraterone, ionizing radiation and their combined treatment.
The data demonstrate that in all the cells tested, the PM-associated GBA1, GBA2, β-Galactosidase and β-Hexosaminidase activities increase after the cell treatments. Conversely, the activity of sphingomyelinase remain constant [35].
The reason leading to the increase in the PM associated glycohydrolase activities has not yet been clarified; it is probably due to an increase expression, an augmented PM translocation or conformational changes of the enzyme structure. This latter hypothesis has already been postulated for

sphingomyelinase by Haimovitz-Friedman et al. [36] and, considering the irradiation energy, it is not surprising that it could modify the enzyme conformation and activity. Moreover, the data show that changes of plasma membrane enzyme activities occur after only 2 hours from cell irradiation, but at this time point is difficult to hypothesize if the increased activity is due to an increased expression. In addition, the rise of the glycohydrolases activity is followed by an increase of ceramide content in the sphingolipid enriched membrane fractions (DRM). The increase of PM Cer in cells subjected to ionizing radiations has been shown to participate to the onset of cell death [40].

These data suggest the involvement of glycohydrolases in plasma membrane Cer production; at this site, Cer may be involved in the molecular mechanisms leading to cell apoptosis. This could enrich the knowledge on the apoptotic pathway induced by ionizing radiation (summarized in Figure 44). The possibility that PM glycohydrolases could participate to the induction of apoptosis in tumor cells opens the way to design and use drugs able to modulate their activity increasing the irradiation-induced cell death. Moreover, the action of the cell surface associated glycohydrolases are not only restricted to GSLs metabolism but also to other cell surface glycoconjugates. Their modifications, which occur during cell irradiation need to be further studied in the future.

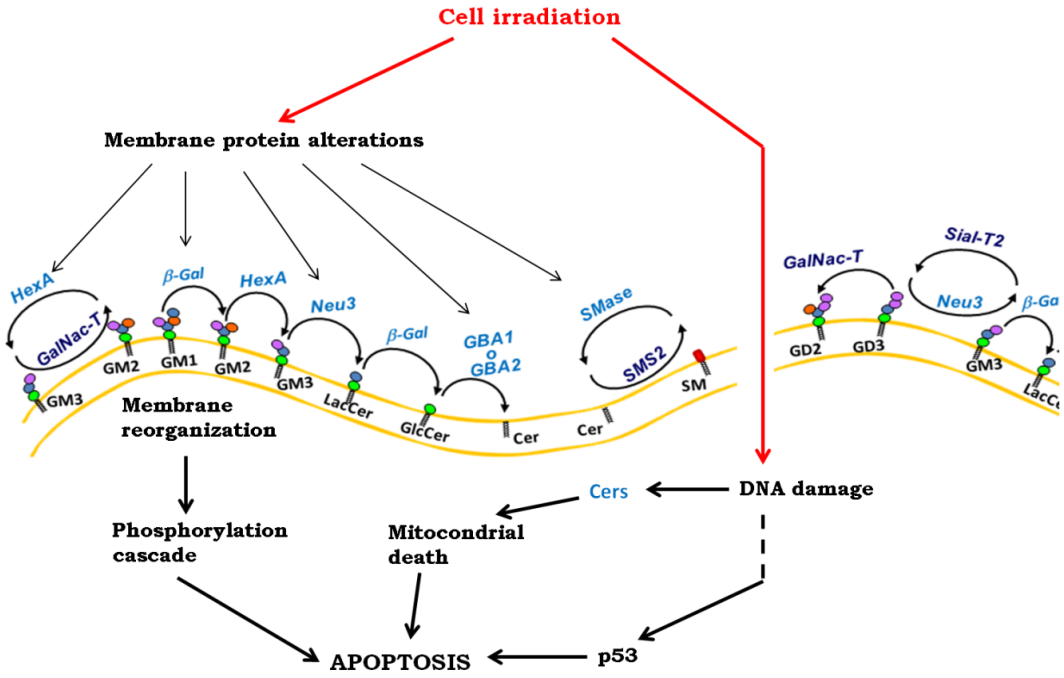

Figure 44. Simplified scheme of the effects of ionizing radiation on cells in culture.

References

1. Jemal A., Siegel R., Ward E., Hao Y., Xu J., Murray T., Thun MJ. (2008) Cancer statistics. CA Cancer J Clin, 58:71-96

2. Kolvenbag G.J., Iversen P., Newling D.W. (2001) Antiandrogen monotherapy: a new form of treatment for patients with prostate cancer. Urology, 58(2 Suppl 1):16-23.

3. Sciarra A., Casale P., Colella D., Di Chiro C., Di Silverio F. (1999) Hormone-refractory prostate cancer? Anti-androgen withdrawal and intermittent hormone therapy. Scand J Urol Nephrol., 33(4):211-6.

4. Akaza H. (2011) Combined androgen blockade for prostate cancer: review of efficacy, safety and cost-effectiveness. Cancer Sci.,102(1):51-6

5. Akaza H., Hinotsu S., Usami M., Arai Y, Kanetake H, Naito S, Hirao Y. (2009) Combined androgen blockade with bicalutamide for advanced prostate cancer: long-term follow-up of a phase 3, double-blind, randomized study for survival. Cancer,115(15):3437-45.

6. Anderson J. (2003) The role of antiandrogen monotherapy in the treatment of prostate cancer. BJU Int., 91(5):455-61.

7. McLeod D.G., Iversen P., See W.A., Morris T., Armstrong J., Wirth M.P. (2006) Bicalutamide 150 mg plus standard care vs standard care alone for early prostate cancer. BJU Int., 97(2):247-54.

8. Schellhammer P.F., Sharifi R., Block N.L., Soloway M.S., Venner P.M., Patterson A.L., Sarosdy M.F., Vogelzang N.J., Schellenger J.J., Kolvenbag G.J. (1997) Clinical benefits of bicalutamide compared with flutamide in combined androgen blockade for patients with advanced prostatic carcinoma: final report of a double-blind, randomized, multicenter trial. Urology., 50(3):330-6.

9. Laufer M., Denmeade S.R., Sinibaldi V.J., Carducci M.A., Eisenberger M.A. (2000) Complete androgen blockade for prostate cancer: what went wrong? J Urol., 164(1):3-9.

10. Lara P.N. Jr., Meyers F.J. (1999) Treatment options in androgen-independent prostate cancer. Cancer Invest., 17(2):137-44.

11. Culig Z., Hobisch A., Hittmair A., Peterziel H., Cato A.C., Bartsch G., Klocker H. (1998) Expression, structure, and function of androgen receptor in advanced prostatic carcinoma. Prostate., 35(1):63-70.

12. Wang C., Uchida T. (1997) Androgen receptor gene mutations in prostate cancer. Nippon Hinyokika Gakkai Zasshi, 88:550-556

13. Henshall S.M., Quinn D.I., Lee C.S., Head D.R., Golovsky D., Brenner P.C., Delprado W., Stricker P.D., Grygiel J.J., Sutherland R.L. (2001) Altered expression of androgen receptor in the malignant epithelium and adjacent stroma is associated with early relapse in prostate cancer. Cancer Res., 61(2):423-427

14. Kinoshita H., Shi Y., Sandefur C., Meisner L.F., Chang C., Choon A., Reznikoff C.R., Bova C.S., Friedl A., Jarrard D.F. (2000) Methylation of the Androgen Receptor Minimal Promoter Silences Transcription in Human Prostate Cancer. Cancer Res, 60; 3623.

15. Feldman B.J., Feldman D. (2001) The development of androgen-independent prostate cancer. Nature Reviews Cancer **1**, 34-45.

16. Damber J.E., Aus G. (2008) Prostate cancer. Lancet., 371(9625):1710-21

17. Hakomori S. (1996) Tumor malignancy defined by aberrant glycosylation and sphingo(glyco)lipid metabolism. Cancer Res., 56(23):5309-18.

18. Kolesnick, R., Fuks, Z.(2003) Radiation and ceramide-induced apoptosis. Oncogene, 22: 5897–5906.

19. Valaperta, R., Chigorno, V ., Basso, L., Prinetti, A., Bresciani, R., Preti, A., Miyagi, T., Sonnino, S.(2006) Plasma membrane production of ceramide from ganglioside GM3 in human fibroblasts. FASEB J. 20: 1227–1229.

20. Aureli, M., Masilamani, A.P., Illuzzi, G., Loberto, N., Scandroglio, F., Prinetti, A., Chigorno, V., Sonnino, S. (2009) Activity of plasma membrane beta-galactosidase and beta-glucosidase. FEBS Lett. 583, 2469–2473.

21. Attard G., Belldegrun A.S., De Bono J.S. Selective blockade of androgenic steroid synthesis by novel lyase inhibitors as a therapeutic strategy for treating metastatic prostate cancer. BJU Int 2005;96:1241-1246.

22. Auchus R.J. Overview of dehydroepiandrosterone biosynthesis. Semin Reprod Med 2004;22:281-288.

23. Locke J.A., Guns E.S., Lubik A.A., Adomat H.H., Hendy S.C., Wood C.A., et al. (2008) Androgen levels increase by intratumoral de novo steroidogenesis during progression of castration-resistance prostate cancer. Cancer Res 2008;68:6407-6415.

24. Montgomery R.B., Mostaghel E.A., Vassella R., Hess D.L., Kalhorn T.F., Higano C.S., et al. (2008) Maintenance of intratumoral androgens in metastatic prostate cancer: a mechanism for castration-resistant tumor growth. Cancer Res, 68:4447-4454.

25. Sonnino, S., Chigorno, V ., Tettamanti, G. (2000) Preparation of radioactive gangliosides, 3H or 14C isotopically labeled at oligosaccharide or ceramide moieties. Methods Enzymol. 311, 639–656.

26. Aureli, M., Loberto, N., Lanteri, P., Chigorno, V ., Prinetti, A., Sonnino, S. (2011) Cell surface sphingolipid glycohydrolases in neuronal differentiation and aging in culture. J. Neurochem. 116, 891–899.

27. Mehlen, P., Rabizadeh, S., Snipas, S.J., Assa-Munt, N., Salvesen, G.S., Bredesen, D.E. (1998) The DCC gene product induces apoptosis by a mechanism requiring receptor proteolysis. Nature 395, 801–804.

28. Overkleeft, H.S., Renkema, G.H., Neele, J., Vianello, P., Hung, I.O., Strijland, A., van der Burg, A.M., Koomen, G.J., Pandit, U.K., Aerts, J.M. (1998) Generation of specific deoxynojirimycin-type inhibitors of the non-lysosomal glucosylceramidase. J. Biol. Chem. 273, 26522–26527.

29. Prinetti, A., Basso, L., Appierto, V ., Villani, M.G., Valsecchi, M., Loberto, N., Prioni, S., Chigorno, V ., Cavadini, E., Formelli, F., Sonnino, S. (2003) Altered Sphingolipid Metabolism in N-(4-Hydroxy- phenyl)- retinamide-resistant A2780 Human Ovarian Carcinoma Cells. J. Biol. Chem. 278, 5574–5583.

30. Kolter, T., Sandhoff, K. (1999) Sphingolipids-their metabolic pathways and the pathobiochemistry of nerodegenrative diseases. Angew. Chem. Int. Ed. 38, 1532–1568.

31. Aureli, M., Loberto, N., Chigorno, V ., Prinetti, A., Sonnino, S. (2010) Remodeling of sphingolipids by plasma membrane associated enzymes. Neurochem Res., 36(9):1636-44

32. Sonnino, S., Aureli, M., Loberto, N., Chigorno, V ., Prinetti, A. (2010) Fine tuning of cell functions through remodeling of glycosphingolipids by plasma membrane-associated glycohydrolases. FEBS Lett. 584, 1914–1922.

33. Goni, F.M., Alonso, A.: Biophysics of sphingolipids I. (2006) Membrane properties of sphingosine, ceramides and other simple sphingolipids. Biochim. Biophys. Acta 1758, 1902–1921.

34. Huschtscha, L.I., Bartier, W.A., Ross, C.E., Tattersall, M.H. (1996) Characteristics of cancer cell death after exposure to cytotoxic drugs in vitro. Br. J. Cancer 73, 54–60.

35. Santana, P., Pena, L.A., Haimovitz-Friedman, A., Martin, S., Green, D., McLoughlin, M., Cordon-Cardo, C., Schuchman, E.H., Fuks, Z., Kolesnick, R. (1996) Acid sphingomyelinase-deficient human lymphoblasts and mice are defective in radiation-induced apoptosis. Cell 86, 189–199.

36. Haimovitz-Friedman, A., Kan, C.C., Ehleiter, D., Persaud, R.S., McLoughlin, M., Fuks, Z., Kolesnick, R.N. (1994) Ionizing radiation acts on cellular membranes to generate ceramide and initiate apoptosis. J Exp Med. 180, 525–535.

37. Ward, J.F. (1994) The complexity of DNA damage: relevance to biological consequences. Int. J. Radiat. Biol. 66, 427–432.

38. Coleman, C.N. (1993) Beneficial liaisons: radiobiology meets cellular and molecular biology. Radiother. Oncol. 28, 1–15

39. Liu C., Zhu Y., Lou W., Nadiminty N., Chen X., Zhou Q., Shi X.B., de Vere White R.W., Gao A.C. (2013) Functional p53 determines docetaxel sensitivity in prostate cancer cells. Prostate. 73(4):418-27.

40. Verheij, M., Bartelink, H. (2000) Radiation-induced apoptosis. Cell Tissue Res. 301, 133–142.

41. Aureli M., Bassi R., Prinetti A., Chiricozzi E., Pappalardi B., Chigorno V., Di Muzio N., Loberto N., Sonnino S. (2012) Ionizing radiations increase the activity of the cell surface glycohydrolases and the plasma membrane ceramide content. Glycoconj J, 29:585–597.

Theme II

Bladder cancer cell growth and motility implicate cannabinoid 2 receptor-mediated modifications of sphingolipids metabolism

Introduction

BLADDER CANCER

Epidemiology and incidence

Bladder cancer (BC) is the most common malignancy form of the genitourinary tract. It's estimated more than 350 000 diagnosed cases each year, with an incidence two fold higher in Caucasians [1] and three fold higher in men than women, which, however, show a more advanced stage of disease and lower chance of survival [2]. Bladder cancer is usually diagnosed in elderly individuals, with an average age of 69 years for men and 71 for women [3].

Risk factors

Several risk factors have been investigated in order to assess a correlation with the occurrence of BC: smoking is the most important risk factor for bladder cancer. Smokers are at least 3 times as likely to get bladder cancer as nonsmokers. Smoking causes about half of the bladder cancers in both men and women. When smokers inhale, some of the carcinogens (cancer-causing chemicals) in tobacco smoke are absorbed from the lungs and get into the blood. From the blood, they are filtered by the kidneys and concentrated in the urine. These chemicals in urine can damage the cells that line the inside of the bladder, which increases the chance of cancer developing [4,5]. Workers in industries that use certain organic chemicals also may be at risk for bladder cancer if exposure is not limited by good workplace safety practices. The industries carrying highest risks include the makers of rubber, leather, textiles, and paint products as well as printing companies. Other workers with an increased risk of developing bladder cancer include painters, machinists, printers, hairdressers (likely because of heavy exposure to hair dyes), and truck drivers (likely because of exposure to diesel fumes) [6]. In addition, chemotherapy and ionizing radiation therapy has been reported increase the risk of bladder cancer: cyclophosphamide is an alkylating agent used in the treatment of lymphomas and leukemias resulting particularly toxic to the lining of the bladder leading to anomalies epithelium [7]. The treatment of a primary tumor with ionizing radiation may lead to the development of a secondary tumor to bladder [8]. Urinary infections, kidney and bladder stones, bladder catheters left in place a long time, and other causes of chronic bladder irritation have been linked with bladder cancer (especially squamous cell

carcinoma of the bladder), but it is not clear if they actually cause bladder cancer. Schistosomiasis (also known as *bilharziasis*), an infection with a parasitic worm called *Schistosoma hematobium* that can get into the bladder, is also a risk factor for bladder cancer. In countries where this parasite is common (mainly in Africa and the Middle East), squamous cell cancers of the bladder are seen much more often. This is an extremely rare cause of bladder cancer in the United States.

Classification and staging

Bladder cancer is a very heterogeneous disease. Histologically can manifest as urothelial carcinoma, adenocarcinoma, squamous cell carcinoma and small cell carcinoma. In more than 90% of cases occur as urothelial or transitional cells, and 70-85% of these are defined and categorized as superficial non-muscle invasive bladder cancer (NMIBC) as opposed to muscle-invasive cancer (MIBC) which affects the deeper layers of the bladder tissue and muscle [9]. The grade of the tumor is a parameter that is considered to have prognostic information and for assessing the progression. The classification was proposed by the World Health Organization (WHO) and the International Society of Urological Pathology (ISUP) in 1973 and then revised in 2004 [10]. This classification provides for the presence of a low and a high degree of carcinoma which differ for a different incidence of the risk of progression and a different cell differentiation (Figure 1).

2004 WHO/ISUP classification	WHO 1973 Classification
Papillary urothelial neoplasm of low malignant potential	Grade 1
Low-grade papillary urothelial carcinoma	Grade 1; Grade 2
High-grade papillary urothelial carcinoma	Grade 2; Grade 3
Carcinoma *in situ*	Carcinoma *in situ*

Figure 1. WHO classification of bladder cancer.

The pathologic stage of urothelial carcinoma is very important to determine prognosis and treatment, and the classification system that takes account of the staging of cancer is the TNM (tumor/node/metastasis), developed in

1946 by the "*Union Internationale Contre le Cancer* " and subsequently revised. This classification allows to evaluate bladder tumors by local extension (T), to the interest of regional lymph nodes (N) and presence of distant metastasis (M) (Figure 2).

Primary tumor (T)
TX Primary tumor cannot be assessed
T0 No evidence of primary tumor
Ta Papillary noninvasive carcinoma
Tis Carcinoma *in situ*
T1 Tumor invades subepithelial connective tissue
T2 Tumor invades the muscularis
T3 Tumor invades into periureteric fat, peripelvic fat, or the renal parenchyma
T4 Tumor invades adjacent organs, or through the kidney into the perinephric fat

Regional Lymph Nodes (N)
Nx Regional nodes cannot be assessed
N0 No regional lymph node metastasis
N1 Metastasis in a single lymph node, 2 cm or less in greatest dimension
N2 Metastasis in a single lymph node, more than 2 cm but not more than 5 cm in greatest dimension; or multiple lymph nodes, none more than 5 cm in greatest dimension
N3 Metastasis in a lymph node, more than 5 cm in greatest dimension

Distant Metastasis (M)
Mx Distant metastasis cannot be assessed
M0 No distant metastasis
M1 Distant metastasis

Figure 2. TNM Classification. The TNM Classification of Malignant Tumours (TNM) is a cancer staging notation system that gives codes to describe the stage of a person's cancer, when this originates with a solid tumor: T describes the size of the original (primary) tumor and whether it has invaded nearby tissue, N describes nearby (regional) lymph nodes that are involved, M describes distant metastasis (spread of cancer from one part of the body to another).

Based on the TNM system pT0, pTa, pT1 and pTis were considered non-muscle invasive tumors and pT2, pT3 and pT4 as muscle invasive tumors [11]. PT0 cancer is a condition in which there is no evidence of residual cancer after an initial diagnosis; stadium pTa is defined as non-muscle-invasive papillary carcinoma with no invasion of the lamina propria; pT1 identifies the invasion of the lamina propria [10-13]. Among the superficial tumors are also identifies carcinoma in situ (CIS). CIS is a non-invasive urothelial carcinoma, consists of cytologically high grade tumour cells [14, 15]. Finally, the stage pT2, pT3 and pT4, are muscle invasive tumors that identify, first, an invasion of the muscularis mucosae, and second, invasion

to perivesical tissue and adjacent organs, such as uterus , vagina, prostate, pelvic and abdominal wall [11] (Figure 3).

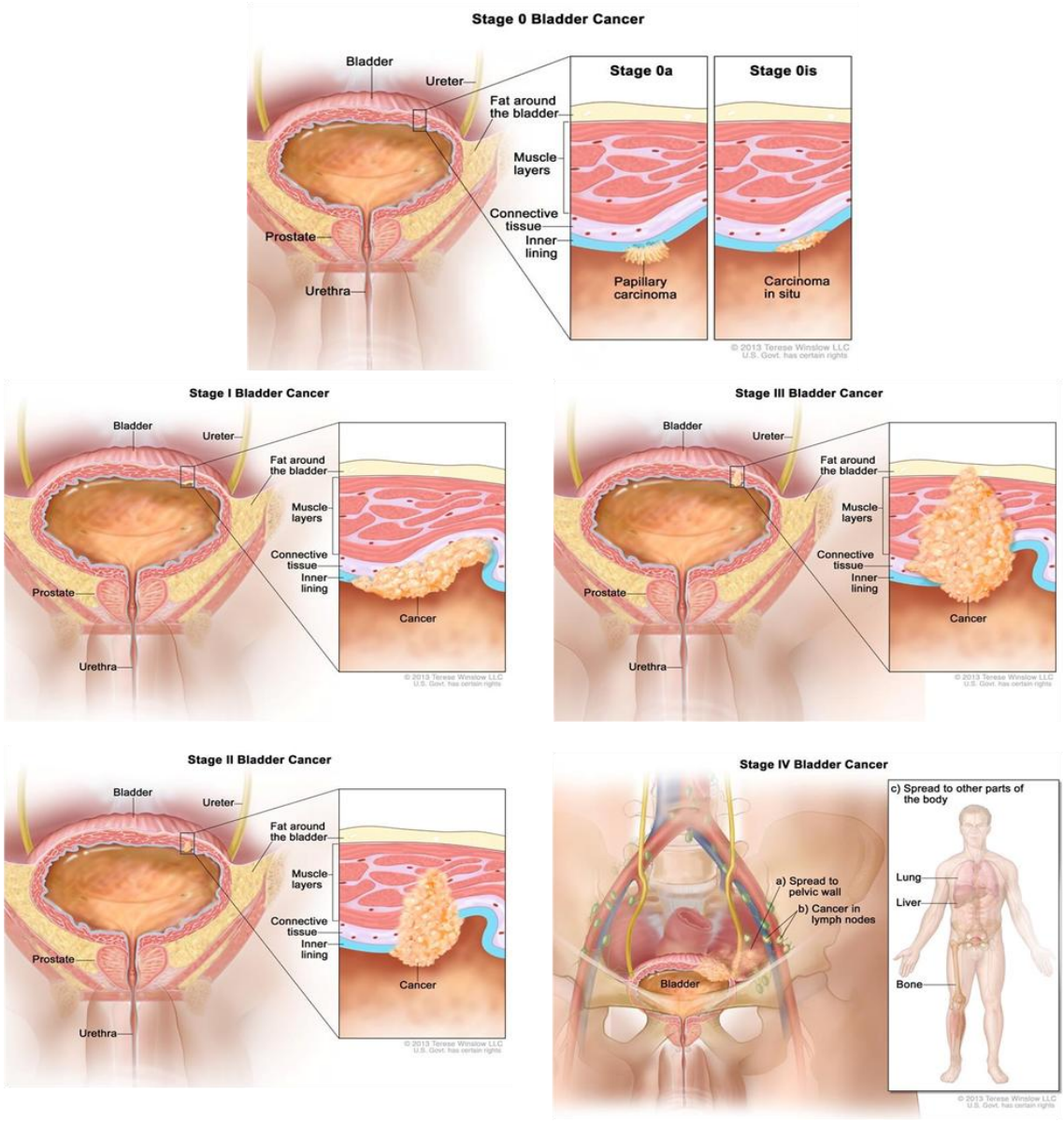

Figure 3. The TNV classification can be integrated into a numerical staging as follows: Stage 0a: Ta, N0, M0, Stage 0is: Tis, N0, M0; Stage I: T1, N0, M0; Stage II: T2a or T2b, N0, M0; Stage III: T3a, T3b, or T4a, N0, M0; Stage IV; any of the following: T4b, N0, M0 any T, N1 to N3, M0 any T, any N, M1.

__Aim__

Clinically, 75-80% of bladder neoplasms correspond to non-muscle-invasive bladder cancer (NMIBC) at diagnosis. After transurethral resection of the tumor followed by adjuvant chemotherapy, 30 to 50% of patients recur, and more than 15% of those undergo progression to muscle-invasive disease [16]. Identification of novel potential targets to reduce recurrence and prevent disease progression represents a medical need for bladder cancer. Among the various putative novel biomarkers or targets recently described for urothelial carcinoma [17], the endocannabinoid system (ECS) expressed by the genitourinary organs has recently gained particular attention. The ECS components such as CB1, CB2 receptors, and the endocannabinoid-degrading enzyme fatty acid amide hydrolase (FAAH) are present in the bladder at the epithelial level and play a role in regulating bladder functions {18-20]. As recently shown, both clinical and experimental evidence has indicated a possible role of the ECS in modulating cancer proliferation, progression and metastasis [21] in several types of neoplastic diseases, including, prostate and breast cancer [22,23]. Of note, little information is available on the possible role of ECS components in proliferation [24] and metastasis of human urothelial carcinoma, or on the mechanisms underlying progression to the muscle invasive phenotype. In this context, glycosphingolipids (GSL) play an important role. As previously reported GSL are components of the cell plasma membranes that change dramatically during differentiation and malignant transformation [25]. Aggressive, muscle-invasive bladder cancer is in fact characterized by a different expression of the glycolipids GM3 and Gb3 [26], suggesting that the metabolism of GSL plays a role in controlling bladder cancer cell invasion and motility [27]. Similarly, the known antiproliferative activity of cannabinoids in cancer models is reported to involve the activation of membrane-associated metabolism of sphingolipids with concomitant accumulation of ceramide (Cer) via *de novo* synthesis [28-30] and possible activation of the Cer/sphingosine-1-phosphate (S1P) rheostat [31]. However, the role of CB2 activators in bladder cancer survival and motility and the interplay with GSL pathways still remains poorly characterized.

The present study is aimed to investigate the expression and activity of CB2 receptor in human bladder cancer in relation to molecular signals mediated by plasma membrane GSL. I have identified a molecular pathway, partly

based on CB2-dependent modulation of GSL, by which bladder cancer survival and progression is possibly mediated.

Materials and Methods

MATERIALS

RPMI 1640 medium, trypsin-EDTA solution, MTT, protease/phosphatase inhibitor cocktail, and JWH015, were purchased from Sigma (Milan, IT). The Fetal calf serum was from Gibco (Euroclone, Milan, IT). Primary antibodies anti-CB1, anti-CB2 and anti-FAAH, anandamide, rimonabant, SR144528, oleoyl ethyl amide and Annexin V/PI detection kit were from Cayman Chemical (Space Import, Milan, IT). The primary antibody anti-GAPDH and HRP conjugated secondary antibodies were from Santa Cruz Biotechnology. Primary antibodies anti-cleaved Caspase-3, Ezrin EZR, pERM were from Cell Signaling Technology (Danvers, MA, USA), while anti SRC/pSRC were from AbCam.

The preparation of isotopically labeled of [1-^{3}H]sphingosine (specific radioactivity, 2.2 Ci/mmole) has been described in detail [32].

METHODS

Immunohistochemical Analysis of Human bladder cancer

After institutional Ethical Committee approval, archival material was obtained from internal pathologists. Histology was carried out on surgical specimens of 13 consecutive patients, not subjected to neoadjuvant chemotherapy, with transitional, muscle-invasive bladder cancer, which were fixed in 4% paraformaldehyde solution in PBS, paraffin embedded, cut at 4 μm and mounted on slides. Sections were stained with either hematoxylin-eosin or for immunohistochemistry by using a LSAB+HRP Kit (DAKO). The specificity of CB1 and CB2 antibodies has been previously described [33,34]. Immunohistochemical staining's were digitally scanned and analyzed by using the Aperio system with color deconvolution algorithm.

Cell cultures and treatments

Human transitional carcinoma cell lines RT112 and RT4 were originally purchased from ATCC. Both tumor cell lines were maintained in RPMI 1640 medium supplemented with 10% FCS. Cells were routinely subcultured by 0.05% trypsinization. Normal human fibroblast were cultured as previously reported [35]. MB49 murine bladder cancer cells were kindly provided by Dr. Angelica Loskog (University of Uppsala, Sweden) and routinely cultured as above. For cell viability assay, cells were seeded in quadruplicates in 96-well plates and incubated in 200 μl of complete RPMI to achieve 60% to 90% confluency. Cannabinoid agonists and/or antagonists were serially diluted (0.1-20 μM) into culture medium; cells were exposed to the compounds ranging from 24 to 120 hours. Cell viability was assayed by standard MTT incorporation. To perform metabolic labeling, cells were pulsed with 3 x 10^{-8} M [1-^{3}H]sphingosine 24 hrs after seeding in a culture dish. Two hours after, cells were replaced with fresh medium without [1-^{3}H]sphingosine containing 20 μM JWH015 and further incubated for 72 hours. Under these conditions, all sphingolipids (including ceramide, sphingomyelin, neutral glycolipids, and gangliosides) were metabolically radiolabeled at a steady state [36].

Immunoblotting analysis of protein patterns

Cells were lysed in ice-cold RIPA buffer containing protease and phosphatase inhibitors. Equivalent protein amounts were separated on SDS-PAGE gels

and transferred onto PVDF membrane by elettroblotting. After blocking with 5% skim milk in TBS-T buffer, membranes were incubated ON at 4°C with primary antibody. After washing, 1 hour (RT) incubation with appropriate HRP-labeled secondary antibodies was done. Immunoblot was revealed by using a chemoluminescence detection kit (Life Technologies, Milan IT). Densitometric analysis was performed with ImageJ (Denovo software).

Lipid extraction and determination

Upon metabolic steady-state radiolabelling of cellular lipids with [1-^{3}H]sphingosine, the content of radioactivity associated with each lipid was analyzed. Radiolabeled cells were harvested in 2-ml ice-cold water and lyophilized. Cellular lipids were then extracted by using a chloroform/methanol/water solution (2:1:0.1 by vol). The total lipid extracts were subjected to a two-phase partitioning and processed as previously described [37].

RNA isolation and RT-PCR analysis

Total RNA was isolated from the bladder cancer cells using a TRIzol Reagent kit (Invitrogen, Carlsbad, CA). Complementary DNA (cDNA) was synthesized from total RNA by using Super ScriptTM III Reverse Transcriptase (RT; Invitrogen). The following primer pairs were used: hCB2 forward 5'-TATGGGCATGTTCTCTGGAA-3', reverse 5'-GAGGAGCACAGCCAACACTA-3'; hCB1 forward 5'-CGCTTTCCGGAGCATGTT-3', reverse 5'-TCCCCCATGCTGTTATCCA-3'; β-actin forward 5'-CGACAGGATGCAGAAGGAG-3', reverse 5'-ACATCTGCTGGAAGGTGGA-3'. Thirty-five cycles were performed at 94°C for 30 sec, 57°C for 1 min and 72°C for 1 min (see suppl. Methods for primer sequences). The PCR products were separated on 1.5% (w/v) agarose gel and visualized by ethidium bromide staining.

Real-time qPCR

One μg of total RNA was reverse-transcribed into cDNA using a High Capacity cDNA kit (Applied Biosystems) according to the manufacturer's protocol. RT-PCR was performed on an ABI Prism 7000 system (Applied Biosystems, Foster City, CA, USA) and the cycling conditions used were 95°C

for 15 sec, 60°C for 1 min, for 40 cycles, followed by a melting point determination for dissociation curves. The relative amount of mRNA was calculated by using standard curves after normalization to the endogenous housekeeping genes GAPDH and HPRT1. PCR primers were designed with the Primer3 program to generate amplicons of 100-150 bp. The following primer pairs were used: GAPDH forward 5'-GGACTCATGACCACAGTCCA; reverse 5'- CCAGTAGAGGCAGGGATGAT; HPRT1, forward 5'-TGCAGACTTTGCTTTCCTTG; reverse 5'- CTGGCTTATATCCAACACTTCG; CB1, forward 5'- CCAGCAGACCAGGTGAACAT; reverse 5'-GGGTTCAGGACCATGAAACACT; CB2 , forward 5'-CCTGTTCATTGGCAGCTTGG; reverse 5'-TCAGCAGGAAGACAGCCTTG; alpha 1,4-galactosyltransferase (A4GALT), forward 5'- TCTGCACCCTGTTCATCATC; reverse 5'- CTTTCTCCTTGGGCTCTCC; ceramide synthase 2 (CERS2), forward 5'- TCCGACTGGGACTCTTAATC; reverse 5'-TGTTGCAGGTGTTCTTCCAT; ceramide synthase 3 (CERS3), forward 5'-GAATCAAGAGAGGCCTTCCA ; reverse 5'-GCAATTCCAGCAACAGTGAT; membrane sialidase 3 (NEU3), forward 5'-CCTGAAGCCACTGATGGAA ; reverse 5'-TTCCTGCCTGACACAATCTG; Lactosylceramide alpha-2,3-sialyltransferase (ST3GAL5); forward 5'-AATTGGCGCTGTTATTTGAGC; reverse 5'-CTGGCAAGAGTTCCAAGAGG; sphingosine kinase 1 (SPHK1), forward 5'-CCCCAGCAAACCGGACCGAC; reverse 5'-CCCCAGCAAACCGGACCGAC; sphingosine kinase 2 (SPHK2), forward 5'-CCCCTCAGACTCAGCGGCCT; reverse 5'-GTGGGCGAGGCAGGTTCCAC.

Wound-healing/invasion assays

Cells were plated at 90% confluence in 5% serum-DMEM. Twenty-four hours after seeding, the monolayers were scratched with a sterile plastic 200-µL micropipette tip, washed, and fed with culture medium containing the appropriate concentrations of DMSO or JWH015 compound. Cell-free area was quantified using ImageJ software (Denovo software). Three measurements were performed for each wound before the addition of agonists and, in a blinded fashion, after 24 hours of stimulation. Each experiment was performed in triplicate at least 3 times. Invasion assay was carried out in BioCoat Matrigel Invasion Chambers (BD Biosciences, Milan, Italy) according to the manufacturer's protocol.

Plasma Membrane (PM) associated glycohydrolase assays

We recently described a simple method, that allows to measure the activity of several glycohydrolases associated with the PMs of intact living cells [38]. This method is based on the observation that the fluorigenic substrates commonly used for the in vitro assay of glycohydrolase activity are not taken up by living cells [39]. In fact, under the appropriate experimental conditions, we did not observe any fluorescence associated with the cells. Moreover, the artificial substrates were not subjected to spontaneous, non-enzymatic hydrolysis nor hydrolyzed in observable entity by secreted enzymes. Thus, their hydrolysis under these experimental conditions is due exclusively to the PM associated enzymatic activities [37,38]. PM associated β-galactosidase (β-Gal), conduritol B epoxide (CBE)-sensitive β-glucosidase GBA1, β-glucosidase GBA2, β-hexosaminidase (β-Hex) and SMase activities were determined in control or differently treated living cells plated in 96-well microplate at different density (depending on the cell lines and by the type of treatment), by a high throughput assay (HTA). For GBA1 and GBA2 assays, the cells were pre-incubated for 30 minutes at room temperature with 5 nM AMP-dNM (adamantane-pentyl-DNM; N-(5-adamantane-1-yl-methoxy-pentyl) deoxynojirimycin) [39] and 1 mM CBE (Sigma) in DMEM-F12, respectively. The β-Gal, β-Hex and β-Glc activities were assayed using the artificial substrates MUB-Gal, MUG and MUB-Glc solubilized in DMEM-F12 without phenol red at pH 6 at the final concentrations of 250 μM, 2 mM and 6 mM respectively. At various times, aliquots of the medium were analyzed fluorometrically by using a microplate reader (Victor, Perkin Elmer) with the addition of 20 volumes of 0.25 M glycine (Sigma), pH 10.7. The data were expressed as n/pmoles of converted substrate/mg cells proteins/hr. Control experiments were performed to exclude any activity released from lysosomes and/or from other intracellular sites.

Enzymatic activities of cell lysates

The enzymatic activities of β-Galactosidase, β-Glucosidase GBA1 and GBA2 and β-Hexosaminidase associated with total cell lysates were determined using fluorigenic substrates as described previously [40] with some modifications. Briefly, cells were washed twice with PBS, harvested, and resuspended in water in the presence of a protease inhibitor. Aliquots of the cell homogenates were transferred into a 96-well microplate and enzymatic

assays performed with three-fold replication. MUB substrates were solubilized in McIlvaine buffer at the same final concentration and the same pH used for the in vivo assay. The reaction mixtures were incubated at 37°C with gentle shaking. The developed fluorescence was detected at various times by a Victor microplate reader (Perkin Elmer) after transferring 10 µl of the reaction mixtures to a microplate and adding 190 µl of 0.25 M glycine, pH 10.7.

Sphingosine kinase 1 (SK1) activity was assayed as previously described [41]. For the analysis of sphingosine-1-phosphate (S1P) production, cells were pulsed with [1-^{3H}]sphingosine for 45 min as previously described [42].

Statistics

All the experiments have been performed threefold in replicate and repeated three times. Data are presented as the mean values ± standard deviations and were tested for significance employing ONE or Two way ANOVA with Bonferroni post-test analysis, as specified in figure legends. The level of significance was set at $p<0.05$.

Other analytical methods

The radioactivity associated with lipid extracts was determined by liquid scintillation counting. The protein assays were carried out using the DC Protein Assay kit (Biorad).

Results

Expression of cannabinoid receptors in human bladder cancer

Immuno-histochemistry on tissue slides showed specific reactivity for both CB1 and CB2 in normal urothelium, vascular endothelium and inflammatory infiltrates. Whereas immunoreactivity for CB1 appeared similar in healthy and neoplastic lesions, signal for CB2 was observed to be increased in tumor tissue. Particularly, by comparing the malignant urothelium and stroma (Figure 1, panel A-B, arrowheads) to the adjacent normal peritumoral tissue (Figure 1, panel A-B, asterisks), the differential level of expression was found to be higher for CB2 (Figure 1B) than for CB1 (Figure 1A). Evaluation of the relative expression carried out by quantitative image analysis (Aperio) on 13 separated tissue specimens having paired normal urothelium and tumor tissue represented on the same slides, revealed a significant higher staining score of CB2 in primary bladder cancer when compared to normal urothelium (Figure 1D). No significant differences were detected for the CB1 (Figure 1C).

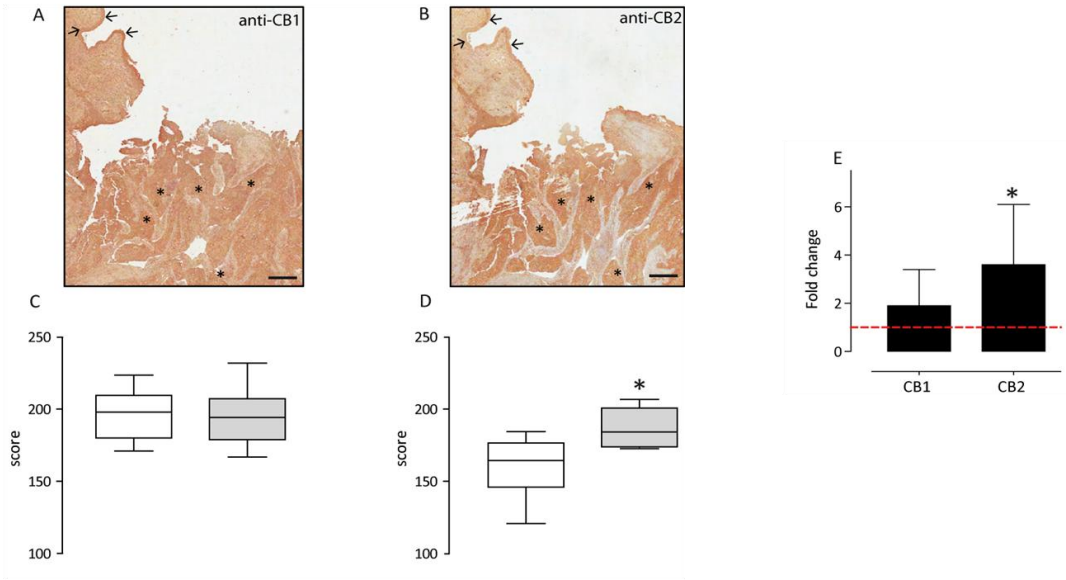

Figure 1. Expression of CB in human BCa. Representative immunoreactivity (scale bars: 500 μm) of cannabinoid CB1 (panel A) and CB2 (panel B) receptors from a representative patient with muscle invasive bladder carcinoma. Tumor lesion (asterisk) and normal urothelium (arrows) are indicated. Formalin-fixed paraffin-embedded sections from 13 different tumor specimens stained with hematoxylin and CB1 and CB2 antibodies (DAB) were analyzed with the Color Deconvolution analysis tool to quantify the DAB staining intensity. Staining score of CB1 (panel C) and CB2 (panel D) receptors were measured on the tumor lesion (grey bars) and normal epithelium (white bars) of 13 different patients in at least triplicate slides for each case. * $p< 0.05$ vs normal urothelium, Student T Test. Control staining in the presence of displacing CB1 and CB2 peptides are shown in Suppl. Fig. 1. Panel E: CB1 and CB2 gene expression analysis of primary muscle invasive BCa (N=5) by quantitative PCR analysis. Data are the mean±sd of quadruplicate fold-increase values over the paired non tumoral tissue (represented by the red dashed line). * $p < 0.05$ vs normal tissue.

The immunoreactivity of both CB1 and CB2 was found to be specific as confirmed by control staining in the presence of competing peptides (Figure 2).

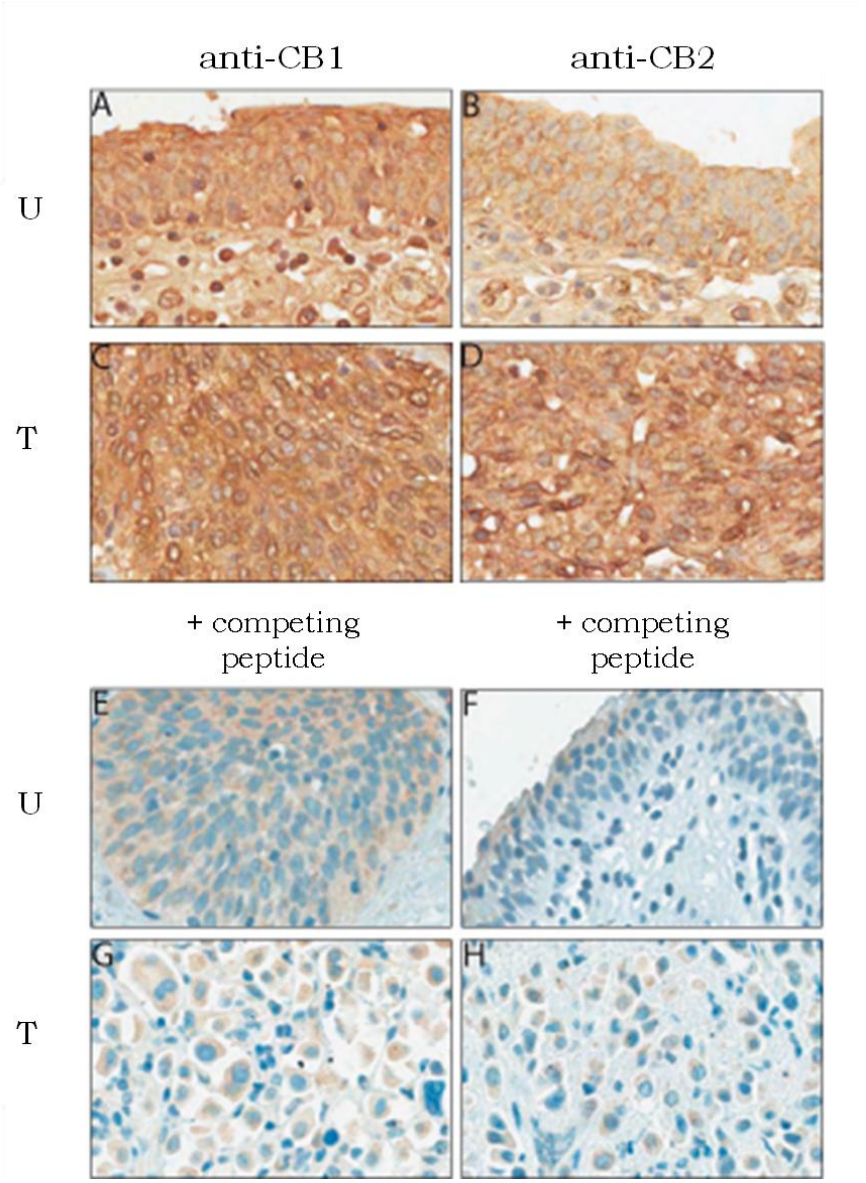

Figure 2. Competing cannabinoid receptor staining. Immunohistochemical analysis of CB1 and CB2 receptor expression in human normal urothelium (U) and muscle invasive urothelial tumor (T), on the same section (magnification 200X).

The presence of CB expression was also assessed and confirmed in five human specimens of primary bladder cancer collected perioperatively. Samples were analyzed by real-time PCR and displayed variable but consistently higher levels of CB2 when compared to normal urothelial tissue specimens from the same patient. CB1 was less expressed in the tumor and not differently expressed in comparison to normal tissue (Figure 1E). As

supportive data, expression of CB2 was analyzed in silico by interrogating the expression data available on bladder cancer patients collected by The Cancer Genome Atlas [43]. As shown in Figure 3 panel A, the expression of CB2 is significantly higher in invasive tumors. Expression of CB1 and CB2 was also evaluated in bladder cancer cells by RT-PCR and WB analyses. Both bladder cancer RT4 and RT112 cell lines were positive for CB1 and CB2 genes and expressed the CB2 protein to a similar extent. Conversely, CB1 protein was only detectable in RT4 cells (Figure 3, panel B-C).

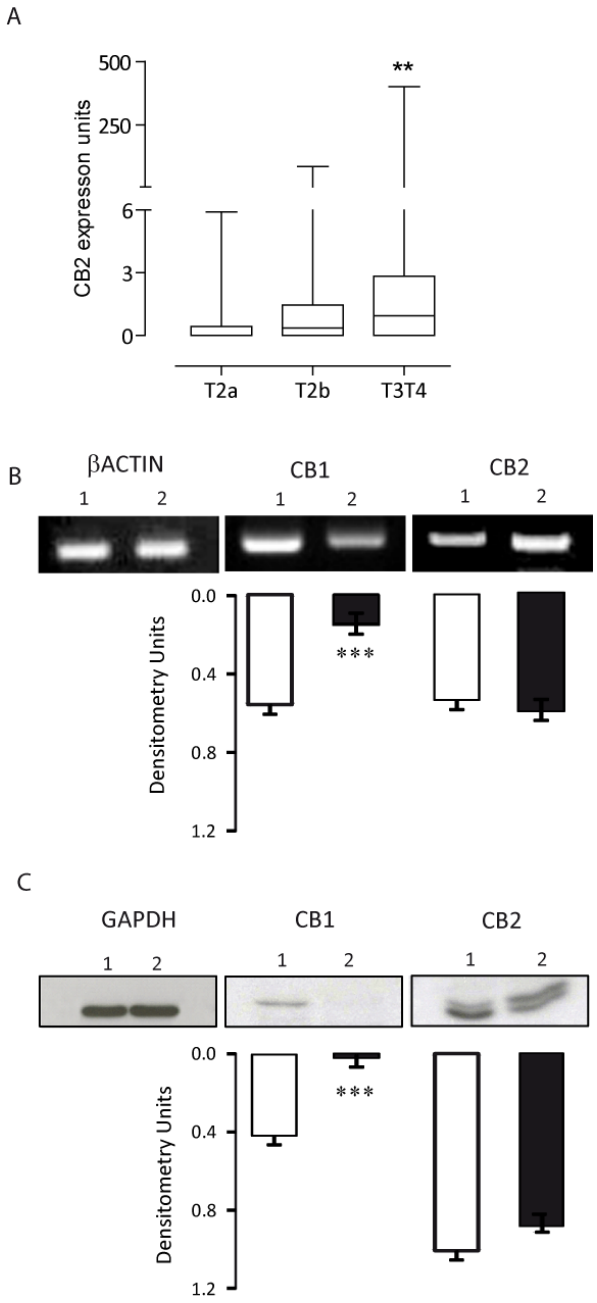

Figure 3. Expression of CB in BCa tumors and cell lines.

Panel A: in silico analysis of the expression of CB2 receptors in primary muscle-invasive bladder cancers. Data are expressed as box-and-whiskers plots encompassing 28 samples of T2a tumors, 37 samples of t2b tumors, and 137 samples of T3T4 tumors. Error bars represent the max value in each group.

Panel B and C: Expression of cannabinoid receptors assessed by RT-PCR (A) and western blot (B) in RT4 (lane 1) and RT112 (lane 2) cells. The densitometric analysis of the relative bands for CB1 (66 bp or 60kDa) and CB2 (141 bp or 40-45 kDa), compared to reference housekeeping gene (β-Actin, 137 bp or GAPDH, 39 kDa), from three separated experiments are shown (*** $p<0.001$ vs lane 1, Student's T test).

Effect of the modulation of endocannabinoids system on human bladder cancer cell viability.

I investigated the effect of the endocannabinoid anandamide (AEA) and the synthetic CB2 ligands JWH015 and JWH133 on the proliferation rate of both RT4 and RT112 cells. AEA has greater affinity for CB1 than CB2, JWH015 exhibits preferential agonist activity on CB2 [44,45], whereas JWH133 is considered CB2-selective [46]. Cells were exposed to increasing concentrations of the drugs over time, and cell viability was evaluated. As expected, AEA (20 μM) displayed a cytotoxic effect that peaked 48 hrs after exposure and allowed 26.4±1.9% and 50±3.6% residual cell viability on RT4 and RT112 cells, respectively. Blockade of CBs with rimonabant (CB1 antagonist) or SR144528 (CB2 antagonist) was tested in AEA-treated RT112 cells. As shown in Figure 4A, data suggested that both receptors contributed to the early CB agonist-induced cytotoxic effects, since both CB1 and CB2 antagonists partially rescued cell viability to approx 50% 24 hrs after AEA exposure. Only CB2 receptor blockade, however, prevented cell death at longer time points, as a max 75% increase of cell viability was evident 48 hrs after AEA exposure and stabilized over time (Figure 4A). Of note, cells exposed to AEA spontaneously regained normal proliferation activity after 5 days (data not shown). Indeed, when cells were co-treated with AEA and oleoyl ethyl amide (OEtA), a specific inhibitor of FAAH enzyme, the cytotoxic effect of AEA potentiated (data not shown), suggesting that the reduced effects of AEA measured 5 days after exposure were mainly due to its degradation. In comparison to AEA, the CB2 specific agonist JWH015 exhibited stronger and concentration-dependent antiproliferative activity on both RT4 and RT112 cell lines (Figure 4B), with the specific IC_{50} value calculated around 5 μM. Kinetics experiments then evaluated cell survival up to 96 hrs after JWH015. As early as 24 hrs after drug exposure, JWH015 induced a significant decrease of cell viability that peaked four days after drug exposure, with a maximal inhibitory effect on RT4 and RT112 cell proliferation that amounted to 85±5% and 88±8% ($p<0.001$), respectively (Figure 4C). Conversely, AEA displayed a maximal inhibitory effect on cell survival by 30±5% (RT4) and 60±13% (RT112), measured 4 days post exposure. Under the same experimental conditions, JWH015 didn’tt induce any changes in the viability of human primary fibroblasts (Figure 4C).

Pretreatment with the CB2 antagonist SR144256 only partially counteracted the JWH015-induced (20 μM) antiproliferative effect by 25.6±3% ($p<0.01$ vs JWH015 alone) measured after 72 hrs incubation. To further support the CB2-mediated effect on cell viability, the agonists JWH015 and JWH133 were tested on RT112 cells in the presence of a more potent CB2 antagonist (AM630). As shown in Figure 4, panel D-E, in both cases, cell viability measured 72 hrs after agonist challenge, was partially but significantly rescued in all the cytotoxic agonist concentrations.

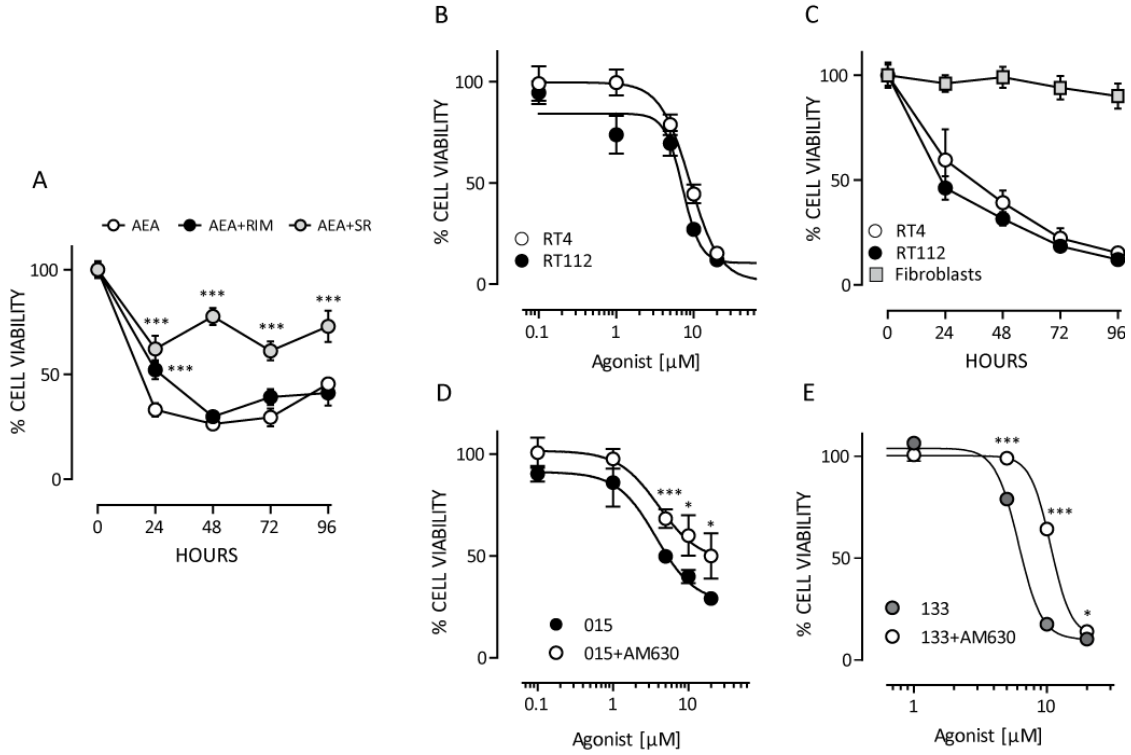

Figure 4. Effect of different cannabinoids (CB2-agonist) on bladder cancer cell proliferation.

Panel A: Antagonistic effect of CB1-specific rimonabant (RIM, 10 μM) and CB2-specific SR144528 (SR, 10 μM) drugs given simultaneously with anandamide (AEA, 20 μM) on CB1/CB2 agonist-induced toxicity of RT112 cells. Concentration of agonist and antagonists were chosen after preliminary experiments to determine optimal agonist cytotoxic effect and reliably measurable blocking effect of the antagonists when simultaneously co-administered to cells. *** $p<0.001$ vs AEA alone, 2-ways ANOVA, Bonferroni post test.

Panel B: Dose-response citotoxicity on RT112 (black symbols) and RT4 (white symbols) cells, measured 72 hours post JWH015.

Panel C: Kinetics () of cytotoxicity after 20 μM JWH015 on both RT4 (white symbols) and RT112 (black symbols) cells. The effect on normal fibroblasts is also shown (grey square symbols).

Panels D and **E**: Effect of the CB2 antagonist AM630 (0.25 μM) on CB-2 agonist-induced RT112 cell toxicity. Cells were pre-treated with AM630 for 30 min before exposure to either JWH015 (015) or JWH133 (133). Cell viability was assayed 72 hrs posr agonist challenge. * $p< 0.05$, *** $p<0.001$ vs agonist alone, 2-ways ANOVA, Bonferroni post test.

As shown in Figure 5, cell cycle analysis carried out by flow cytometry 48 hours after CB2 agonist exposure demonstrated a significant higher accumulation of cells in the sub-G1 phase (28.2 ± 1%, $p<0.01$) compared to control cells (2.2 ± 0.9%). This finding was accompanied by an evident apoptotic phenotype, as the frequency of annexin-V$^+$/PI$^+$ cells increased 6.7±0.3 ($p<0.01$) fold over untreated cells. The apoptotic phenotype was also confirmed by activated form of caspase 3 that accumulated over time (Figure 5, panel A-B) following exposure to increasing concentrations of JWH015 (Figure 5B). Caspase induction was not detectable earlier than 24 hrs after CB2 agonist exposure on RT112 cells, even in the presence of an autophagy inducer such as rapamycin (Figure 3C).

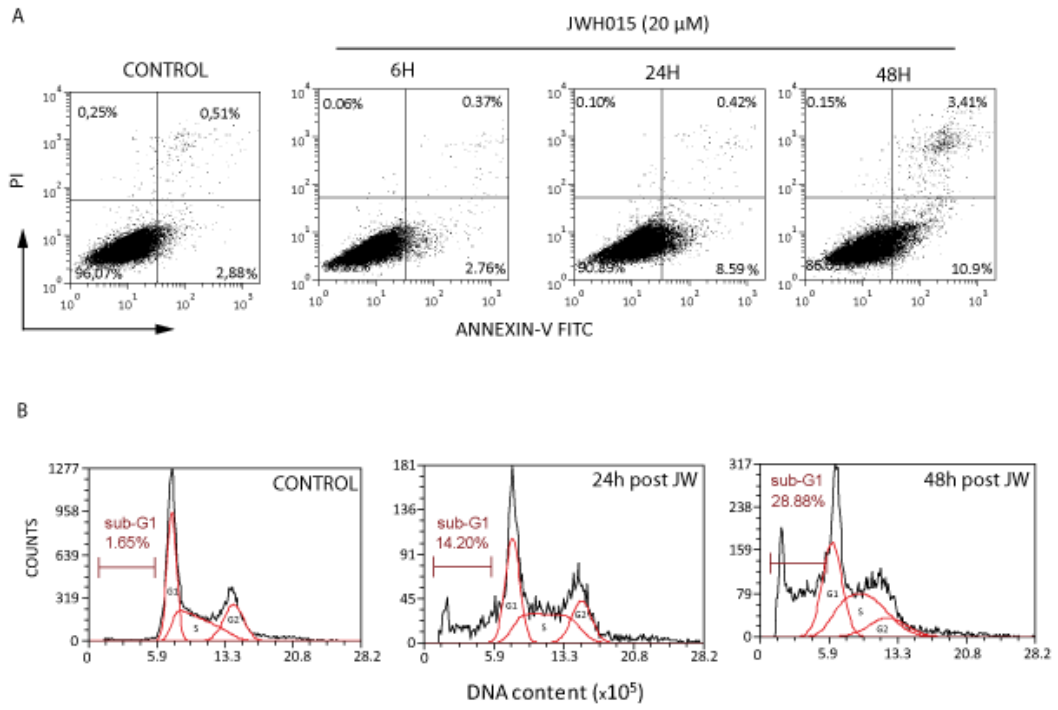

ID	% G1	% S	% G2
CONT	40.1±1.1	35.5±0.4	24.3±1.1
+ JW 24H	39.3±2.2	34.3±5.3	26.3±5.1
+ JW 48H	47.1±5.8	40.0±3.6	27.8±15

Figure 5. Cell Cycle analysis.
Panel A: representative FACS plots of annexin V/PI + cells induced by JWH015 exposure over time.
Panel B: cell cycle analysis of RT112 cells treated with JWH015 (20 µM). The frequency of sub G1 phase population is shown. The table summarizes the % of cells for each phase. Histogram plots are overlaid with the interpolation model used to calculate the cell cycle phases (red line).

Cannabinoids were previously reported to promote cell death by modulating membrane sphingolipids and inducing autophagy in tumors [47,48].

I further assessed if CB activation in bladder cancer cells triggered autophagy, induced apoptosis secondary to the accumulation of Cer, and modified related sphingolipids. As shown in Figure 6B, in RT112 cells increasing concentrations of JWH015 induced conversion from the soluble form of LC3 (LC3-I) to the lipidated and autophagosome-associated form (LC3-II, a hallmark of autophagy) that peaked 24 hours after agonist exposure. Similar results were obtained with RT4 cells (not shown). This finding was also supported by LC3 quantitative immunostaining carried out on RT112 cells 24-48 hrs after JWH015 treatment (Figure 7, panel A-C). In RT112 cells, JWH015-mediated inhibition of mTORc1, evaluated as reduced phosphorylation of p70S6, was detected already 6 hrs after agonist stimulation and counteracted by an autophagy inhibitor (Figure 7D). Analysis of temporal AKT activation (Figure 6D) in JWH015-treated cells revealed that, after an initial upregulation detected 24-48 hours after drug exposure, AKT phosphorylation was significantly reduced at day 3 and 4, consistently with the cytotoxic effect. The up regulation of pAKT measured 24 hrs after JWH015 challenge in RT112 cells was reversed (Figure 6E) by co-treatment with CB2 antagonist (SR144528) but not with CB1 antagonist (Rimonabant), suggesting a selective receptor-dependent effect. The effects of cannabinoids on the sphingolipids metabolism and in particular on Cer production were evaluated upon metabolic steady-state radiolabeling with [1-^{3}H]sphingosine, before and after exposure to JWH015. Independently of the basal cell membrane SL composition, which was different between the two cell lines tested, JWH015-treated cells exhibited 2-5-fold increased ($p<0.001$) Cer levels over the untreated cells baseline (Figure 6F). On the other hand, the levels of the pro-survival signal S1P were reduced by approximatively 40% in both cell lines ($p<0.001$; Figure 6F). Exposure to JWH015 did not change the amount of sphingomyelin (SM) (Figure 7), thus, accumulation of Cer in JWH015-treated cells probably isn't a consequence of SM hydrolysis. However, given that the prominent increase in the Cer levels detected in bladder cancer cells after JWH015 cannot be completely explained by the moderated rise of the S1P formation (Figure 6F), we carried out further investigations to quantify, before and after stimulation with JWH015, the

enzymatic activities of the intracellular and plasma membrane-associated glycohydrolases.

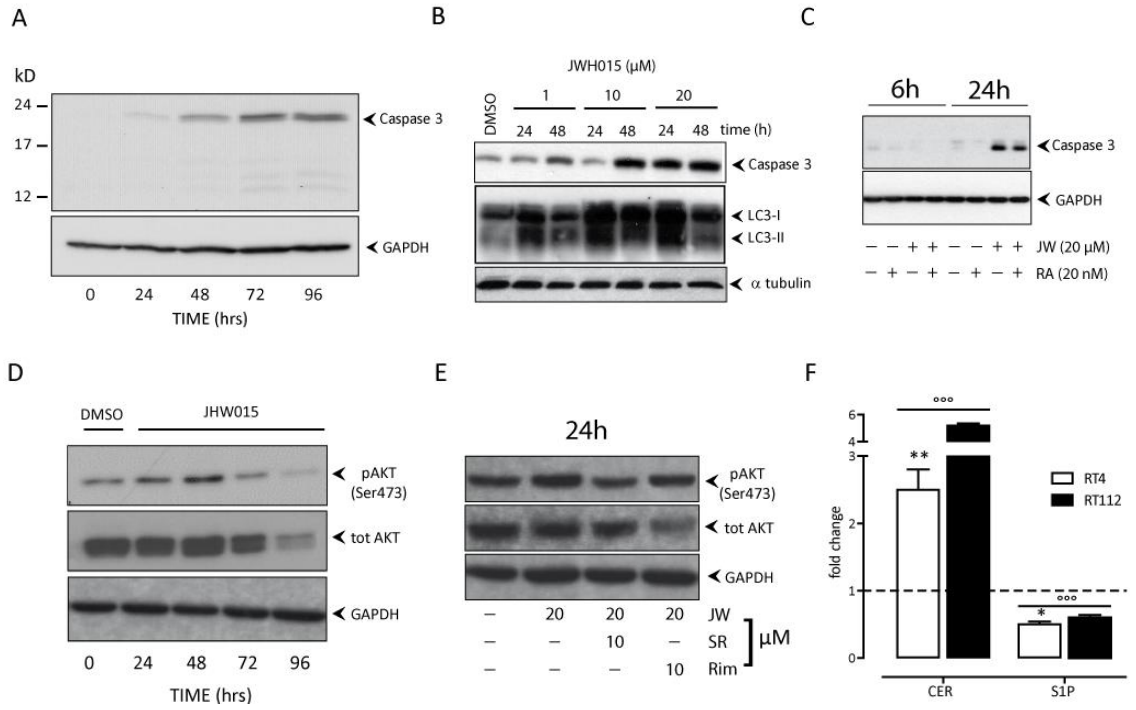

Figure 6. Molecular events driving JWH015 citotoxicity. Representative Western blot experiments showing the effect of JWH015 on apoptosis and autophagy mediators in RT112 cells. Data are expressed as fold change with respect to untreated control cells (dashed line) and are the means ± SD of three different experiments. °°° $p<0.001$ vs untreated cells baseline (dashed line); * $p< 0.05$ vs RT112. ** $p< 0.01$ vs RT112, 2-tails Student' T test.

Panel A: JWH015-mediated (20 μM) induction of caspase 3 over time (0-96 hrs).

Panel B: Dose-effect of JWH015 (1-20 μM) in inducing caspase 3 and LC3I-II 24-48 hrs post exposure.

Panel C: JWH015-mediated (JW, 20 μM) induction of caspase 3 6-24 hrs after Exposure with or without addition of rapamycin (RA, 20 nM).

Paned D: modulation of pAKT by JWH015 (20 μM) over time.

Panel E: Effect of CB1 (rimonabant, Rim, 10 μM) or CB2 (SR14452, SR, 10 μM) antagonists when simultaneously administered to cells together with the CB2 agonist (JWH015, JW, 20 μM) upon 24 hrs incubation. Untreated (DMSO) control cells were tested both at time 0 and after 96 hrs of culture with similar results. A single experiment is shown as representative of three independent ones with similar results.

Panel F: Ceramide (CER)/sphingosine 1-phosphate (S1P) rheostat levels in RT4 and RT112 cells treated with JWH015(20 μM). Cell lipids were metabolically labeled with [1-3H]sphingosine after 48 h JWH015 incubation. Radioactive lipids were visualized by digital autoradiography and quantified with specific Beta-Vision software.

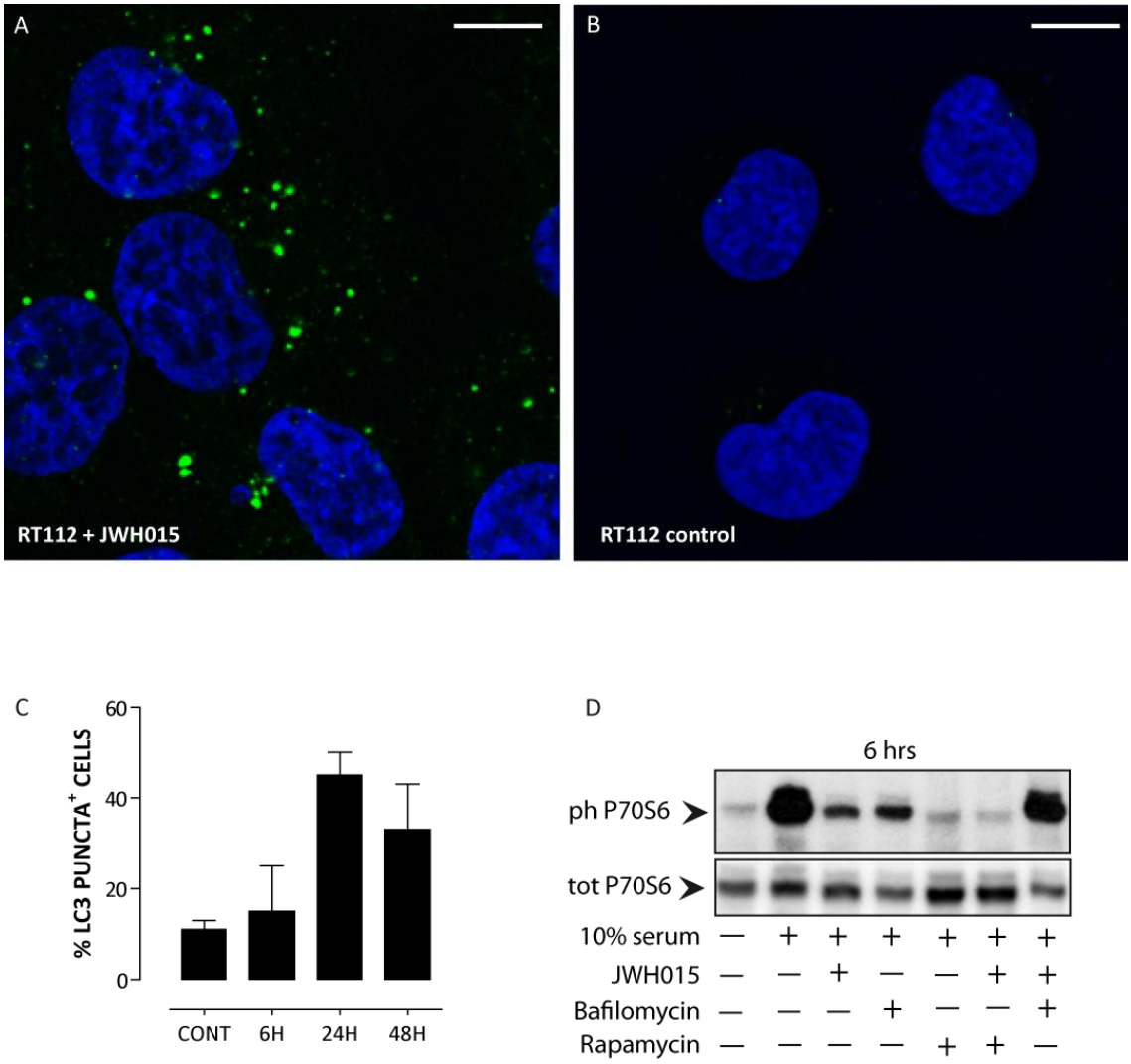

Figure 7. Autophagy occurring in RT112 upon exposure to CB2 agonist.
The conversion of the soluble form of LC3 (LC3-I) to the lipidated and autophagosome-associated form (LC3-II) was evaluated on RT112 cells upon 24 hrs exposure with JWH015 (20 μM) (Panel A) in comparison to the vehicle-treated control (Panel B). Fluorescence microscopy analysis was carried out by using a specific LC3 antibody followed by alexa-green labeled secondary pAb. Nuclei were labeled with DAPI (blue). Scale bars= 4 μm. The insoluble form of LC3 is evidenced by more intensely and condensed green-labeled intracellular localizations. Quantification of LC3 puncta^{+} cells is shown in Panel C. The percentage of cells with more than 5 LC3 punctae was calculated by counting at least 6 fields. Data are the mean±sd of quadruplicate counts in two independent experiments. Panel D: immunoblot analysis of p70SP phosphorylation in RT112 cells measured 6 hrs after JWH015 challenge (20 μM) with or without 30 min pre-treatment with rapamycin (20 nM) or bafilomycin (100 nM).

As summarized in Table 1, the activity of the enzyme devoted to sphingomyelin (SM) catabolism, namely sphingomyelinase (SMase) did not increase following JWH015 exposure, confirming that SM hydrolysis did not contribute to the build-up of ceramide. In addition, the plasma membrane-associated glycohydrolases GBA1/GBA2, β-Galactosidase and β-Hexosaminidase displayed a significant increment in the enzymatic activity 48 hrs after JWH015 exposure (Table 1). This JWH015-mediated effect on glycohydrolases appeared to be preferential at the plasma membrane level, since the same enzyme activities measured in the total cell lysate did not change (Table 2). Along with this, I also assessed Cer synthase (CERS) gene expression by qPCR and found that in JWH015-treated cells the levels were significantly higher in RT112 (+200%) as well as in RT4 (+120%) cells compared to controls (not shown), indicating additional contribution via *de novo* synthesis to the final Cer level in JWH015-treated cells.

		Enzyme activity in plasma membrane (pmoles/mg protein/hours)				
		GBA1	**GBA2**	**β-Hex**	**β-Gal**	**SMase**
RT4	**ctrl**	0.098 ± 0.001	0.0531 ± 0.009	0.569 ± 0.002	0.023 ± 0.002	2.8 ± 0.2
	JWH015	0.17 ± 0.01*	1.25 ± 0.03*	2.2 ± 0.2*	0.049 ± 0.001*	2.1 ± 0.3
RT112	**ctrl**	0.156 ± 0.001	ND	0.256 ± 0.003	0.0125 ± 0.001	2.5 ± 0.3
	JWH015	0.32 ± 0.03*	0.75 ± 0.02*	1.26 ± 0.01*	0.046 ± 0.003*	1.25 ± 0.05*

Table 1. Plasma-membrane associate glycohydrolases measured in RT4 and RT112 cells treated with JWH015. Cells were treated or untreated for 48h with 20 μM JWH015 and subjected to enzymatic assays. The activity associated with the cell surface was measured directly on living cells. Data are expressed as picomoles of formed metabolite per milligram of cell protein per hour and are the mean ± SD of at least three separate experiments. Comparisons between groups were made using Student's t test. *$p<0.005$ vs untreated cells.

		Enzyme activity in total cell lysate (nmoles/mg protein/hours)					
		GBA1	**GBA2**	**β-Hex**	**β-Gal**	**Neu3 §**	**SMase §**
RT4	**ctrl**	3.2 ± 0.2	2.3 ± 0.1	2500 ± 157	186 ± 13	3.77 ± 0.4	250 ± 10
	JWH015	4.8 ± 0.3	2.2 ± 0.1	1723 ± 145	166 ± 23	4.23 ± 0.32	153 ± 20
RT112	**ctrl**	1.5 ± 0.2	1.1 ± 0.09	1150 ± 213	115 ± 8	8.23 ± 0.56°	103 ± 9
	JWH015	1.7 ± 0.4	1.0 ± 0.07	650 ± 33	94 ± 8	10.6 ± 0.21*	123 ± 5

Table 2. Enzyme activity in total cell lysate measured in RT4 and RT112 cells treated with JWH015. Cells were treated or untreated for 48h with 20 μM JWH015 and subjected to enzymatic assays. . The activity associated with the total cell lysate was evaluated as described above. Data are expressed as picomoles/nanomoles of formed metabolite per milligram of cell protein per hour and are the mean ± SD of at least three separate experiments. Comparisons between groups were made using Student's t test.
° $p<0.005$ vs RT4, *$p<0.005$ vs untreated cells, §: picomoles per milligram of protein per hours.

Bladder cancer cell motility is modulated by cellular GSL

I found a significant differential expression of some GSL (Figure 8) between RT4 and RT112 cell lines. Previous reports had already demonstrated how cellular GSL, in particular gangliosides, may dramatically change during differentiation and malignant transformation promoting cellular motility [49]. As depicted in Figure 8A, the levels of the globotriesosylceramide, Gb3, previously described as cell motility-promoting sphingolipid [27], was found 15-fold higher ($p<0.001$) in RT112 cells than in RT4 cells. Conversely, RT4 cells showed a 5-7-fold higher levels ($p< 0.01$) of both the cell migration-inhibiting ganglioside GM3 [27,49,50] and of glucosylceramide (GlcCer) respectively (Figure 9A). In addition, the lower levels of GM3 detected in RT112 cells compared to RT4 cells strongly correlated with the increased enzymatic activity (+55.4±5%, $p<0.01$) of the specific sialidase Neu3 (Table 1), which is devoted to hydrolyze gangliosides, such as GM3, at the cell plasma membrane level. Furthermore, we detected a 4-fold increase ($p< 0.05$) in the expression levels of the GM3 synthase gene (SAT1) in RT4 cells if compared with RT112 (not shown).

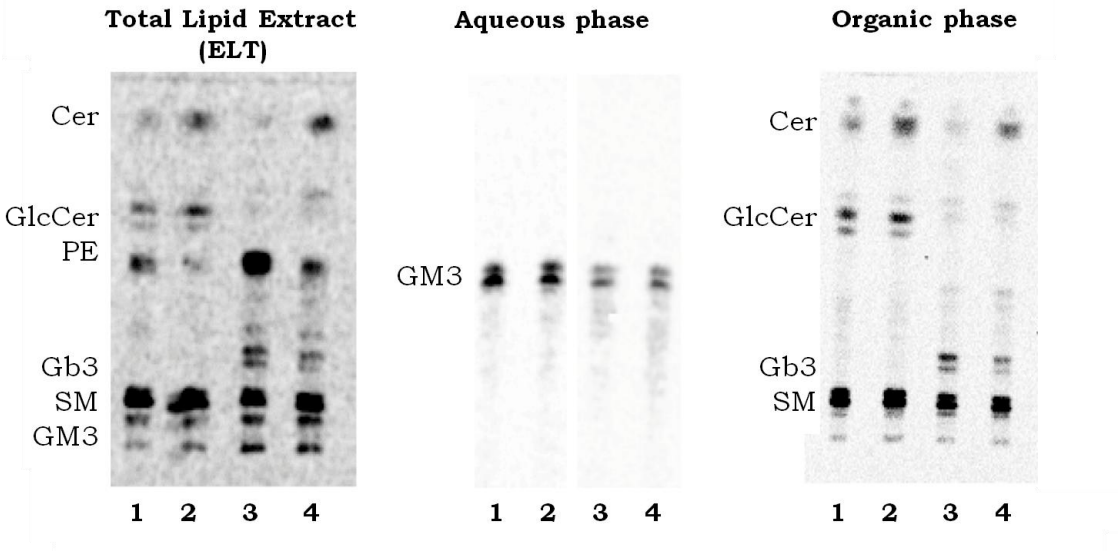

Figure 8. Representative TLC showing lipid composition of BCa cells before and after JWH015 treatment. After metabolic labeling with 2h pulse of [1-^{3}H]sphingosine, RT4 (lanes 1–2) and RT112 (lanes 3-4) cells were chased with vehicle (lanes 1 and 3) or 20μM JWH015 for 24 h (lanes 2 and 4). Cellular lipids were then extracted and subjected to phase separation as described in Materials and Methods. The total lipid extracts (panel A), spotted as equal amount of total radioactivity and equal volumes of partitioned lipids in the aqueous (panel B) and organic (panel C) phase, corresponding to same amount of total cell lipid radioactivity, were separated by HPTLC and visualized by digital autoradiography. Radioactive lipids were identified by using the appropriate standards: ceramide (Cer), glucosylceramide (GlcCer), phosphoethanolamine (PE), globotriaosylceramide (Gb3), sphingomyelin (SM).

The different GSL pattern between RT112 and RT4 cell lines were, in turn, associated with different functional features in terms of cellular motility. As depicted in Figure 9, RT112 and RT4 cells, independently of their comparable proliferation rates (not shown), displayed a differential motility. In a wound-healing assay (Figure 9, panel B-G), we found that RT112 cells reconstituted more than 70% of the scratched area within 48 hrs (Figure 9, panel D-E-F), while, in the same time frame, RT4 cells only populated 5% of the free available surface (Figure 9, panel B-C-F) The invasivity features of RT112 cells were also markedly different from the RT4 cells, as demonstrated by a classical matrigel-based invasion assay (Figure 9G). To sum up, considering the nature of the constitutive GSL, the associated metabolic enzymes, and the differential cell mobility and invasivity, RT112 and RT4 cells can reasonably be considered as models of high- and low-grade malignancy, respectively. In addition to these evidences, along with the recent findings that demonstrated the strong link between plasma membrane GSL and the activation of ERM proteins in driving cancer progression mechanisms [51,52], I showed that the levels of phospho-ERM detected in RT112 cells were significantly higher compared to RT4 (Figure 9H), suggesting a cytoskeletal rearrangement in high-grade bladder cancer cells. Previous data [53] demonstrated that the phosphorylation level of ERM was strictly linked to the level of S1P. Consistently with this, the content of S1P we measured in high-motility RT112 cells was 3-fold higher than the one in low-motility RT4 cells (3.8±0.56 vs 1.43±0.36 nCi $mg^{-1;}$ $p<0.01$); in addition, the sphingosine kinase 1 (SK1) was upregulated in both gene expression (5-fold) and enzymatic activity (891±94 vs 283±71 pmoles $hour^{-1}$ $mg^{-1;}$ $p<0.01$) in RT112 cells compared to RT4 cells. Finally, in order to directly relate the GSL metabolism with cell motility, RT112 cells were pretreated either with an inhibitor of GSL synthesis (AMP-dNM) or a migration-inhibitory GSL (GM3) before measuring the cell migration in the scratch assay. As shown in Figure 9I, both AMP-dNM and exogenous GM3 were able to significantly reduce the motility of RT112 cells.

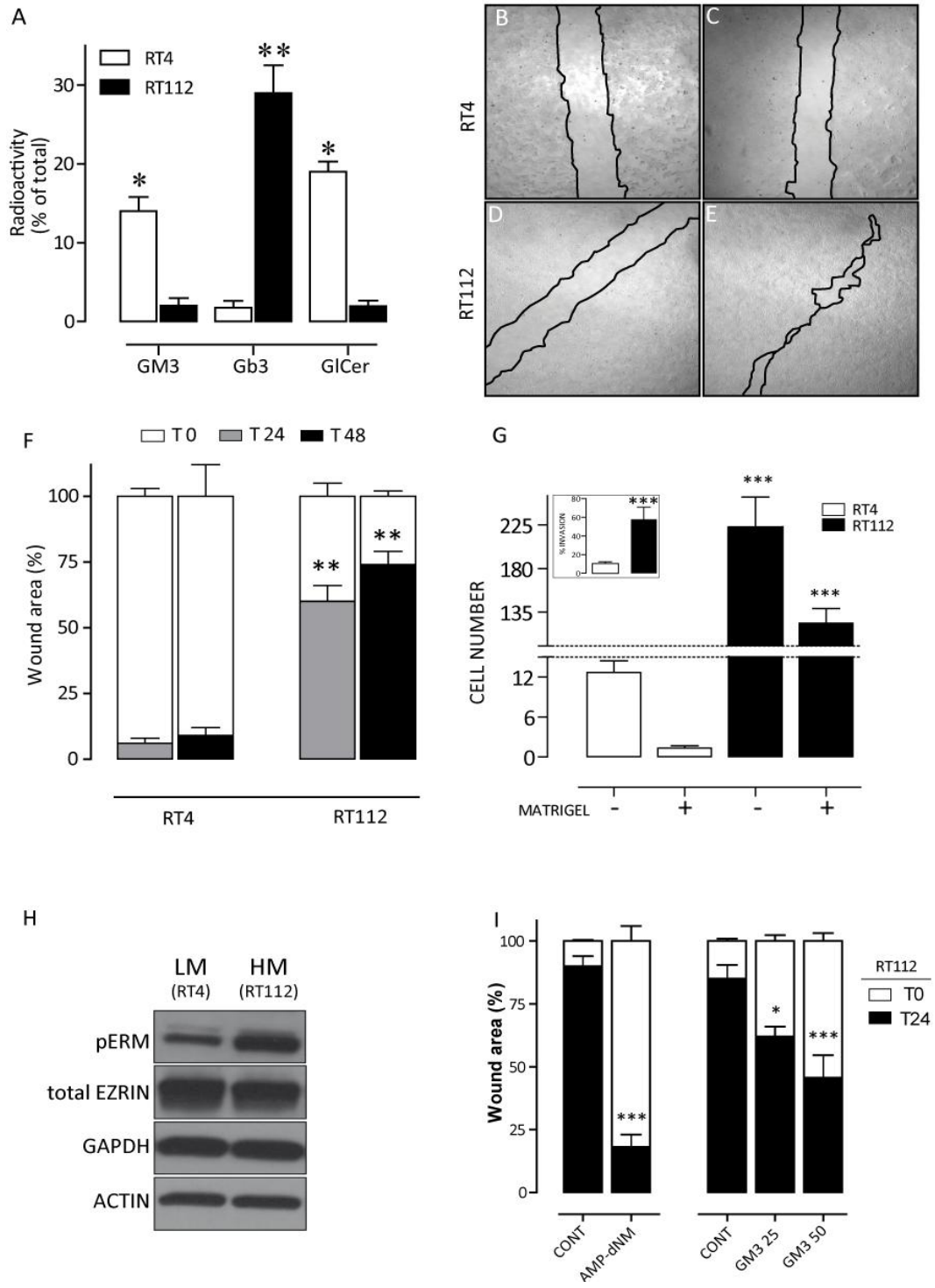

Figure 9. Differential GSL composition and motility between high and low grade BCa cells.
Panel A: Sphingolipid composition of RT4 and RT112 cells. Cell lipids were metabolically labeled with [1-^{3}H]sphingosine at the steady-state. Lipids were then extracted separated by HPTLC, visualized by digital autoradiography and quantified with specific Beta-Vision software. Data are expressed as the percentage of total radioactivity incorporated into sphingolipids and are the means ± SD of three different experiments. * $p< 0.05$ versus RT112. ** $p< 0.01$ versus RT112.
Panels B-E: Representative pictures of wound-healing assays in either RT4 cells at T0 (panel B) and 48 h after scratch (panel C) or RT112 cells at T0 (panel D) and 48 h after scratch (panel E). Wound edges were artificially highlighted by drawing a black line.

Panel F: Quantification of cell migration evaluated as % of cell-covered area at 24 h (gray bars) and 48 h (black bars) compared to the cell-free wound area at time 0 (white bars). Data are the mean±sd of three independent experiments done in triplicate. ** $p<0.01$ vs RT4 cell, ANOVA, Dunnett's T test.
Panel G: invasion assay on RT4 and RT112 cells. Data ate expressed as number of migrated cells through the pores with or without the presence of matrigel. The percent of invasion thru the matrigel is show in the panel inset. Data are the mean±sd of quadruplicates from 2 independent experiments. *** $p< 0.01$ vs RT4 cells.
Panel H: Phospho-ERM WB quantification on low-motility (LM, RT4) and high-motility (HM, RT112) cells. EZRIN, GAPDH and β-Actin proteins were used as control.
Panel I: Cell motility quantification of RT112 cells in the presence of GSL metabolism modulators evaluated as % of re-populated scratched area, compared to control (CONT). Wounded RT112 cultures were incubated with vehicle (DMSO), AMP-dNM (0.4 μM) or exogenous GM3 (25-50 μM) for 24 hrs. Data are the mean±sd of three experiments done in triplicate.

Previous reports associated cannabinoids with reduced metastatic and invasive behaviors in cancer, both in vitro and in vivo [54]. We then evaluated the effect of non-cytotoxic concentrations of JWH015 on the migration capability of high grade RT112 cells. As shown in Figure 10, RT112 cells were prevented from migrating upon exposure to escalating doses of JWH015. In particular, 1 μM JWH015 significantly inhibited by approx. 50% the reconstitution of the cell monolayer (Figure 10, panel D-G) 24 hours after stimulation, as compared to untreated control cells (Figure 10, panel B-G). The maximal effect was achieved with the highest JWH015 concentration (20 μM) and accounted for almost 90% inhibition (Figure 10, panel E-F-G). This effect, however, was accompanied by an increase in the frequency of apoptotic and necrotic phenotype, which accounted for 40±3% in cells treated with 20 μM JWH015, compared to 3±2% in 1 μM-treated cells or 3.5±2% in control cells ($p<0.01$). The functional effect on the migratory properties in aggressive RT112 cells was accompanied by a change in the levels of the motility-promoting globoside Gb3, which reduced after JWH015 treatment (Figure 10H, $p<0.01$) in RT112 cells, while it remained unchanged in low motility RT4 cells. As expected, both in high grade (RT112) and low grade (RT4) cells, agonist-mediated CB2 activation increased the level of the Cer precursor GlcCer (Figure 10H).

To further test the anti-migratory effects of cannabinoids we assayed the level of phospho-Src in its inactive state. The activation of the c-SRC protein is associated with enhanced migratory features, cell transforming potential and cancer progression [55]. As shown in Figure 10I, the inactive form of c-Src, which is phosphorylated in Tyr-530, was consistently up-regulated over time in cells treated with the CB2 agonist JWH015. The effects of JWH015 on cell migration was partly reverted by the pharmacological inhibition of GSL metabolism, which increased the cell motility (Figure 10J) and reduced the inactive form of p-Src (Figure 10K).

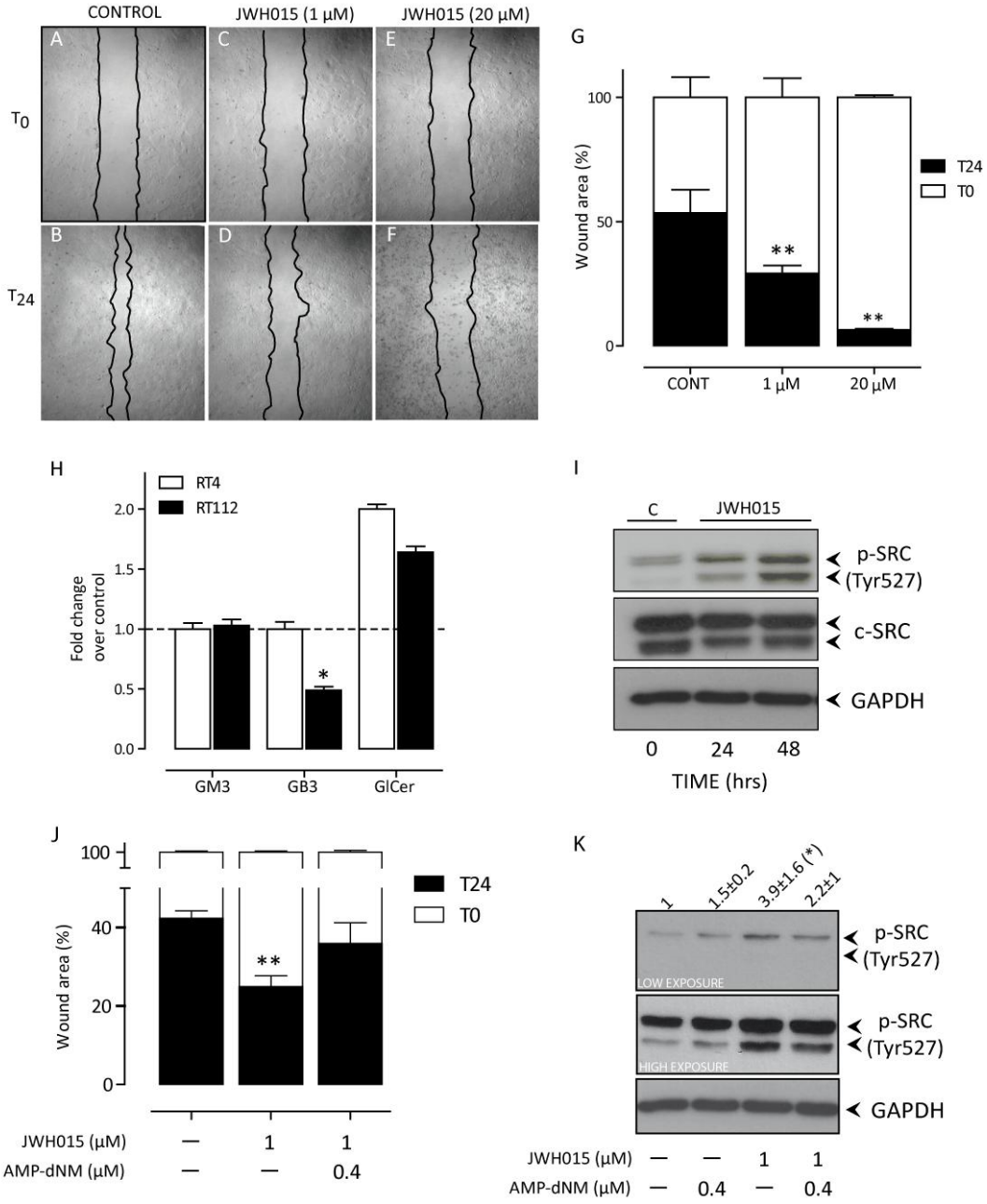

Figure 10. Effect of JWH015 treatment in high motility RT112 cells.
Panels A-F: Representative pictures of RT112 wound healing assay evaluated 24 hrs post scratch. Wound edges were artificially highlighted by drawing a black line.
Panel G: Cell migration was quantified as % of cell-covered area at 24 h (black bars) compared to the cell-free wound area at time 0 (white bars). Data are the mean±sd of three independent experiments in triplicate. ** $p<0.01$ vs T0, ANOVA, Dunnett's T test.
Panel H: Levels of measured GSL (GM3, Gb3, and GlcCer) in RT4 and RT112 cells after exposure to JWH015 (1 μM) for 24 h. Data are the mean±sd of three independent experiments and expressed as fold chance over the level measured in untreated cells and indicated by the dashed line. * $P<0.05$ vs RT4, ANOVA, Dunnett'sT test.
Panel I: immunoblotanalysis of inactive c-Src (p-Src Tyr527) 24 and 48 hrs after JWH015 (1 μM) exposure in RT112 cells. Similar results were obtained in two other independent experiments.

Panel J: Effect of GSL synthesis inhibition by AMP-DNM (0.4 μM) on JWH015 (1 μM) -modulated RT112 cell migration evaluated as % of re-populated scratched area. Data are the mean±sd of quadruplicate values.
Panel K: Immunoblot analysis of inactive c-Src (pSRC Tyr527) in RT112 cells treated with JWH015 (1 μM) with or without AMP-DNM (0.4 μM). The calculated fold-increase of band density (mean±sd, n=4) is shown above the panel. Both low and high exposure blots are shown.

Effects of the CB2 agonists on a murine model of an orthotopically implanted urothelial cancer

In order to gain a formal proof of concept that local exposure to CB2 agonists may prevent tumor growth in vivo, we used a relevant murine model of an orthotopically implanted urothelial cancer. As shown, intravesical instillations of JWH015, started three days after mucosal tumor implantation, significantly delayed the onset macro-hematuria, a specific symptom of tumor uptake and reduced the frequency of tumor-positive animals (Figure 11A). Terminal evaluation of the tumor load evaluated as bladder weight measured 2 weeks after tumor implantation demonstrated that intravesical instillations successfully reduce the tumor burden compared to vehicle-instilled animals (Figure 11B). The data support the effect of the CB2 agonists in inhibiting both tumor progression and growth.

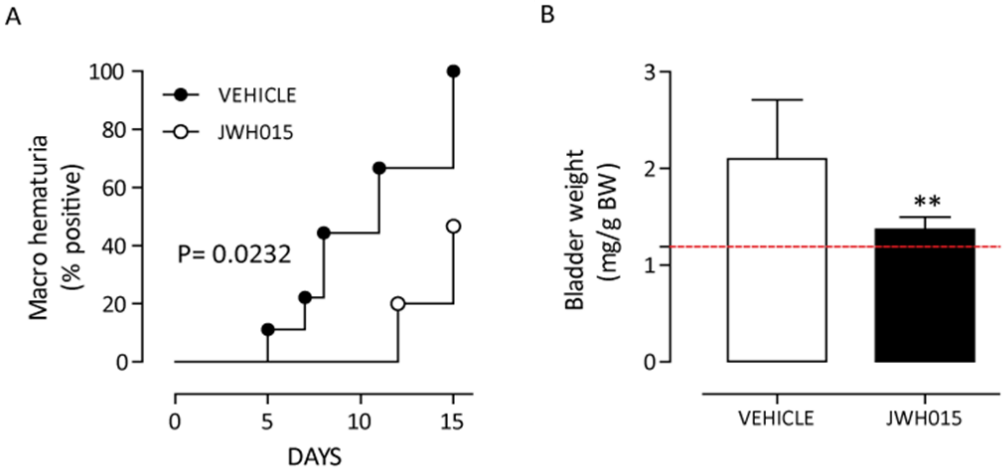

Figure 11. Effect of JWH015 on orthotopic bladder tumor uptake and growth in vivo.

Panel A: Frequency of macro hematuria-positive animals. Animals were engrafted with BCa cells as previously describe in Matherials and Methods. Three days after tumor instillations mice were treated intravesically with vehicle (n=9) or 20 μM JWH015 (n=6). Treatments were repeated other two times 4 days apart.

Panel B: quantification of tumor burden evaluated as increment of bladder weight. Data are normalized and expressed as the mean±ds of mg bladder over g body weight. Horizontal dashed line represent the normality cut-off of bladder weight in naïve, untreated animals.

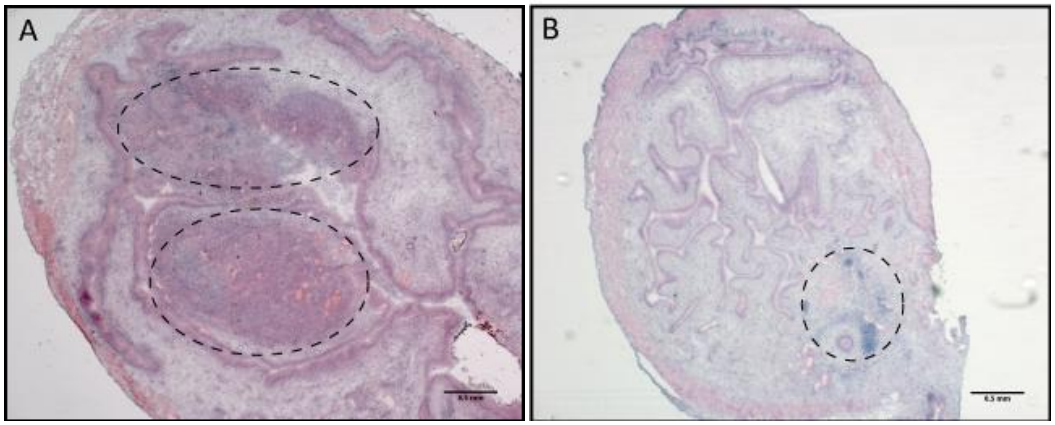

Figure 12. Histological evaluation of tumor bearing bladders. Representative image of a bladder of vehicle-treated (Panel A) and JWH015-treated animals (Panel B). Tumor lesions are indicated by the circle. Scale bars= 0.5 mm

Discussion

My study suggests CB2 as a putative novel target for innovative treatments and diagnostic/prognostic tools in BCa., I describe also previously unrecognized links between the endocannabinoid system and the glycosphingolipid pathway, as CB2-mediated modulation of cancer cell proliferation are conveyed by specific lipidic signals that also control cell motility and malignancy of urothelial cancer cells.

CB2 receptor as potential target in BCa

Recent data describe CB1 and CB2 receptors in all layers of the normal human bladder [18,20]. It Has already been described for other tumor types [56,57], we found that in primary BCa, the expression of CB2 is consistently higher in the neoplastic lesion, when compared to paired normal urothelial and stromal counterparts. This finding may support the specific use of CB2 as target of therapeutic and diagnostic approaches [58].

My results also demonstrate that CB2 receptors which are expressed in bladder cancer cells are functional, as indicated by the effect of the CB2-selective synthetic agonists on cellular functions, which was partially prevented by CB2-selective antagonism, but not by a CB1 antagonist. Notably, and consistent with previous findings [54,59,60], the JWH015-induced arrest of proliferation appears to be selective for tumor cells, while no significant effects are detected if the cells present a low proliferation rate, such as normal human fibroblasts, upon exposure to the CB2-agonist. Hence, stimulation of CB2 may be coupled to the activation of signaling pathways that are differently regulated between transformed and non-transformed cells [54]. I cannot exclude the involvement of a third related receptor, such as the GPR55, which may also interact with JWH015 [61,62]. This receptor is however contradictory reported to be associated with signals that promote either cancer cell proliferation or antiproliferative effects [63,65]. Further studies are needed to elucidate the role of GPR55 also in bladder cancer.

CB2-mediated cytotoxic mechanisms in BCa cells

Previous reports [48,54,65] demonstrated that tumor cell autophagy is induced by cannabinoids as an early event. I found that BCa cells react to the cannabinoid-induced stress by initially activating autophagy as defective

survival signal that is eventually taken over by the apoptotic response. Also, some molecular events, such as mTORC1 inhibition, predisposing the autophagy machinery are occurring before the cannabinoid-mediated caspase 3 activation, confirming that cellular and possibly defective autophagy, is indeed preceding the JWH015-induced cytotoxicity of bladder cancer cells. Furthermore, Cer-mediated inhibition of the pro-survival signal Akt is a well-recognized mechanism of mTORC1 inactivation and apoptosis conversion [48,66].. In my experimental setting, however, this effect is preceded by a transient increase in the phosphorylated form of Akt, indicating an initial possible activation of this system. These apparently contrasting results may be partly explained by either a cellular homeostatic loop that transiently switches on in an attempt to maintain Akt activity upon its inhibition, as it has been previously described [56], or by speculating a possible effect of the JWH015 compound on the GPR55 receptor that is reported to upregulate Akt in other tumors [63,64,67].

To better understand the mechanism of action of CB2-mediated apoptosis in bladder cancer cells, I investigated the role of sphingolipids metabolism in the modulation of cell survival/death pathways. Cer, indeed, is well known pro-apoptotic lipid, which is described to act as a second messenger of the cannabinoid-mediated actions in various model systems [68]. CB1 activation, for instance, induces Cer accumulation in primary astrocytes and glioma cells through both SM hydrolysis and de novo synthesis [28,69]. Recently, CB2 activation has been shown to induce cell apoptosis through the stimulation of Cer *de novo* synthesis in a number of human tumors, including glioma [28,69], leukemia [70], and pancreatic cancer [71].

The mechanisms involved in the CB2–mediated induction of Cer are still largely unknown. my data demonstrate that CB2 activation may indeed stimulate Cer synthesis also in bladder cancer cells. The molecular event underlying Cer accumulation upon exposure to CB2 agonists is most likely not due to sphingomyelin hydrolysis, whose cellular level remains unchanged, but are rather mediated by reduced metabolism of S1P. Cer is produced by dephosphorylation of S1P, operated by two specific phosphatases (SPP1 and SPP2), to sphingosine, which eventually is converted to Cer by CERS. In addition, conversion of the sphingosine to S1P operated by the sphingosine kinases could also play a pivotal role in this process [72]. We investigated the role of different enzymes involved in the

GSL metabolism to analyze the biochemical pathways leading to Cer-induced apoptosis in bladder cancer cells upon exposure to cannabinoids. Like Cer, S1P may also act as a second messenger in the regulation of cell survival/death pathways, with an opposite, anti-apoptotic effect [31]. Thus, conversion of S1P into sphingosine and eventually Cer shifts the ratio between anti-apoptotic to pro-apoptotic signals (namely S1P and Cer) towards cell death. The increase of Cer, with the concomitant reduction of S1P, perfectly reflects the well-known sphingolipid rheostat which controls cell proliferation/apoptosis. In fact, a high level of Cer associated with a low amount of S1P is usually resulting in cell growth arrest, whereas the opposite situation corresponds to an increased cell proliferation [31]. The large increase in Cer content that I measured is however not completely attributable to the moderate, but significant, reduction of S1P. Since Cer may also derive from *de novo* biosynthesis as well as GSL catabolism, I demonstrated that the CB2 agonist JWH015 triggers Cer accumulation also via the known mechanism [73], which implies the sequential activation of different GSL-converting glycohydrolases located in the cell membrane. Overexpression of Neu3 and production of LacCer have been demonstrated to provide antiapoptotic effects in tumors [74,75]. In contrast, I detected a significant increase of Neu3 activity after CB2 activation. This effect may be explained either by a CB2-mediated apoptotic signal that originates from Neu3-mediated GM3 hydrolysis and ends up to Cer via activation of downstream glycohydrolases, or by an ineffective attempt of the bladder cancer cells to survive by increasing the levels of LacCer. Thus, my data support the hypothesis that, in bladder cancer cells, the initial accumulation of the lipid ceramide, in response to JWH015 treatment, is due to multiple and coordinated series of biochemical pathways leading to apoptosis activation.

Role of GSL metabolism in BCa cell motility and its modulation by CB2 engagement

The models which has been shown of bladder cancer are characterized by significant differences in the GSL patterns, particularly reminiscent of the described differential GSL composition reported for invasive and papillary bladder cancer [27]. I show that bladder cancer cells expressing high Gb3 and low GM3 gangliosides in fact display enhanced cell mobility, which

characterizes the RT112 cells as a suitable model for invasive bladder cancer. This feature is further reinforced by the evidence demonstrating that, in high-motility bladder cancer cells (RT112), a robust inverse correlation exists between the cellular levels of S1P [53] and up-modulated phospho-ERM proteins. Phosho-ERMs have previously been recognized to play a pivotal role in driving cancer progression mechanisms through its increased levels that control the cytoskeletal rearrangement [51,52].

Along with these evidences, I have shown that the agonist-mediated activation of CB2 receptors in high grade bladder cancer cells have a profound impact on GSL, which are components of the plasma membrane that dramatically change during cell differentiation and malignant transformation [76]. The molecular mechanisms involved in the downstream activation of CB2 receptor appear complicated and further studies are indeed necessary. Still, I show that cell motility in bladder cancer cells, a hallmark feature of aggressive cancer, may be controlled by agonist-mediated CB2 activation, in a way that possibly interferes with the FAK-Src [55] pathway. Consistently, I have detected a significant increase of the inactive form of p-Src after CB2 activation, which resulted in reduced cell motility. This effect, as well as the activation of programmed cell death, is likely mediated by early events that impact on GSL metabolism. In attempt to illustrate a molecular model, as depicted in Figure 13, it's reasonable to suggest that, upon agonist-induced CB2 activation in high grade bladder cancer cells, a dual action inhibiting the sphingosine kinase enzyme and upregulating the ceramidase takes place. This in turn favors a reduction of S1P and an increase of Cer that shift the balance of the cellular rheostat towards apoptosis and cell cycle arrest. On the other hand, the plasma membrane-associated enzymatic hydrolysis of GSL is activated and produces a signaling cascade that may modulate cytoskeletal changes via p-ERM and cell migration via Src. Into this picture though, it is important also to consider the already reported receptor-independent effects of cannabinoids [77], which may play an important role in our system.

The present study, however, strongly associates the anti-metastatic properties of cannabinoids, which are described in the recent literature, [78-81], with a molecular mechanism involving CB2 contribution that implicates GSL metabolism. This finding, together with the in vitro antiproliferative effect, the in vivo efficacy on tumor progression, and the tumor-specific up-

regulation of CB2 in primary bladder cancer may play a role in the identification of novel therapeutic and diagnostic targets for treating bladder cancer. In addition, the use of non psycho-tropic cannabinoid agonists may warrant further studies to implement a more effective adjuvant treatment in transitional BCa aimed to prevent both tumor recurrence and progression.

References

1. Kirkali Z.C.T., Manoharan M., Algaba F., Busch C., Cheng L., Kiemeney L., Kriegmair M., Montironi R., Murphy W.M., Sesterhenn I.A., Tachibana M., Weider J. (2005) Bladder Cancer: epidemiology, staging and grading, and diagnosis. Urology,p. 4-34.

2. Fajkovic H., et al. (2011) Impact of gender on bladder cancer incidence, staging, and prognosis. World J Urol, 29(4): p. 457-63.

3. Scosyrev E., Noyes K., Feng C., Messing E. (2009) Sex and racial differences in bladder cancer presentation and mortality in the US. Cancer.,115(1): p. 68,74.

4. Freedman N.D., Silverman D.T., Hollenbeck A.R., Schatzkin A., Abnet C.C. (2011) Association between smoking and risk of bladder cancer among men and women. JAMA,306: p. 737-745.

5. Zeegers M.P.A., Tan F.E.S., Dorant E., Van den Brandt P.A. (2000) The Impact of Characteristics of Cigarette Smoking on Urinary Tract Cancer Risk: A Meta-Analysis of Epidemiologic Studies. American Cancer Society, 89(3): p. 630-639.

6. Kogevinas M., Mannetje A., Cordier S., Ranft U., González C.A., Vineis P., Chang-Claude J., Lynge E., Wahrendorf J., Tzonou A., Jöckel K.H., Serra C., Porru S., Hours M., Greiser E., Boffetta P. (2003) Occupation and bladder cancer among men in Western Europe. Cancer Causes Control, 14: p. 907-914.

7. Knight A., Askling J., Granath F., Sparen P., Ekbom A. (2004) Urinary bladder cancer in Wegener's granulomatosis: risks and relation to cyclophosphamide. Ann Rheum Dis, 63: p. 1307-1311.

8. Abern m.r., et al. (2013) The characteristics of bladder cancer after radiotherapy for prostate cancer. Urologic oncology,31(8): p. 1628-1634.

9. Griffiths T.R.L. (2013) On behalf of Action on Bladder Cancer: Current perspectives in bladder cancer management. Int J Clin Pract, 65(5): p. 435-448.

10. Anastasiadis A., de Reijke T.N. (2012) Best practice in the treatment of nonmuscle invasive bladder cancer. Ther Adv Urol, 4(1): p. 13-32.

11. Cheng L., Montironi R., Davidson D.D., Lopez-Beltran A. (2009) Staging and reporting of urothelial carcinoma of the urinary bladder. Modern Pathology, 22: p. S70-S95.

12. Kirkali Z., Chan T., Manoharan M., Algaba F., Busch C., Cheng L., Kiemeney L., Kriegmair M., Montironi R., Murphy W.M., Sesterhenn I.A., Tachibana M., Weider J. (2005) Bladder Cancer: epidemiology, staging and grading, and diagnosis. Urology, 66(6 Suppl 1): p. 4-34.

13. Grasso M. (2008) Bladder Cancer: A Major Public Health Issue. European Urology, Suppl 7: p. 510-515.

14. Sylvester R.J., et al. (2005) High-grade Ta urothelial carcinoma and carcinoma in situ of the bladder. Urology, 66(6 Suppl 1): p. 90-107.

15. Van der Meijden A.P., Sylvester R.J., Oosterlinck W., Solsona E., Boehle A., Lobel B., Rintala E. (2005) EAU guidelines on the diagnosis and treatment of urothelial carcinoma in situ. European Urology, 48(3): p. 363-371.

16. Sylvester R.J., Van der Meijden A.P., Oosterlinck W., Witjes J.A., Bouffioux C., Denis L., Newling D.W., Kurth K. (2006) Predicting recurrence and progression in individual patients with stage Ta T1 bladder cancer using EORTC risk tables: a combined analysis of 2596 patients from seven EORTC trials. Eur Urol 49: 466-465; discussion 475-477.

17. Richter S., Sridhar S.S. (2012) New directions for biologic targets in urothelial carcinoma. Molecular Cancer Therapeutics, 11:1226-1235

18. Gratzke C., Streng T., Park A., Christ G., Stief C.G., Hedlund P., Andersson K.E. (2009) Distribution and function of cannabinoid receptors1 and 2 in the rat, monkey and human bladder. J Urol, 181:1939-1948.

19. Gratzke C., Streng T., Sitef C.G., Downs T.R., Alroy I., Rosenbaum J.S., Andersson K.E., Hedlund P. (2010) Effects of cannabinor, a novel selective cannabinoid 2 receptor agonist, on bladder function in normal rats. Eur Urol, 57:1093-1100.

20. Strittmatter F., Gandaglia G., Benigni F., Bettiga A., Rigatti P., Montorsi F., Gratzke C., Stief C., Colciago G., Hedlund P. (2011) Expression of Fatty Acis Amide Hydrolase (FAAH) in human, mouse, and rat urinaly bladder and effects of FAAH inhibition on bladder function in awake rats. Eur Urol, 61(1):98-10.

21. Bifulco M., Laezza C., Pisanti S., Gazzerro P. (2006) Cannabinoids and cancer: pros and cons o fan antitumour strategy. Br J Pharmacol, 148:123-135.

22. Alexander A., Smith P.F., Rosengren R.J. (2009) Cannabinoids in the treatment of cancer. Cancer Lett, 285: 6-12.

23. Hermanson D.J., Marnett L.J. (2011) Cannabonoids, endocannabinoids, and cancer. Cancer and Metastasis Reviews, 30:599-612.

24. Gasperi V., Evangelista D., Oddi S., Florenzano F., Chiurchiu V., Avigliano L., Catani M.V., Maccarone M. (2014) Regulation of inflammation and proliferation of human bladder carcinoma cells by type-1 and type-2 cannabinoid receptors. Life Sci, 138:41-41.

25. Ogretmen B., Hannun Y.A. (2004) Biologically active sphingolipids in cancer pathogenesis and treatment. Nat Rev Cancer, 4:604-616.

26. Ohyama C. (2008) Glycosylation in bladder cancer. Int J Clin Oncol, 13:308-313.

27. Kawamura S., Ohyama C., Watanabe R., Satoh M., Saito S., Hoshi S., Gasa S., Orikasa S. (2001) Glycolipid composition in bladder tumor: a crucial role of GM3 ganglioside in tumor invasion. International Journal of Cancer, 94:343-347.

28. Galve-Roperh I., Sanchez C., Cortes M.L., Gomez del Pulgar T., Izquierdo M., Guzman M. (2000) Anti-tumoral action of cannabinoids: involvement of sustained ceramide accumulation and extracellular signal-regulated kinase activation. Nat Med, 6:313-319.

29. Cianchi F., Papucci L., Schiavone N., Lulli M., Magnelli L., Vinci M.C., Messerini L., Manera C., Ronconi E., Romagnani P., Donnini M., Perigli G., Trallori G., Tanganelli E., Capaccioli S., Masini E. (2008) Cannabinoid receptor activation induces apoptosis through tumor necrosis factor alpha- mediated ceramide de novo synthesis in colon cancer cells. Clinical Cancer Research, 14:7691-77000.

30. Gustafsson K., Sander B., Bielawski J., Hannun Y.A., Flygare J. (2009) Potentiation of cannabinoid-induced cytotoxicity in mantle cell lymphoma through modulation of ceramide metabolism. Molecular Cancer Research, 7:1086-1098.

31. Maceyka M., Payne S.G., Milstien S., Spiegel S. (2002) Sphingosine kinase, sphingosine-1-phosphate, and apoptosis. Biochimica et Biophysica Acta-Molecular and Cell Biology of Lipids, 1585:193-201.

32. Sonnino, S., Chigorno, V ., Tettamanti, G. (2000) Preparation of radioactive gangliosides, 3H or 14C isotopically labeled at oligosaccharide or ceramide moieties. Methods Enzymol. 311, 639–656.

33. McIntosh H.H., Song C., Howlett A.C. (1998) CB1cannabinoid receptor: cellular regulation and distribution in N18TG2 neuroblastoma cells. Brain Res Mol, 53:163-173.

34. Shire D., Calandra B., Rinaldi-Carmona M., Oustric D., Pessegue B., Bonnin-Cabanne O., Le Fur G., Caput D., Ferrara P. (1996) Molecular cloning, exprression and function of the murine CB2 peripheral cannabinoid receptor. Biochim Biophys Acta, 107:132-136.

35. Leroy J.G., HO M.W., MacBrinn M.C., Zielke K., Jacob J., O'Brien J.S. (1972) I-cell disease: biochemical studies. Pediatr Res, 6:752-757.

36. Prinetti A., Millimaggi D., D'Ascenzo S., Clarkson M., Bettiga A., Chigorno V., Sonnino S., Pavan A., Dolo V. (2006) Lack of ceramide generation and altered sphingolipid composition are associated with drug resistance in human ovarian carcinoma cells. Biochemical Journal, 395: 311-318.

37. Scandroglio F., Loberto N., Valsecchi M., Chigorno V., Prinetti A., Sonnino S. (2009) Thin layer chromatography of gangliosides. Glycoconjugate Journal, 26:961-973.

38. Aureli M., Loberto N., Lanteri P., Chigorno V., Prinetti A., Sonnino S. (2011) Cell surface sphingolipid glycohydrolases in neuronal differentiation and aging in culture. Journal of Neurochemistry, 166:891-899.

39. Overkleeft H.S., Renkema G.H., Neele J., Vianello P., Hung I.O., Strijland A., van der Burg A.M., Koomen G.J., Pandit U.K., Aerts J.M. (1998) Generation of specific deoxynojirimycin-type inhibitors of the non-lysosomal glucosylceramidase. J Biol Chem, 273(41):26522-7.

40. Aureli M., Loberto N., Lanteri P., Chigorno V., Prinetti A., Sonnino S. (2011) Cell surface sphingolipid glycohydrolases in neuronal differentiation and aging in culture. Journal of Neurochemistry, 166:891-899.

41. Pitman M.R., Pham D.H., Pitson S.M. (2012) Isoform-selective assays for sphingosine kinase activity. Methods Mol Biol, 874:21-31.

42. Riboni L., Viani P., Tettamanti G. (2000) Estimating sphingolipid metabolism and trafficking in cultured cells using radiolabeled compounds. Sphingolipid Metabolism and Cell Signaling, Pt A, 311:656-682.

43. Network CGAR (2014) Comprehensive molecular characterization of urothelial bladder carcinoma. Nature, 507:315-322.

44. Berglund B.A., Boring D.L., Wilken G.H., Makriyannis A., Howlett A.C. (1998) Structural requirements for arachidonylethanolamide interaction with CB1 and CB2 cannabinoid receptors: pharmacology of the carbonyl and ethanolamide groups. Prostaglandins Leukotrienes and Essential Fatty Acids, 59:111-118.

45. Showalter V.M., Compton D.R., Martin B.R., Abood M.E. (1996) Evaluation of binding in a transfected cell line expressing a peripheral cannabinoid receptor (CB2): identification of cannabinoid receptor subtype selective ligands. Journal of Pharmacology and Experimental Therapeutics, 278:989-999.

46. Huffman J.W., Liddle J., Yu S., Aung M.M., Abood M.E., Wiley J.L., Martin B.R. (1999) 3-(1',1'-Dimethylbutyl)-1-deoxy-delta8-THC and related compounds: synthesis of selective ligands for the CB2 receptor. Bioorg Med Chem, 7:2905-2914.

47. Velasco G., Galve-Ropher I., Sanchez C., Blazquez C., Haro a., Guzman M. (2005) Cannabinoids and ceramide: two lipids acting hand-by-hand. Life Sciences, 77:1723-1731.

48. Salazar M., Corracedo A., Salanueva I.J., Hernandez-Tiedra S., Lorente M., Egia A., Vazquesz P., Blasquez C., Torres S., Garcia S., Nowak J., Fimia G.M., Piacentini M., Cecconi F., Pandolfi P.P., Gonzales-Feria L., Iovanna J.L., Guzman M., Boya P., Velasco G. (2009) Cannabinoid action induces autophagy-mediated cell death through stimulation of ER stress in human glioma cells. J Clin Invest, 119:1359-1372.

49. Prinetti A., Cao T., Illuzzi G., Prioni S., Aureli M., Gagliano N., Tredici G., Rodriguez-Menendez V., Chigorno V., Sonnino S. (2011) A glycosphingolipid/Caveoilin-1 signaling complex inhibits motility of human ovarian carcinoma cells. Journal of Biological Chemistry, 286:40900-40910.

50. Prinetti A., Aureli M., Illuzzi G., Prioni S., Nocco V., Scandroglio F., Gagliano N., Tredici G., Rodriguez-Menendez V., Chigorno V., Sonnino S. (2010) GM3 synthase overexpression results in reduced cell motility and in caveolin-1 upregulation in human ovarian carcinoma cells. Glycobiology, 20:62-77.

51. Leiphrakpam P.D., Rajput A., Mathiesen M., Agarwal E., Lazenby A.J., Are C., Brattain M.G., Chowdhury S. (2014) Ezrin expression and cell survival regulation in colorectal cancer. Cell Signal, 26:868-879.

52. Luo Y, Zheng C., Zhang J., Lu D., Zhuang J., Xing S., Feng J., Yang D., Yan D., Yan X. (2012) Recognition of CD146 as an ERM-binding protein offers novel mechanisms for melanoma cell migration. Oncogene, 31:306-321.

53. Gandy K.A.O., Adada M., Canals D., Carrol B., Roddy P., Hannun Y.A., Obeid L.M. (2013) Epidermal growth factor-induced cellular invasions requires sphingosine-1-phosphate/sphingosine-1-phosphate 2 receptor-mediated ezrin activation. Faseb Journal, 27:3155-3166.

54. Velasco G., Sãinchez C., Guzmãin M. (2012) Towards the use of cannabinoids as antitumour agents. Nat Rev Cancer, 12:436-444.

55. Guarino M. (2010) Src signaling in cancer invasion. J Cell Physiol, 223:14-26.

56. Han E.K.H., Leverson J.D., McGonigal T., Shah O.J., Woods K.W., Hunter T., Giranda V.L. (2007) Akt inhibitor A-443654 induces rapid Akt Ser-473 phosphorylation independent of mTORC1 INHIBITION. Oncogene, 26:5655-5661.

57. Preet A., Qamri Z., Nsser M.W., Prasad A., Shilo K., Zou Z.H., Groopman J.E., Genju R.K. (2011) Cannabinoid receptors, CB1 and CB2, as novel targets for inhibition of non-small cell lung cancer growth and metastasis. Cancer Prevention Research, 4:65-75.

58. Sarfaraz S., Afaq F., Adhami V.M., Mukhtar H. (2005) Cannabinoid receptor as a novel target for the treatment of prostate cancer. Cabcer Res, 65:1635-1341.

59. Casanova M.L., Blazquez C., Martinez-Palacio J., Villanueva C., Fernandez-Acenero M.J., Huffman J.W., Jorcano J.L., Guzman M. (2003) Inhibition of skin tumor growth and angiogenensis in vivo by activation of cannabinoid receptors. Journal of Clinical Investigation, 111:43-50.

60. McAllister S.D., Chan C., Taft R.J., Luu T., Abood M.E., Moore D.H., Aldape K., Yount G. (2005) Cannabinoids selectively inhibit proliferation and induce death of cultured human glioblastoma multiforme cells. Journal of Nuero-Oncology, 74:31-40.

61. Ryberg E., Larsson N., Sjogren S., Hjorth S., Hermansson N.O., Leonova J., Elebring T., Nilsson K., Drmota T., Greasley P.J. (2007) The orphan receptor GPR55 is a novel cannabinoid receptor. Br J Pharmacol, 152:1092-10101.

62. Lauckner J.E., Jensen J.B., Chen H.Y., Lu H.C., Hille B., Mackie K. (2008) GPR55 is a cannabinoid receptor that increases intracellular calcium and inhibits M current. Proceedings of the National Academy of Sciences of the United States of America, 105:2699-2704.

63. Pineiro R., Maffucci T., Falasca M. (2011) The putative cannabinoid receptor GPR55 defines a novel autocrine loop in cancer cell proliferation. Oncogene, 30:142-152.

64. Hu G., Ren G., Shi Y. (2011) The putative cannabinoid receptor GPR55 promotes cancer cell proliferation. Oncogene, 30:139-141.

65. Vara D., Salazar M., Olea-Herrero N., Guzman M., Velasco G., Diaz-Laviada I. (2011) Anti-tumoral action of canabbinoids on hepatocellular carcinoma: role of AMPK-dependent activation of autophagy. Cell Death Differ, 18:1099-10111.

66. Shrivastava A., Kuzontkoski P.M., Groopman J.E., Prasad A. (2011) Cannabidiol induces programmed cell death in breast cancer cells by coordinating the cross-talk between apoptosis and autophagy. Molecular Cancer Therapeutics, 10:1161-1172.

67. Schmuhl E., Ramer R., Salamon A., Peters K., Hinz B. (2014) Increase of mesenchymal stem cell migration by cannabidiol via activation of p42/44 MAPK. Biochemical Pharmacology, 87:489-501.

68. Tirodkar T.S., Voelkel-Johnson C. (2012) Sphingolipids in apoptosis. Exp Oncol, 34:231-342.

69. Sanchez C., de Ceballos M.L., del Pulgar T.G., Rueda D., Corbacho C., Velasco G., Galve-Roperh I., Huffman J.W., Cajal S.R.Y., Guzman M. (2001) Inhibition of glioma growth in vivo by selective activation of the CB2 cannabinoid receptor. Cancer Research, 61:5784-5789.

70. Herrera B., Carracedo A., Diez-Zaera M., del Pulgar T.G., Guzman M., Velasco G. (2006) The CB2 cannabinoid receptorsignals apoptosisi via ceramide-dependent activation of the mitocondrial intrinsic pathway. Experimental Cell research, 312:2121-2131.

71. Carracedo A., Gironella M., Lorente M., Garcia S., Guzman M., Velasco G., Iovanna J.L. (2006) Cannabinoids induce apoptosis of pancreatic tumor cells via endoplasmic reticulum stress-related genes. Cancer Res, 66:6748-6755.

72. Hannun Y.A., Obeid L.M. (2008) Principles of bioactive lipid signalling: lessons from sphingolipids. Nature Reviews Molecular Cell Biology, 9:139-150.

73. Valaperta R., Chigorno V., Basso L., Prinetti A., Bresciani R., Preti A., Miyagi T., Sonnino S. (2006) Plasma membrane production of ceramide from ganglioside GM3 in human fibroblats. Faseb Journal, 20:1227-1229

74. Kawamura S., Sato I., Wada T., Yamaguchi K., Li Y., Li D., Zhao X., Ueno S., Aoki H., Tochigi T., Kuwahara M., Kitamura T., Takahashi K., Moriya S., Miyagi T. (2012) Plasma membrane-associated sialidase (NEU3) regulates progression of prostate cancer to androgen-indipendent growth through modulation of androgen receptor signaling. Cell Death and Differentiation, 19:170-179.

75. Kakugawa Y., Wada T., Yamaguchi K., Yamanami H., Ouchi K., Sato I., Miyagi T. (2002) Up-regulation of plasma membrane-associated ganglioside sialidase (Neu3) in human colon cancer and its involvement in apoptosis suppression. Proc Natl Acad Sci U.S.A., 99:10718-10723.

76. Sonnino S., Prinetti A. (2010) Gangliosides as regulators of cell membrane organization and functions. Sphingolipids as Signaling and Regulatory Molecules, 688:165-184.

77. Chakravarti B., Ravi J., Ganju R.K. (2015) Cannabinoids as therapeutic agents in cancer: current status and future implications. Oncotarget, 5:5852-5872.

78. Ramer R., Merkord J., Rohde H., Hinz B. (2010) Cannabidiol inhibits cancer cell invasion via upregulation of tissue inhibitor of matrix metalloproteinases-1. Biochem Pharmacol, 9:955-966.

79. Ramer R., Rohde A., Merkord J., Rohde H., Hinz B. (2010) Decrease of plasminogen activator inhibitor-1 may contribute to the anti-invasive action of cannabidiol of human lung cancer cells. Pharm Res, 27:2162-2174.

80. Portella G., Laezza C., Laccetti P., De Petrocellis L., Di Marzo C., Bifulco M. (2003) Inhibitory effects of cannabinoid CB1 receptor stimulation on tumor growth and metastatic spreading: actions on signals involved in angiogenesis and metastasis. FASEB J, 17:1771-1773.